NASA Contractor Report 159791

(NASA-CR-159791) SENSOR FAILURE AND MULTIVARIABLE CONTROL FOR AIRBREATHING PROPULSION SYSTEMS Ph.D. Thesis - Dec. 1979 Final Report (Toledo Univ.) 244 p HC A11/MF A01 CSCL 01B G3/01

N83-16279

Unclas 08312

SENSOR FAILURE ANALYSIS AND MULTIVARIABLE CONTROL FOR AIRBREATHING PROPULSION SYSTEMS

Khosrow Behbehani

University of Toledo
Toledo, Ohio

March 1980

Prepared for

NATIONAL AERONAUTICS AND SPACE ADMINISTRATION
Lewis Research Center
Under Grant NSG-3084

TABLE OF CONTENTS

An Abstract of

SENSOR FAILURE ANALYSIS AND MULTIVARIABLE

CONTROL FOR AIRBREATHING PROPULSION SYSTEMS

Khosrow Behbehani

Submitted in partial fulfillment
of the requirements of the
Doctor of Philosophy Degree

University of Toledo
December 1979

A new sensor/actuator failure analysis technique for turbofan jet engines is developed. The technique utilizes redundant information embedded in the engine model residual and does not require multiple hardware redundancy.

Three phases of failure analysis, namely detection, isolation, and accommodation are considered. Failure detection and isolation techniques are developed by utilizing the concept of Generalized Likelihood Ratio (GLR) tests. These techniques are applicable to both time-varying and time-invariant systems. Three GLR detectors are developed for: (1) hard-over sensor failure; (2) hard-over actuator failure; and (3) brief disturbances in the actuators. The probability distribution of the GLR detectors and the detectability of sensor/actuator failures are established. Failure type is determined by the maximum of the GLR detectors. Failure accommodation is accomplished by extending the Multivariable Nyquest Array (MNA) control design techniques to nonsquare system designs.

The performance and effectiveness of the failure analysis technique are studied by applying the technique to a turbofan jet engine, namely the Quiet Clean Short-Haul Experimental Engine (QCSEE). Single and multiple sensor/actuator failures in the QCSEE are simulated and analyzed and the effects of model degradation are studied.

ACKNOWLEDGMENTS

I would like to acknowledge the support of the National Aeronautics and Space Administration's Graduate Research Program in Aeronautics and the Lewis Research Center for this research.

My special thanks go to the members of the Dynamics and Controls Branch of the Lewis Research Center for their continuous support and invaluable technical advice. In particular, I wish to express my gratitude to Dr. Walter C. Merrill for his continued interest, encouragement and excellent technical and editorial assistance.

I also wish to thank my advisor, Dr. Gary G. Leininger, for his ideas, guidance and generous assistance during the entire period of my doctoral studies. Furthermore, I would like to thank the co-chairman of my advisory committee, Dr. James B. Farison as well as Dr. Donald J. Ewing, Jr., Prof. John D. Hansell, Dr. O. William Muckenhirn, and Dr. R. Kenneth Wolfe for serving on the committee.

Next, I would like to thank Florence Sprosty and Millie Hutchison for their patience and perfection in typing the final manuscript of this thesis.

Finally, I wish to offer my appreciation to my family and S. B. Grantham for their ceaseless support and encouragement.

CHAPTER I

INTRODUCTION

1.1 Overview of Dissertation

The objective of this dissertation is to develop a sensor failure detection, isolation, and accommodation technique for air breathing propulsion systems. For this purpose a new detection and isolation technique based on testing the engine model residuals (the difference between the engine output and an engine model) is developed. The technique uses the redundant information available in dissimilar output measurements, thus eliminating the need for hardware redundancy. The concept of the Generalized Likelihood Ratio (GLR) (Ref. 31) is used to extract the detection information from the model residuals. Isolation of a failed sensor is achieved by estimating the direction and magnitude of the failure in the output space. Since in the proposed scheme a model of the engine would be available, the accommodation of a failed sensor can be achieved in three alternative ways. The first method is to replace the lost measurement with the corresponding measurement from the model. In the second method the control design configuration is changed by discarding the lost measurement and substituting a different measurement from the engine. Finally, as a third alternative, the failed sensor is discarded and a new design incorporating fewer sensors is implemented. To accomplish the reconfiguration of the control design a new nonsquare Multivariable Nyquist Array design procedure is developed. The detection, isolation, and accommodation techniques

developed in this dissertation are compatible with an on-board digital realization of an engine control system.

The remaining sections of this chapter provide a description of motivations, objectives and the necessary background for the development of the failure analysis technique. The organization of these sections is as follows. A brief description of the jet engine operation is presented in the next section. The engine control requirements and the future control systems of the jet engine are discussed in Section 1.3. Since the development of the detection technique is closely related to the design of the engine control system, the applications of control design techniques to the problem of engine control is reviewed in Section 1.4. In Section 1.5 three phases of sensor failure analysis are discussed. A brief review of the failure analysis techniques is presented in Section 1.6. Finally in Section 1.7 the objectives of this dissertation are defined and the outline of the proposed solution is presented.

1.2 Jet Engines

The history of the jet engine goes back to the year 1908. In that year, Rene Lorin, a French engineer proposed the use of hot gas pulses that would be expelled through a nozzle to generate propulsive thrust. However, it was not until the 1940's that the first jet engine was used to propel an aircraft (Ref. 64).

The main purpose of the jet engine is to generate thrust. To understand jet engine operation, consider the schematic diagram of a single spool turbojet engine and the corresponding ideal fluid processes diagram in Figure 1.1. The engine generates thrust by expelling high-velocity gases from the exhaust nozzle. This is achieved by the

following processes (ideal case):

0 - 1 : Large quantities of air are brought into the engine through the inlet duct. This will either accelerate or decelerate the air. There is a pressure and temperature increase associated with this process while the entropy remains constant (isentropic process).

1 - 2 : The velocity of the air is decreased through the inlet diffuser while the pressure and temperature continue to increase. In this process the entropy remains constant.

2 - 3 : The air is compressed in the compressor raising its pressure to the maximum cycle pressure. The rise in pressure is accompanied by an increase in air temperature, but the entropy does not change.

3 - 4 : The compressed air is passed on to the combustion chamber where the fuel is sprayed into the front of the chamber. The mixture of the air and fuel is burned, thus increasing the air temperature to the maximum cycle temperature. The pressure remains constant and the entropy increases.

4 - 5 : The hot gases produced in 3 - 4 are expanded through the turbine blades producing rotation of the turbine rotors. During this process the pressure and temperature drop and the entropy stays constant.

5 - 6 : The exhaust gases from the turbine are expelled through the nozzle thus increasing the air velocity.

The ideal turbojet engine cycle in Figure 1.1 corresponds to a temperature-entropy diagram of a Brayton cycle (Ref. 41).

To start a jet engine the compressor is turned using a starter motor. Simultaneously, fuel is added and spark ignited in the combustion chamber. When the compressor is rotating at sufficient speed, the starter and the ignitors are turned off. The engine will continue operating as long as fuel and air are supplied to the engine in proper proportions. Controlling the proper fuel-air ratio in the mixture is a must for safe operation of the engine. Excessive fuel could result in exceedingly high rotor speed, high turbine inlet temperature, and perhaps engine damage by violating its physical constraints. On the other hand, very lean fuel-air mixture could result in the engine shutting off. The problem of controlling the proper fuel-air ratio can be divided into two parts. The first part is how to accelerate the engine without violating its physical constraints and the second part is how to maintain steady-state operation as disturbances occur. These control requirements and the increased demand for higher thrust-weight ratio led jet engine designers to develop engines with more controls in addition to the fuel flow. Variable nozzle area, variable fan pitch angle, variable compressor vane position, and variable inlet guide vane are examples of the additional controls which are now available on the more sophisticated jet engines (see, e.g., Ref. 47). The addition of these input controls to the engine increases the complexity of the engine control problem. Hence, more sophisticated control systems are required to fully utilize the benefits of the additional input controls. A brief discussion of the control systems used to solve the engine control problem is presented in the next section.

1.3 Engine Control System

A general configuration of the engine control system is shown in Figure 1.2. The sensors measure engine output variables such as speed, pressure, and temperature. A separate set of sensors measure environmental conditions such as altitude, atmospheric pressure and temperature. The engine output measurements and the environmental conditions are transferred to the computation apparatus of the control system. The physical constraints of the engine such as maximum allowable rotor speed and turbine inlet temperature are normally stored in the computing element. The computation apparatus utilizes the environmental and engine measurements to compute the difference between the desired output and the actual engine output. Based on the engine physical constraints and the output discrepancies the appropriate input signals are computed. The input signals are then transferred to the actuators (e.g., a fuel metering valve and a motor that changes the engine nozzle area are examples of typical jet engine actuators) (Ref. 45).

At first the main requirement of the engine control was to achieve the desired speed without violating physical constraints. The control input to the engine was fuel flow and simple hydromechanical devices were used to achieve this control objective. For example, a simple flyball speed governor that directly controlled the fuel input was used to maintain steady-state speed. As the engines became more sophisticated in order to deliver higher thrust and provide faster response, more complex hydromechanical control systems evolved. Today, hydromechanical controls are still the most commonly used types of control. However, hydromechanical controls will gradually be giving their place to the electronic controls. This is due to two

major reasons. First, future aircraft engines will have a more complex structure, thus requiring the controls to manipulate more than six variables which is the practical limit of the hydromechanical controls (Ref. 9). The second reason is that high performance aircrafts require control integration between the engine and the aircraft. Hence, the future engine control system must be capable of processing more information and manipulating more inputs.

The physical limitations and complex structure of hydromechanical controls motivated the designers of jet engine control systems to consider electronic control as an alternative. Initially, the electronic controls were analog and they are still the most commonly used type of electronic control. The analog computer, however, is sensitive to time and environmental changes and, hence, it is inherently less accurate than a digital computer. Furthermore, the modification of the programs in the analog computers are not easily achieved. Due to these considerations, the researchers raised the question of analog and/or digital computers for future engine control in the mid 1960's. Predictions since then indicate that future engine controls will be digital. The main reasons for such predictions are the flexibility of programming and the capability of storing large amounts of data. Also, the modification of the digital computer after its development is usually more feasible than the analog computers.

From an economical point of view, the application of digital controls will result in a substantial saving. In their study Sevich and Newrith (Ref. 10) indicate that the savings will be in fuel consumption, lower life-cycle cost, and reduced engine maintenance. According to Yafee (Ref. 11) a savings of 1% in fuel consumption results in

a savings of four (4) billion gallons of fuel per year for just the wide-body transports in service (based on 1976 data).

Reliability of the digital electronic controls is still a major problem in the application of these controls. System reliability can be improved however in several areas. With the advancement in solid-state electronics, more logic transfers and circuit hardware can be incorporated per chip, hence reducing the number of components. The reduction in the number of components improves the overall reliability of the control system. Reliability can also be improved by using redundant components. This is referred to as hardware redundancy. Recently researchers have considered using the redundant information that is available from dissimilar components to detect a failure. The redundant information is referred to as analytical redundancy. The main advantage of using analytical redundancy is that it eliminates the need for redundant components. This is particularly of interest for future jet engines as the number of inputs and outputs on these engines will be higher and the use of hardware redundancy might be impractical. The sensor failure detection technique developed in this dissertation utilizes the concept of analytical redundancy.

In summary, the trend in the research and development of the jet engine control system indicates that the future control system will be digital. The major concern about the digital controls is the reliability of such systems. Due to the complexity of future aircrafts it is not feasible to use hardware redundancy to improve the reliability of the control system. The advent of high speed digital computers with large storage capability has made it possible to consider the use of analytical redundancy. The development of failure detection

techniques which utilize analytical redundancy is affected by the design of the control system. Therefore, the next section is devoted to the discussion of modern control design techniques for jet engines.

1.4 Design of the Control System

In achieving the desired engine performance, the design methodology of the engine control system plays an important role. In the past control laws were designed by classical frequency response techniques. During this period, techniques were limited to single input-single output linear time-invariant systems. The application of the classical technique to a multivariable engine resulted in control laws that were designed for each input independently. When these independently designed control laws were implemented, severe interaction resulted and performance degradation occurred. Alternatively, the increase in complexity of future engines to achieve higher performance (e.g., high thrust-weight ratio) has also contributed to the need for multivariable engine controls. The classical control techniques cannot be used to design these systems unless cross coupled interactions are taken into consideration. Therefore, researchers have considered the use of multivariable design techniques in both the frequency and time domain (Ref. 16).

Some multivariable design techniques utilize all the relationships between inputs and outputs to achieve the desired engine response, hence using input interaction in a favorable manner. One such time-domain technique is Linear Quadradic Regulator (LQR) theory. Applications of this theory to jet engine control were studied by Michael and Farrar (Ref. 13), Merrill (Ref. 6), Beattie and Spock (Ref. 42), and De Hoff and Hall (Ref. 43). Recently a practical altitude test

cell demonstration of LQR theory application to a F100 turbofan engine was reported by Lehtinen et al (Ref. 22).

In the area of frequency domain techniques McMorran (Ref. 14) used the Inverse Nyquist Array to design a controller for a gas turbine. Other applications of Inverse Nyquist Array to jet engines has been reported by Leininger (Ref. 19), Spang (Ref. 21), and Sain et al (Ref. 44). Recently the use of alternative multivariable control design technique for jet engines has been addressed in numerous studies. An excellent collection of these studies can be found in reference 16. The volume of the research and the recent practical demonstration of the multivariable control techniques indicate that such techniques will be the design tools of future engine control systems.

Among the multivariable frequency domain techniques the Inverse Nyquist Array (INA), (Ref. 17) and the Direct Nyquist Array (DNA), (Ref. 18) are the natural extension of the classical frequency response techniques. In these Multivariable Nyquist Array (MNA) techniques the cross-coupled system interaction is reduced by making the transfer matrix diagonally dominant. After the dominance is achieved the control loops are designed separately by utilizing the classical frequency response tools. The use of tools such as Nyquist and Bode diagrams and Nichols chart is particularly appealing to a broad range of designers. Designing each control loop separately provides insight for MNA designers about the input-output relations in the system. Application of the MNA to the jet engine control problem (Refs. 14,19,20,21) results in a set of simple compensators

which provide the desired response. These studies conclude that MNA promises to be a viable alternative design method for the jet engine application.

Successful application of the MNA techniques, like any other design method, depends on the information provided to the control system by the sensors. Loss of information due to a sensor failure decreases the control system effectiveness, thus degrading the engine performance. Therefore, it is essential to identify the failed sensor and take appropriate corrective action. When multiple redundant sensors for the lost measurement are not available, then a failure must be accommodated in one of the following ways. The first method is to synthesize or estimate the lost measurement from the other measurements. The second approach is to reconfigure the control system. In rearranging the engine control system, the design methodology plays a significant role. Since in the MNA method each loop is designed separately, a relative independence exists among the loops that can be used to reconfigure the controls. It is one objective of this dissertation to develop this new approach for failure accommodation.

In summary, the design tools for future engine control systems will be the multivariable design techniques. Control systems designed by such techniques rely on sensors for output information. Therefore, in the event of a sensor failure it must be detected and accommodated. The MNA design technique promises to facilitate the accommodation of the failure. In the next section sensor failures and different phases of sensor failure analysis are discussed further.

1.5 Sensor Failure Problem

A jet engine control system depends on the engine output information to maintain the high level of performance. The output information is supplied to the control system by temperature, speed, and pressure sensors. If a sensor in the control loop (see Fig. 1.2) fails, the control system will be affected directly and hence the performance of the engine will be degraded. The level of degradation due to a sensor failure depends on the type of the failed sensor (i.e. temperature, pressure, or speed sensor) and also on the reaction of the control system to the failure. Thus, the reliability and safety of the engine control and ultimately the engine itself is related to the reliability of the sensors and the actions of the control system after the sensor failure.

Sensor failures are generally categorized into two groups: soft and hard failures. For this purpose the sensor output is viewed as a combination of the true measurement and a random noise. In case of no failure the mean of the sensor output is the true measurement and the variance is the same as the variance of the noise. If the mean of the sensor output deviates from the true measurement by a large margin, then a hard failure has occurred. Alternatively, when the variance of the sensor output exceeds a certain tolerable value, a soft failure is declared.

A complete sensor failure analysis of any system can be divided into three phases: detection, isolation, and accommodation. In the detection phase, the concern is to establish the occurrence of the failure. Ideally, a detection technique should detect both soft and hard failure. This, however, is not easily accomplished in a dynamic

system. After the detection it is necessary to isolate the failed sensor so that the effect of the failure can be reduced. The task of isolating a failed sensor becomes more complicated when multiple hardware redundancy does not exist. This is, of course, due to the fact that the output of redundant sensors cannot be compared with each other. It is, however, possible to utilize the available redundant information from dissimilar sensors to isolate a failure. The third phase of sensor failure analysis is to accommodate the failed sensor in the system. Specifically, the accommodation of a failure is to identify and implement the necessary changes in the control system to maintain safe operation with minimal performance loss. The methods of accommodating a failure when analytical redundancy is used can be divided into two groups: fixed and variable. If the measurement corresponding to the failed sensor can be synthesized or estimated, the control configuration can remain unchanged or fixed and the estimate is used in place of the failed sensor output. For variable accommodation the control loops are reconfigured to provide the control action without utilizing the output corresponding to the failed sensor.

Based on the discussion in this section, the main objectives of any sensor failure analysis are: detection, isolation, and accommodation. Utilizing analytical redundancy - a must for future complex engines - requires more sophisticated failure analysis methods. A brief review of such techniques is presented in the next section.

1.6 Failure Analysis Techniques

Traditionally, the problem of sensor failure is solved by utilizing multiple redundant sensors. A simple majority voting system will determine the failed sensor by comparing the output of the

redundant sensors. The output of the failed sensor is disregarded and the output of a similar unfailed sensor is substituted. For the detection of a failure at least three independent measurements of the same variable must be available. Although the voting technique does not necessarily require that each variable be sensed by three identical sensors, it does require that a large number of redundant sensors be added to the system. On the other hand, if one takes advantage of unlike sensors to compute duplicates of the measurements, the detection logic becomes complicated. The voting technique has generally been used for hard failure detection. An application of this method is reported by Gilmor and McKern (Ref. 25). Pejsa (Ref. 26) developed an optimum arrangement for redundant sensors. However, the basic drawback of voting techniques is the requirement of multiple redundancy. Since future engines will require more sensors the multiple redundancy requirement would make a voting technique too complex to be useful.

The complexity of future engine control systems dictates the use of an on-board digital computer for engine control purposes. The recent advances in solid state electronics allows design of small computers with large storage and high computation speed for on-board utilization. The storage and speed capabilities of the on-board computers provide an opportunity for the development of failure detection techniques which use analytical redundancy. The main idea behind such techniques is to extract the failure detection information from the output of dissimilar sensors.

In recent years researchers have proposed various analytical approaches to the problem of sensor failure. One approach is to use

Kalman filters (Ref. 27) to remove the effects of the failure from the outputs of the engine. For this purpose a set of Kalman filters were designed that are sensitive to abrupt changes in the system (e.g., see Jazwinski, Ref. 28). Increasing the sensitivity of the filters, however, may severely degrade the performance of the system under the normal operation without any failure. Another drawback is that the failure sensitive filters do not provide any isolation capability. To add the isolation capability to this method, Kerr (Ref. 29) has included the failure biases as states. Then a large estimate of the bias state indicates the failure. Inclusion of the failure biases as states increases the dimension of the system and may degrade the performance of the system (Ref. 30). Two successful attempts in the area of failure-sensitive filters have recently been made by Beard (Ref. 58) and Jones (Ref. 59) which have an isolation capability. They design a filter such that its residual carries the detection and isolation information. The filter, however, is suboptimal and the implementation logic is considerable.

A more popular approach in the development of the computational techniques has been to use the innovations of Kalman filters to test for failure in the system. Montgomery et al (Refs. 12,32) by associating different hypotheses with each failure mode use the innovation process to test these hypotheses statistically. A major difficulty with hypothesis testing is the need for a bank of filters for generating the innovations. In a similar fashion Wells (Ref. 60) formulates a Baysian risk function which incorporates the risk associated with various modes of failure. He selects the hypothesis which minimizes the risk function. Wells has studied the application

of this technique to jet engine sensor failure; however, he indicates that due to the requirement of a bank of filter the on-line implementation is impractical. In a somewhat different approach Mehra and Peschon (Ref. 33) have developed a chi-squared test for examining the whiteness of the innovations. The application of this simple technique by Willsky et al (Ref. 34) has produced mixed results. The method does not provide any isolation information and only those failures which significantly effect the innovations are detected. More subtle failures are difficult to detect with this technique.

In their study of sensor failures in jet engines Corley and Spang (Ref. 35) have used engine measurement errors and an engine model to test for sensor failures. Assuming white Gaussian plant and measurement noise, they compare the absolute value of the measurement errors in each sample interval against a threshold to test for the failure. The major disadvantage of this technique is that it only utilizes the information contained in one sample interval for failure detection.

An alternative way of testing the innovations for failure detection is to use the concept of Generalized Likelihood Ratio (GLR). The concept of GLR is described by Sage and Melsa (Ref. 31) and by Van Trees (Ref. 36). Willsky and Jones (Ref. 37) used the concept of GLR to develop a jump failure detection technique for linear systems. In their approach they use the innovations of a Kalman-Bucy type filter to develop the likelihood ratio. Since this ratio has a known distribution it can be used to test the hypothesis of no failure versus failure. The GLR method has been applied to the detection of cardiac arrhythmias and the results have been extremely

impressive (Ref. 38). The advantage of GLR is that it provides both an estimate of the size of the jump and the time of the failure. The GLR is mainly a detection technique, but under additional assumptions (Ref. 37) it provides isolation information. However, GLR does not accommodate the failure and it has to be complemented with an accommodation technique.

The preceding techniques are mainly compatible with a control system designed by a multivariable time domain control technique. On the other hand, the potential advantages that new multivariable frequency domain control techniques can offer with respect to the sensor failure detection/accommodation problem are yet to be explored. This dissertation is an attempt to respond to the need for such exploration. In the next Section the objectives of this dissertation are defined and the proposed approach is outlined.

1.7 Dissertation Objectives

The development of a sensor failure analysis for a jet engine is highly influenced by the design philosophy of the engine control system. This influence can ultimately effect the speed and accuracy of the failure detection system. Most of the failure detection techniques are developed to operate with a control system designed by the multivariable time domain techniques. The recent development of the Multivariable Frequency Domain (MVFD) techniques (e.g., Refs. 18,39) has opened a new frontier in sensor failure detection analysis. The Multivariable Nyquist Array (MNA) (Refs. 19,20), a MVFD technique, is particularly of interest. In the MNA design the estimation of system states is not required and each input-output is designed separately. These two characteristics of the MNA design and the

successful application of the MNA technique to the jet engine control problem (Ref. 16) suggests that MNA is an excellent candidate for exploring the potential benefits of MVFD techniques. Specifically, it is important to determine the logic simplifications and the computational savings that result from the use of MNA design. In response to this need the objectives of this dissertation are defined as follows:

1 - To introduce the failure accommodation capability in the MNA design and develop the reconfiguration scheme for on-board utilization.

2 - To develop a failure detection and isolation technique based on the MNA design for on-board implementation.

The proposed solutions to the problems corresponding to the above objectives are presented in the following chapters. In Chapter II a new approach for failure detection is proposed and by utilizing the concept of Generalized Likelihood Ratio (GLR) a failure detection technique is developed. Important statistical properties of this detection technique are derived in Chapter III. Chapter IV is devoted to the application results of the proposed failure analysis technique to a Quiet Clean Short-haul Experimental Engine (QCSEE). The problem of failure accommodation is addressed in Chapter V where a new accommodation technique based on MNA design methodology is developed. The application results of the accommodation technique to QCSEE are also presented in Chapter V. Finally, in Chapter VI a summary of the dissertation and recommendations for future research are discussed.

CHAPTER II

GENERALIZED LIKELIHOOD RATIO DETECTION TECHNIQUE

2.1 Introduction

The value of an on-board digital computer for future jet engine control was examined in Chapter I. With the availability of low-cost digital computers and their increased storage and speed capabilities, more advanced failure detection techniques can be studied in order to improve overall engine reliability and performance. In this chapter a sensor-actuator failure detection technique based on the concept of the Generalized Likelihood Ratio (GLR) (Ref. 36) is developed. The technique consists of performing hypothesis testing on the difference between the engine output measurements and the output of an engine model. The hypotheses correspond to various modes of failure in the system sensors or actuators. The technique provides a simple decision function and an estimate of the time of the failure. Also estimates of bias in the outputs or states due to a sensor or actuator failure can be easily computed. The technique is developed for linear dynamic systems and, therefore, its application is not restricted to jet engines. Prior to the mathematical development of the technique the configuration of the detection scheme is described in the next section. Then a general formulation of the technique for time-varying systems is presented in Section 2.3. In Section 2.4 the special case of failure detection in a time-invariant system is treated and then in Section 2.5 recursion relations for computer implementation of the time-invariant case are de-

veloped. A brief treatment of soft failures in output sensors is presented in Section 2.6. Finally, a summary and discussion of the developments in this chapter are presented in Section 2.7.

2.2 Generalized Likelihood Ratio Detection Scheme

The idea of using a Generalized Likelihood Ratio (GLR) test for failure detection in dynamic systems has been investigated by Willsky and Jones (Ref. 1). Figure 2.1 illustrates their proposed detection scheme. Under this scheme, a Kalman-Bucy filter is used to estimate the output of the plant. The estimated output is then subtracted from the actual plant output. The difference between the estimated and actual measurement, referred to as the residual, is used to test for failure occurrence in the plan. The development of the technique is based on the assumption that under no-failure operation each residual is a zero mean white Gaussian noise process. If a component fails, however, the residuals will no longer have zero mean. Based on these assumptions the detection of a failure is equivalent to testing the mean of the residuals for deviation from zero. Testing the mean of the residuals can be achieved statistically by testing the hypotheses corresponding to failure and no-failure modes. Specifically

H_0: No failure occurred

(i.e., the mean of the residuals is zero)

H_1: A failure occurred

(i.e., the mean of the residual is nonzero)

To test the above hypotheses the GLR method is used. For this purpose the likelihood function corresponding to hypothesis H_1 is divided into the liklihood function for H_0. Based on the desired degree of confidence in the detection results, a threshold can be selected as the

upper limit of the value of the likelihood ratio under no failure. A failure is declared if the likelihood ratio exceeds this threshold. This is called the decision rule.

To estimate the outputs, a Kalman-Bucy filter must estimate the states. State estimates from the Kalman-Bucy filter (Fig. 2.1) can, at the same time, be used for the purpose of controlling the plant. This, of course, would be the case only if state estimates are required in the design of the control system. Such is the case in standard linear quadratic state regulator designs. Alternatively, if the control design of the plant is based on a technique which does not require state estimates (e.g., as in the case of the Multivariable Nyquist Array technique) then the Kalman-Bucy filter will only serve the purpose of generating residuals for failure detection. In this case alternative means for generating the residuals can be considered. The motivation for such consideration is as follows. The output estimates from the Kalman-Bucy filter are dependent on the plant output measurements. Thus a failure in either sensors or actuators would not only affect the output of the plant but also the state estimates and hence the output estimates. The dependence of the output estimates on plant measurements excludes the option of replacing the lost measurement, in case of a failure, with its estimate. In addition, since the state estimates (and, consequently, the residuals) are affected by sensor output, then even brief and scattered sensor disturbances have to be considered in the failure detection. This increases the number of failure modes and hence reduces the speed of detection, isolation, and accommodation of a failure. Therefore, it is important to consider alternative means of generating residuals.

One possible alternative for generating the residuals is to use a model of the plant that follows the dynamics of the plant closely and at the same time depends only on the input to the plant. In Figure 2.2 the Kalman-Bucy filter is replaced by a plant model. The model is required to follow the engine dynamics so that under a no-failure condition the difference between the actual plant output and the model output will be a zero mean white Gaussian noise process. Comparing Figures 2.1 and 2.2 reveals that while the output estimate from the Kalman-Bucy filter depends on both the input and output of the system, the model outputs are only functions of the input and plant dynamics. Thus, if a sensor fails the model output will not be affected and could replace the lost measurement. Also the detection of brief disturbances in the sensors is no longer essential. This eliminates one mode of failure from consideration. As will be shown later the mathematical formulation of the GLR detection will be simpler when a model is used to generate the residuals. This modification in the failure detection scheme requires that the likelihood ratio decision function be rederived for residuals computed by subtracting model outputs from plant measurements. In the next section the preliminary concepts and definitions for the development of the new detection technique are discussed and then the general formulation of the technique for linear time-varying systems is presented.

2.3 Generalized Likelihood Ratio for Time-Varying Systems

In the previous section an overview of the proposed Generalized Likelihood Ratio (GLR) detection scheme was presented. In this section the mathematical development of the GLR technique for the proposed detection plan (see Fig. 2.2) will be discussed. For this purpose it is first necessary to develop the system model.

2.3.1 The System Model

The development of the failure detection technique in this section is based on the assumption that the dynamics of the system under study can be represented by the following linear time-varying discrete equations:

$$X(k+1) = \phi(k)X(k) + B(k)U(k) + F_a(k,t) \quad (2\text{-}1)$$

$$Z(k) = H(k)X(k) + J(k)U(k) + Y(k) + F_s(k,t) \quad (2\text{-}2)$$

where the symbols in the above equations are defined as:

$X(k)$	:	$n \times 1$	State column vector
$\phi(k)$	:	$n \times n$	System matrix
$B(k)$	:	$n \times m$	Input matrix
$U(k)$	:	$m \times 1$	Input column vector
$F_a(k,t)$	:	$n \times 1$	Actuator failure function vector
$H(k)$	:	$g \times n$	Output matrix
$J(k)$	:	$g \times m$	Matrix (relating inputs to outputs)
$Y(k)$	:	$g \times 1$	Zero mean Gaussian white noise process with the covariance matrix $V(k)$
$F_s(k,t)$	:	$g \times 1$	Sensor failure function vector
k	:		Number of observations
t	:		Time of failure occurrence.

The functions $F_a(k,t)$ and $F_s(k,t)$ are used to model the failure modes of interest. Such failure modes are hard-over actuator, a brief disturbance in the actuator, and hard-over sensor failures which are of main interest in a jet engine application. It should be mentioned that

even if only the detection of a sensor failure is of interest it may still be necessary to consider the other modes of failure because the effect of other failures on the residuals may resemble the effect of a sensor failure. Typically, hard-over failures in actuators and sensors are modeled as step changes in the outputs of actuators or sensors. For brief disturbances in the actuator, a jump function is used to model the failure. In the following a hard-over actuator and sensor failure will often be referred to as state-step and sensor-step failure, respectively. The brief disturbances in the actuator will be referred to as a state-jump failure. These three modes of failure are modeled as follows.

1. Hard-Over Actuator

For this type of failure the function $F_a(k,t)$ has the following form

$$F_a(k,t) = \nu\sigma_{k+1,t} \tag{2-3}$$

where ν is a $n \times 1$ column vector that denotes the unknown magnitude and direction of the failure and σ_{ij} is the unit step function defined as

$$\sigma_{ij} = \begin{cases} 0 & i < j \\ 1 & i \geq j \end{cases} \tag{2-4}$$

Setting the first subscript to $k + 1$ in (2-3) assures that the effect of the actuator failure will be reflected in the output without any delay.

2. Actuator Brief Disturbances (Jump Failure)

The function $F_a(k,t)$ for this type of failure is

$$F_a(k,t) = \nu\delta_{k+1,t} \tag{2-5}$$

where ν is defined in the same way as above and $\delta_{i,j}$ is the Kronecker delta function representing a pulse at $i = j$, i.e.,

$$\delta_{i,j} = \begin{cases} 0 & i \neq j \\ 1 & i = j \end{cases} \tag{2-6}$$

3. Hard-Over Sensor Failure

The failure function $F_S(k,t)$ for this type of failure can be written as:

$$F_S(k,t) = \nu\sigma_{k,t} \tag{2-7}$$

where ν is a $g \times 1$ column vector that represents the unknown magnitude and direction of the failure in the output space and σ_{ij} is the unit step function as was defined in equation (2-4).

With the completion of modeling the system dynamics and different modes of failure, the next step is to model the residuals for the three failure modes.

2.3.2 The Residual Model

In the proposed GLR detection plan (see Fig. 2.2) the residuals are defined as the difference between the actual output of the plant and the output of the plant model. The main assumption here is that under no failure, the residuals are a zero-mean white Gaussian noise process. Let $r(k)$ denote the residuals and let $r_1(k)$ represent the residuals under no failure operation then

$$r(k) = r_1(k) \tag{2-8}$$

where $r_1(k) \epsilon R^g$ and is a zero mean white Gaussian noise process with known covariance matrix $V(k)$. When one of the three types of hard failure (explained above) occurs the residuals will no longer remain

equal to $r_1(k)$. In fact the residuals will reflect the deviation that the failure induces in the plant output from the model output. Therefore, when a failure occurs the residuals will have the following form:

$$r(k) = r_1(k) + r_2(k) \tag{2-9}$$

where $r_2(k)$ is the unknown but nonrandom effect of the failure on the residuals. The term $r_2(k)$ not only signals the occurrence of the failure but it also carries the information concerning the type of the failure. To extract this information from $r_2(k)$, the effect of each failure mode on the residuals must be studied. Hence, for each type of failure the form of $r_2(k)$ will be determined.

1. Hard-Over Actuator (State Step) Failure

To calculate the effect of hard-over (state step) failure on the residuals, consider the following equations

$$X_p(k + 1) = \phi(k)X_p(k) + B(k)U(k) \tag{2-10}$$

$$X_f(k + 1) = \phi(k)X_f(k) + B(k)U(k) + \sigma_{k+1,t}{}^{\nu} \tag{2-11}$$

where $X_f(k)$ is the value of the plant state due to failed conditions and X_p is the state value for unfailed conditions. The effect of the failure on the states can be calculated by subtracting equation (2-11) from (2-10) and the result can be written as:

$$X_2(k + 1) = \phi(k)X_2(k) + \sigma_{k+1,t}{}^{\nu} \tag{2-12}$$

where

$$X_2(k) = X_f(k) - X_p(k) \tag{2-13}$$

is the change in the value of the states due to the failure. Note that $X_2(k) = 0$ for $k < t$ and for $k \geq t$ $X_2(k)$ is calculated from equation (2-12) where t is the time of the failure.

The closed form solution for equation (2-12) can be written as

$$X_2(k) = \begin{cases} \left[\sum_{j=t}^{k} Q(k,j)\nu\right] & k \geq t \\ 0 & k < t \end{cases} \tag{2-14}$$

where $Q(k,j)$ is the discrete transition matrix obtained from solution of equation (2-12) as

$$Q(k,j) = \phi(k-1)\phi(k-2) \ldots \phi(j) \tag{2-15}$$

where

$$Q(j,j) = I .$$

The effect of hard-over failure $r_2(k)$ on the residuals in equation (2-9) can be written as

$$r_2(k,t) = \begin{cases} H(k)\left[\sum_{j=t}^{k} Q(k,j)\right]\nu & k \geq t \\ 0 & k < 0 \end{cases} \tag{2-16}$$

since $r_2(k) = H(k)X_2(k)$, which follows from insertion of equation (2-14) into equation (2-2). For ease of reference equation (2-16) can be re-written as

$$r_2(k,t) = G_1(k,t)\nu \tag{2-17}$$

where

$$G_1(k,t) = \begin{cases} H(k)\left[\sum_{j=t}^{k} Q(k,j)\right] & k \geq t \\ 0 & k < t \end{cases} \tag{2-18}$$

the subscript 1 of $G_1(k,t)$ refers to the type of failure (i.e., hard-over actuator failure).

2. Actuator Disturbance (Jump) Failure

The effect of a brief disturbance on the value of the states can be computed by following the same approach as in the case of hard-over actuator failure. In this case the change in the value of the states can be obtained by replacing $\sigma_{k+1,t}$ with $\delta_{k+1,t}$ in equations (2.11) and (2.12) yielding

$$X_2(k+1) = \phi(k)X_2(k) + \delta_{k+1,t}\nu \tag{2-19}$$

where $X_2(k)$ is the change in the value of the states due to the jump failure alone and $\phi(k)$, $\delta_{k+1,t}$, and ν are the system matrix, Kronecker delta function, and failure vector, respectively. Note that $X_2(k) = 0$ for $k < t$ and the solution to equation (2-19) can be written as

$$X_2(k) = \begin{cases} Q(k,t)\nu & k \geq t \\ 0 & k < t \end{cases} \tag{2-20}$$

where $Q(k,t)$ is the discrete transition matrix as defined in equation (2-15). Therefore, the effect of this type of failure on the residuals can be calculated by multiplying $X_2(k)$ in equation (2-20) by the output matrix $H(k)$

$$r_2(k,t) = \begin{cases} H(k)Q(k,t)\nu & k \geq t \\ 0 & k < t \end{cases} \tag{2-21}$$

The above equation for $r_2(k,t)$ can be rewritten as

$$r_2(k,t) = G_2(k,t)\nu \tag{2-22}$$

where

$$G_2(k,t) = \begin{cases} H(k)Q(k,t) & k \geq t \\ 0 & k < t \end{cases} \qquad (2\text{-}23)$$

The subscript 2 of $G_2(k,t)$ refers to the type of failure (i.e., actuator jump failure).

3. Hard-Over (Step) Sensor Failure

A hard-over sensor failure affects the residuals directly (see Fig. 2.2). Therefore, the corresponding $r_2(k,t)$ can be written as:

$$r_2(k,t) = \sigma_{k,t}\nu \qquad (2\text{-}24)$$

where $\sigma_{k,t}$ and ν are the unit step function and the failure vector defined in equations (2-4) and (2-7), respectively. Then equation (2-24) can be written as:

$$r_2(k,t) = G_3(k,t)\nu \qquad (2\text{-}25)$$

where $G_3(k,t)$ is a null matrix for $k < t$ and a $g \times g$ identity matrix for $k \geq t$. This completes the calculation of the effect of failures on the residuals.

In summary, to develop the GLR decision function it is necessary to determine how each type of failure affects the residuals. To achieve this, the hard-over failures and the brief disturbances were modeled as step and jump functions (see eqs. (2-3), (2-5), and (2-7)). Using these models, it was shown that (eqs. (2-17), (2-22), and (2-25)) the effect of the actuator and sensor failures on the residuals can be expressed in the general form of:

$$r_2(k) = G_i(k,t)\nu \qquad \text{for} \quad i = 1,2,3 \qquad (2\text{-}26)$$

where $G_i(k,t)$ for $i = 1,2,3$ corresponds to hard-over actuator, brief disturbance in the actuator, and hard-over sensor failure, respectively.

The formulation in equation (2-26) proves to be particularly helpful in the mathematical development of GLR which will be discussed next.

2.3.3 The Generalized Likelihood Ratio

Application of GLR concept to the problem of failure detection rests on two basic assumptions. The first assumption is that for a no-failure mode the residuals are zero mean white Gaussian noise processes. Under the second assumption when a hard failure (any of the three types discussed in Section 2.3.1) occurs the residuals will no longer have zero mean but their Gaussian property is retained. Based on these assumptions, testing the hypothesis regarding the detection of a failure is equivalent to testing the hypothesis concerning the zero mean of the residuals. The null and the alternative hypotheses can be written as:

H_0: No failure occurred

(i.e., the mean of the residuals is zero)

H_i: Failure of type i has occurred

(i.e., the residuals mean is nonzero)

The type $i = 1,2,3$ refers to hard-over actuator, brief disturbances in the actuator, and hard-over sensor failures, respectively. The null and the alternative hypotheses can be expressed in terms of $r(k)$ as:

$$H_0: \quad r(k) = r_1(k)$$
$$H_i: \quad r(k) = r_1(k) + G_i(k,t)\nu \tag{2-27}$$

where $r_1(k)$ is defined in equation (2-9) and $G_i(k,t)\nu$ for $i = 1,2,3$ are defined in equations (2-18), (2-23), and (2-25), respectively. The likelihood function for the above hypotheses can be established by considering a sample of k residuals

$$F_0 = \text{Prob. } (r(1), r(2), \ldots, r(k)/H_0) \tag{2-28}$$

$$F_i = \text{Prob. } (r(1), r(2), \ldots, r(k)/H_i) \tag{2-29}$$

where F_0 is the likelihood function for null hypothesis H_0, and $r(j)$ denotes the jth residual and t and ν are the failure time and failure vector, respectively, and F_i is the likelihood function for the hypothesis corresponding to ith type of failure. The likelihood function F_i depends on both time of the failure, t, and the failure vector ν which are unknown. Since the probability distribution of the residuals is Gaussian the likelihood functions F_0 and F_i can be written as:

$$F_0 = \prod_{j=1}^{k} \left\{ (2\pi)^{g/2} \left[\text{Det } V(j)\right]^{-1/2} \exp\left[-\frac{1}{2} r^T(j) V^{-1}(j) r(j) \right] \right\} \tag{2-30}$$

$$F_i = \prod_{j=1}^{k} \left\{ (2\pi)^{g/2} \left[\text{Det } V(j)\right]^{-1/2} \exp\left[-\frac{1}{2} \left[r(j) - G_i(j,t)\nu \right]^T V^{-1}(j) \times \left[r(j) - G_i(j,t)\nu \right] \right] \right\} \tag{2-31}$$

where $V(j)$ is the covariance matrix of the residuals. Based on the Neymann-Pearson lemma (Ref. 46), the ratio of the likelihood functions is formed to test the occurrence of a type i failure:

$$A(k) = \frac{F_i}{F_0}. \tag{2-32}$$

If $A(k)$ exceeds the threshold limit ε then a failure is declared. Since F_i is a function of t and ν, the likelihood ratio $A(k)$ is also a function of these variables. Both t and ν are unknown and

they must be estimated before the Neymann-Pearson test can be applied. To estimate t and ν the likelihood ratio $A(k)$ is maximized with respect to these variables. The algebra of maximization can be simplified if the logarithm of $A(k)$ is maximized instead of the $A(k)$. Consider the natural logarithm of $A(k)$:

$$\ln A(k) = \ln F_i - \ln F_0 = \frac{1}{2}\left\{\sum_{j=1}^{k} r^T(j)V^{-1}(j)r(j) - \sum_{j=1}^{k}\left[r(j) - G_i(j,t)\nu\right]^T V^{-1}(j)\left[r(j) - G_i(j,t)\nu\right]\right\}. \quad (2\text{-}33)$$

It can be shown (Ref. 51) that maximizing $\ln A(k)$ is equivalent to maximizing $A(k)$ with respect to t and ν, because the logarithmic function is monotonic. Thus the values of ν, t which maximize $\ln A(k)$ will also maximize $A(k)$. Taking the partial derivative of $\ln A(k)$ with respect to ν and equating the derivative to zero, yields

$$\hat{\nu} = \left\{\sum G_i^T(j,t)V^{-1}(j)G_i(j,t)\right\}^{-1}\left\{\sum G_i^T(j,t)V^{-1}(j)r(j)\right\}. \quad (2\text{-}34)$$

To simplify the notation the following terms are defined:

$$C_i(k,t) = \sum_{j=1}^{k} G_i^T(j,t)V^{-1}(j)G_i(j,t) \quad (2\text{-}35)$$

and

$$D_i(k,t) = \sum_{j=1}^{k} G_i^T(j,t)V^{-1}(j)r(j) \tag{2-36}$$

therefore, $\hat{\nu}$ can be expressed in terms of $C_i(k,t)$ and $D_i(k,t)$ as

$$\hat{\nu} = C_i^{-1}(k,t)D_i(k,t). \tag{2-37}$$

Substituting the equations $C_i(k,t)$ and $D_i(k,t)$ from equations (2-35) and (2-36), respectively, into equation (2-33) the expression for ln A(k) becomes

$$\ln A(k) = \frac{1}{2}\left[\nu^T D_i(k,t) + D_i^T(k,t)\nu - \nu^T C_i(k,t)\nu\right] \tag{2-38}$$

Substituting $\hat{\nu}$ from equation (2-37) for ν in equation (2-38) yields:

$$2 \ln A(k) = \hat{\nu}^T D_i(k,t) \tag{2-39}$$

or alternatively

$$2 \ln A(k) = D_i^T(k,t)C_i^{-1}(k,t)D_i(k,t) \tag{2-40}$$

In equation (2-40) the time of the failure, t, is still unknown and it must be estimated. Using equation (2-40) in place of equation (2-33) the maximum likelihood estimate of t can be obtained by maximizing the likelihood ratio with respect to t. Therefore, the Generalized Likelihood Ratio for testing the occurrence of the ith type of failure can be expressed as

$$L_i^*(k,\hat{t}) = 2 \ln A(k) = \max_{\hat{t}} D_i^T(k,t)C_i^{-1}(k,t)D_i(k,t) \tag{2-41}$$

where $L_i^*(k,\hat{t})$ represents the likelihood ratio for the ith type of failure and it is referred to as GLR index.

In order to calculate $L_i^*(k,\hat{t})$ from equation (2-41) the term on the right-hand side of equation (2-40) must be computed for all possible t (i.e., $0 < t \leq k$) and the maximum value of these terms is $L_i^*(k,\hat{t})$. The corresponding t is the estimate of the failure time. Thus, to compute $L_i^*(k,\hat{t})$ and estimate $\hat{t}$ more of the terms of equation (2-40) must be computed as k, the number of observations, increases.

To make the estimation of $\hat{t}$ more feasible Wilsky and Jones (Ref. 1) suggest using a finite size window to restrict the range of $\hat{t}$ to the interval $k - M \leq \hat{t} \leq k - N$ where M and N denote the window limits. Further suggestions in reference 1 include:

1. Restricting the direction of failure vector, ν, to a set of known directions in the state and output space. The GLR formulation resulting from this simplification is referred to as constrained GLR (CGLR).
2. Selecting only one direction for the failure vector (e.g., the direction corresponding to the failure of a component with the highest probability of failure). The GLR formulation corresponding to this type of simplification is called the Simplified GLR (SGLR).

The development of constrained GLR (CGLR) follows directly from equation (2-40). Substituting αf_j for ν in equation (2-33), where α is an unknown scalar and f_j is the jth vector of the preselected directions, and maximizing with respect to α yields:

$$2 \ln A(k) = \frac{\left[f_j^T D_i(k,t)\right]^2}{f_j^T C_i(k,t) f_j} \qquad (2\text{-}42)$$

The maximum likelihood estimate of α corresponding to equation (2-41) is

$$\hat{\alpha} = \frac{f_j^T D_i(k,t)}{f_j^T C_i(k,t) f_j} . \tag{2-43}$$

In equation (2-42) the time of the failure, t, and the direction of the failure, j, are unknown. Thus the expression on the right-hand side has to be maximized with respect to t and j. The maximization can be expressed as:

$$L_i(k,\hat{t},\hat{j}) = \underset{\hat{j},\hat{t}}{\text{Max}} \left\{ \frac{\left[f_j^T D_i(k,t) \right]^2}{f_j^T C_k(k,t) f_j} \right\} \tag{2-44}$$

The development of the Simplified GLR (SGLR) is based on the assumption that the failure vector, ν, can only assume a known direction and value. This assumption eliminates the need for estimation of ν. Substituting $\nu = \nu_0$, where ν_0 is the known vector, in equation (2-38) results in

$$2 \ln A(k) = 2\nu_0^T \sum_{j=1}^{k} G_i^T(j,t) V^{-1}(j) r(j) - \nu_0^T \times \left[\sum_{j=1}^{k} G_i^T(j,t) V^{-1} G_i(j,t) \right] \nu_0 \tag{2-45}$$

or

$$2 \ln A(k) = 2 \nu_0^T D_i(k,t) - \nu_0^T C_i(k,t) \nu_0 . \tag{2-46}$$

The time of the failure, t, in equation (2-46) is unknown and it must be estimated. Maximization of $2 \ln A(k)$ in equation (2-46) with re-

spect to t can be expressed as

$$L_i^*(k,\hat{t}) = \max_{\hat{t}} \left[2\nu_0^T D_i(k,t) - \nu_0^T C_i(k,t)\nu_0\right] \qquad (2\text{-}47)$$

The restrictions imposed on failure directions will make the detection scheme more responsive to the predetermined directions and less sensitive to the nonspecified directions. As a result, these restrictions may only be useful if sufficient information about the nature of the failures in the system is available. The development of the GLR for the two simplifications suggested in reference 1 concludes the study of GLR for time-varying system.

In summary, three types of failures, namely the hard-over actuator failure, brief disturbance in the actuator, and the hard-over sensor failure, were considered. Examination of the results generated for these failures indicates that the Generalized Likelihood Ratio indices for the three types of failure can be expressed in a common form as:

$$L_i(k,t) = D_i^T(k,t)C_i^{-1}(k,t)D_i(k,t) \qquad \text{for } i = 1,2,3 \qquad (2\text{-}48)$$

where $D_i(k,t)$ and $C_i(k,t)$ are defined in equations (2-35) and (2-36), respectively. The source of distinction between $D_i(k,t)$'s and $C_i(k,t)$'s for the three types of failure is the different $G_i(k,t)$ matrices. The matrix $G_i(k,t)$ reflects the effect of type i failure on the residuals. Therefore, the successful detection and isolation of a failure depends on how well the $G_i(k,t)$ matrix represents the true effect of type i failure on the residuals. A summary of the GLR formulation for the three types of failures is given in Table 2.1. A design regarding the occurrence and the type of a failure is made as

TABLE 2.1

SUMMARY OF GLR FORMULATION FOR TIME-VARYING SYSTEMS

GLR Index

$$L_i(k,t) = D_i^T(k,t)C_i^{-1}(k,t)D_i(k,t)$$

$$D_i(k,t) = \sum_{j=1}^{k} G_i^T(j,t)V^{-1}(j)r(j)$$

$$C_i(k,t) = \sum_{j=1}^{k} G_i^T(j,t)V^{-1}(j)G_i(j,t)$$

For $i = 1,2,3$

Hard-Over Actuator (state step)

$$G_1(k,t) = \begin{cases} H \sum_{j=t}^{k} Q(k,t) & k \geq t \\ 0 & k < t \end{cases}$$

Brief Disturbance in the Actuator (state jump)

$$G_2(k,t) = \begin{cases} HQ(k,t) & k \geq t \\ 0 & k < t \end{cases}$$

Hard-Over Sensor (sensor step)

$$G_3(k,t) = \begin{cases} I & k \geq t \\ 0 & k < t \end{cases}$$

follows. The $L_i^*(k,\hat{t})$ from equation (2-41) is compared with a threshold ε and if $L_i^*(k,\hat{t})$ exceeds ε then the occurrence of a failure of type i at time $\hat{t}$ is declared. When more than one type of failure is considered then the selection of the failure type is achieved by maximizing $L_i^*(k,\hat{t})$ over i, the type of the failure. The procedure for selecting ε is given in the next chapter. Due to the importance of time-invariant systems in practical applications, the next section is devoted to the discussion of the GLR failure detection for these systems.

2.4 Application of GLR to Time-Invariant Systems

The development of GLR detection technique for time-invariant systems is indeed a special case of the time-varying formulation of the technique. The importance of studying failure detection for time-invariant systems stems from the fact that in most practical applications the systems are assumed to be time-invariant. As in the time-varying case, the first step is to develop the system model.

2.4.1 The System Model

The state and output equations for a time-invariant system can be written as:

$$X(k+1) = \phi X(k) + BU(k) + F_a(k,t) \tag{2-49}$$

$$Z(k) = HX(k) + JU(k) + Y(k) + F_s(k,t) \tag{2-50}$$

where all the symbols are defined in the same way as in equations (2-1) and (2-2) except that ϕ, B, H, and J are not functions of k any longer. The failure functions $F_a(k,t)$ and $F_s(k,t)$ are used to model the three types of failure in exactly the same manner as in equations (2-3) through (2-7). The next step is to model the effect of the failures on the residuals of the time-invariant system.

2.4.2 The Residual Model

The definitions and the assumptions of Section 2.3.2 regarding the modeling of the residuals also apply to time-invariant systems. However, the matrices ϕ and H are constant and this simplifies the formulation of the $G_i(k,t)$ matrix. The effect of each type of failure on the residuals of time-invariant systems will be developed as follows.

1. Hard-Over Actuator (State Step) Failure

The change in the value of the states due to a hard-over actuator failure can be calculated from the following equation:

$$X_2(k+1) = \phi X_2(k) + \sigma_{k+1,t}\nu \qquad (2\text{-}51)$$

$$X_2(k) = 0 \qquad \text{for} \quad k < t$$

where ϕ, σ_{ij}, ν, and $X_2(k)$ are defined in the same way as in equations (2-1), (2-3), and (2-10), respectively. The closed form solution for equation (2-51) is as follows:

$$X_2(k) = \begin{cases} \sum_{j=t}^{k} Q(k,t)\nu & k \geq t \\ 0 & k < t \end{cases} \qquad (2\text{-}52)$$

where $Q(k,t)$ is the discrete transition matrix obtained by solving equation (2-51). Specifically

$$Q(k,j) = \phi \cdot \phi \cdot \phi \cdots \phi = \phi^{k-j}. \qquad (2\text{-}53)$$

The equation (2-52) can also be derived directly from equation (2-15) by substituting ϕ for $\phi(k)$, $\phi(k-1)$, ... etc. The effect of the failure on the residuals can be calculated by multiplying $X_2(k)$ by H:

$$r_2(k) = \begin{cases} H \sum_{j=t}^{k} \phi^{k-j} \nu & k \geq t \\ 0 & k < t \end{cases} \tag{2-54}$$

Using the notation introduced in equation (2-26):

$$G_1(k,t) = \begin{cases} H \sum_{j=t}^{k} \phi^{k-j} & k \geq t \\ 0 & k < t \end{cases} \tag{2-55}$$

The equation (2-55) indicates that G_1 is only a function of $d = k - t$ which allows equation (2-55) to be rewritten as:

$$G_1(d) = \begin{cases} H \sum_{s=0}^{d} \phi^{d-s} & d \geq 0 \\ 0 & d < 0 \end{cases} \tag{2-56}$$

2. Brief Disturbance in Actuator

The effect of a brief disturbance in the actuator on the states is evaluated from the following equation.

$$X_2(k+1) = \phi X_2(k) + \delta_{k+1,t} \nu. \tag{2-57}$$

The closed form solution for the above equation can be derived as:

$$X_2(k) = \begin{cases} Q(k,t) & k \geq t \\ 0 & k < t \end{cases} \tag{2-58}$$

where

$$Q(k,t) = \phi^{k-t}. \tag{2-59}$$

Therefore, the effect of the failure on the residuals can be written as:

$$r_2(k) = \begin{cases} H\phi^{k-t}\nu & k \geq t \\ 0 & k < t \end{cases} \tag{2-60}$$

The $G_2(k,t)$ corresponding to $r_2(k) = G_2(k,t)\nu$ is

$$G_2(k,t) = \begin{cases} H\phi^{k-t} & k \geq t \\ 0 & k < t \end{cases} \tag{2-61}$$

It is easily seen that $G_2(k,t)$ may be written as a function of $d = k - t$:

$$G_2(d) = \begin{cases} H\phi^{d} & d \geq 0 \\ 0 & d < 0 \end{cases} \tag{2-62}$$

3. Hard-Over Sensor (Sensor Step) Failure

Consider the effect of a hard-over sensor failure on the residuals in equation (3-21):

$$r_2(k,t) = \sigma_{k,t}\nu \tag{2-53}$$

It can easily be seen that the effect of a hard-over sensor failure on the residual is independent of the system equations. That is, the effect of a sensor step failure on the residuals is the same for both

time-invariant and time-varying system. Therefore, $G_3(k,t)$ corresponding to $r_2(k) = G_3(k,t)v$ can be written as:

$$G_3(k,t) = \begin{cases} I & k \geq t \\ 0 & k < t \end{cases} \qquad (2\text{-}64)$$

or, alternatively, it can be expressed as

$$G_3(d) = \begin{cases} I & d \geq 0 \\ 0 & d < 0 \end{cases} \qquad (2\text{-}65)$$

where $d = k - t$. With the completion of modeling the residuals, the GLR for the time-invariant system will be derived.

2.4.3 The Generalized Likelihood Ratio

Consider the derivation of the GLR for time-varying systems in equations (2-27) through (2-41). Direct substitution of $G_i(d)$ (from eqs. (2-56), (2-62), and (2-65)) into equations (2-27) through (2-41) yields the corresponding GLR relationships for time-invariant system. A summary of these relationships for time-invariant systems is given in Table 2.2. Since G_i's for the time-invariant system are functions of $d = k - t$, C_i's will also be functions of d only. This is true since the covariance matrix of the residuals is constant (i.e., $V(j) = V$). Therefore, the C_i for time-invariant systems can be derived from equation (2-35) by direct substitution of $G_i(d)$:

$$C_i(d) = \sum_{j=0}^{d} G_i^T(j)V^{-1}G_i(j) \qquad (2\text{-}66)$$

Although $D_i(k,t)$ remains a function of both k,t, it may be expressed in terms of d and t as follows. Consider the equation

TABLE 2.2

SUMMARY OF GLR FORMULATION FOR TIME-INVARIANT SYSTEMS

GLR Index

$$L_i(d,t) = D_i^T(d,t)C_i^{-1}(d)D(d,t)$$

$$D_i(d,t) = \sum_{j=0}^{d} G_i^T(j)V^{-1}r(j+t)$$

$$C_i(d) = \sum_{j=0}^{d} G_i^T(j)V^{-1}G_i(j)$$

$$d = k - t$$

Hard-Over Actuator (state step)

$$G_1(d) = \begin{cases} H\sum_{j=0}^{d} \phi^{d-j} & d \geq 0 \\ 0 & d < 0 \end{cases}$$

Brief Disturbance in the Actuator (state jump)

$$G_2(d) = \begin{cases} H\phi^d & d \geq 0 \\ 0 & d < 0 \end{cases}$$

Hard-Over Sensor (sensor step)

$$G_3(d) = \begin{cases} I & d \geq 0 \\ 0 & d < 0 \end{cases}$$

$$D_i(k,t) = \sum_{j=1}^{k} G_i^T(j - r)V^{-1}r(j). \qquad (2\text{-}67)$$

Since

$$G(j - t) = 0 \qquad \text{for } j < t$$

then

$$D_i(d,t) = \sum_{j=0}^{d} G_i^T(j)V^{-1}r(j + t) \qquad (2\text{-}68)$$

where $d = k - t$.

The derivation of GLR relationships for time-invariant systems is of considerable significance for practical implementation of the technique. In a typical jet engine application the relationships in Table 2.2 will be implemented on a digital computer. Two observations can be made in this regard. The first observation is that for time-invariant systems $G_i(d)$ and $C_i(d)$ (see Table 2.2) are only functions of $d = k - t$ (where k is the number of the current observation and t is the time of the failure), therefore, they can be computed off line for on-board utilization. This property is important when storage and computation cycle time are critical. The second observation that can be made is that the GLR relationships resulting from the proposed detection scheme (Fig. 2.2) can easily be written in a recursive format. The recursion relationships yield a simple procedure for computing GLR indices. The development of these recursion relationships is the subject of the next section.

2.5 Recursion GLR Relationships for Time-Invariant Systems

In this section a set of recursion relationships for calculation

of the GLR detection index for the time-invariant systems is developed. The main utility of these relations is to facilitate the computer programming of the proposed GLR detection scheme. Consider the GLR equations for time-invariant systems in Table 2.2. In order to calculate the GLR index, $L_i(d,t)$, it is essential to compute $C_i(d)$ and $D_i(d,t)$ first. The matrix $C_i(d)$ is the summation of the matrices $G_i^T(j)V^{-1}G_i(j)$, for $j = 1,2,\ldots,d$, hence, it can be written in the recursion format by inspection as follows:

$$C_i(d) = C_i(d-1) + G_i^T(d)V^{-1}G_i(d). \tag{2-69}$$

Simularly the column vector $D_i(d,t)$ can be written as

$$D_i(d,t) = D_i(d-1,t) + G_i^T(d)V^{-1}r(t+d). \tag{2-70}$$

It follows from equations (2-69) and (2-70) that the computation of $C_i(d)$ and $D_i(d,t)$ depends directly on the $G_i(d)$ matrix. Therefore, the derivation of recursion relations for $G_i(d)$ is necessary. The relations for each of the three types of failure will be developed.

1. Hard-Over Actuator Failure

For the hard-over actuator the $G_1(d)$ was derived in equation (2-50) as:

$$G_1(d) = \begin{cases} H\sum_{s=0}^{d}\phi^{d-s} & d \geq 0 \\ 0 & d < 0 \end{cases} \tag{2-71}$$

From equation (2-71), for $d \geq 0$ the $G_i(d)$ can be written as:

$$G_1(d) = H\left[\phi^d + \phi^{d-1} + \ldots + I\right] \tag{2-72}$$

or

$$G_1(d) = H\left[I + \phi + \ldots + \phi^d\right] \tag{2-73}$$

thus

$$G_1(d) = H \sum_{s=0}^{d} \phi^s \ . \tag{2-74}$$

It follows from equation (2-74) that

$$G_1(d) = \begin{cases} H & d = 0 \\ G_1(d-1) + H\phi^d & d > 0 \\ 0 & d < 0 \end{cases} \tag{2-75}$$

2. Brief Disturbance in Actuator

Examination of the form of $G_2(d)$ in equation (2-62) indicates that $G_2(d)$ can be written as:

$$G_2(d) = \begin{cases} H & d = 0 \\ G_2(d-1)\phi & d > 0 \\ 0 & d < 0 \end{cases} \tag{2-76}$$

The derivation of equation (2-76) is achieved in the following manner

$$\begin{aligned} G_2(0) &= H \\ G_2(1) &= H\phi = G_2(0)\phi \\ G_2(2) &= H\phi^2 = G_2(1)\phi \\ &\cdot \\ &\cdot \\ &\cdot \\ G_2(d) &= H\phi^d = G_2(d-1)\phi. \end{aligned} \tag{2-77}$$

Equations (2-75) and (2-76) can be combined into one equation for calculation of $G_1(d)$ as follows:

$$G_1(d) = G_1(d-1) + G_2(d) \qquad d \geq 0. \tag{2-78}$$

Equation (2-78) implies that $G_1(d)$ is the cumulative sum of $G_2(d)$. This is, of course, expected because the $G_1(d)$ reflects the effect of a persistent actuator failure while $G_2(d)$ reflects the effect of the actuator failure over one sample interval. Another implication of equation (2-78) is that after the $G_2(d)$ matrix is calculated the $G_1(d)$ matrices can be computed by simple matrix addition.

3. Hard-Over Sensor

Consider $G_3(d)$ in equation (2-65), this matrix is simply a $g \times g$ identity matrix for $d \geq 0$, i.e., $G_3(d)$ is a constant matrix for $d \geq 0$. Since $G_3(d)$ is a constant matrix $C_3(d)$ takes a simple form as

$$C_3(d) = \sum_{j=0}^{d} V^{-1} = (d+1)V^{-1} \qquad d \geq 0 \tag{2-79}$$

A summary of the recursion relationships for $G_i(d)$ is given in Table 2.3.

The development of the detection technique for hard failure is concluded at this point. The study of statistical properties of the detection technique will be discussed in the next chapter. Prior to examination of the statistical properties of GLR, a brief discussion of soft failures in sensors is presented in the next section.

2.6 Sensor Soft Failure

In this Section a failure detection technique for sensor soft failures in time-invariant systems using the proposed detection scheme (Fig. 2.2) will be presented. The objective is to demonstrate the

TABLE 2.3

SUMMARY OF RECURSION FORMULAS FOR $G_1(d)$

(Time-Invariant Case)

Hard-Over Actuator

(state step)

$$G_1(d) = \begin{cases} H & d = 0 \\ G_1(d-1) + H\phi^d & d > 0 \\ 0 & d < 0 \end{cases}$$

or

$$G_1(d) = \begin{cases} H & d = 0 \\ G_1(d-1) + G_2(d) & d > 0 \\ 0 & d < 0 \end{cases}$$

Brief Disturbance in the Actuator

(state jump)

$$G_2(d) = \begin{cases} H & d = 0 \\ G_2(d-1)\phi & d > 0 \\ 0 & d < 0 \end{cases}$$

Hard-Over Sensor

(sensor step)

$$G_3(d) = \begin{cases} 0 & d < 0 \\ I & d \geq 0 \end{cases}$$

applicability of the proposed detection technique to the problem of soft failure.

A sensor soft failure can be defined as an increase in the known variance of the sensor output. Figure 2.3 illustrates the definition of a sensor soft failure. In order to test a sensor for soft failure two hypotheses are set up

$$\begin{aligned} H_0&: \text{ No failure has occurred} \\ H_1&: \text{ A sensor soft failure has occurred} \end{aligned} \tag{2-80}$$

Testing of the above hypotheses is accomplished by utilizing the model residual. Several assumptions regarding the model residual are made. It is assumed that under no-failure hypothesis, H_0, the model residuals are zero mean white Gaussian noise with known constant variance, V. The second assumption is that when a failure occurs the variance matrix changes to some unknown matrix V* while the mean remains the same and the Gaussian and whiteness properties are retained.

Based on the above assumptions the hypotheses in equation (2-80) can be expressed in terms of the variance of the residuals as

$$\begin{aligned} H_0&: \text{ Residual variance } V \text{ (known)} \\ H_1&: \text{ Residual variance } V^* \text{ (unknown)} \end{aligned} \tag{2-81}$$

Both V and V* are diagonal and positive definite. The matrix V* has at least one element larger than the corresponding elements in V. To test the hypothesis in equation (2-81) the method of Generalized Likelihood Ratio will be used. For this purpose consider the likelihood function for hypothesis H_0:

$$L_0 = \text{Prob.}\left[r(1), r(2), \ldots, r(k)/H_0\right] \tag{2-82}$$

or

$$L_0 = (2\pi)^{-gk/2} |V|^{-k/2} \exp\left[-\frac{1}{2}\sum_{j=1}^{k} r^T(j)V^{-1}r(j)\right] \tag{2-83}$$

where L_0 is the probability that the k observations of the model residuals are from a population with Gaussian distribution and covariance matrix V, and g is the dimension of the residual vector r(j). Similarly the likelihood function for alternate hypothesis, H_1, can be written as

$$L_1 = \text{Prob.}\left[r(1),r(2),\ldots,r(k)/H_1\right] \tag{2-84}$$

or

$$L_1 = (2\pi)^{-gk/2} |V^*|^{-k/2} \exp\left[-\frac{1}{2}\sum_{j=1}^{k} r^T(j)V^{*-1}r(j)\right] \tag{2-85}$$

where L_1 is the probability that k model residuals, r(j), are from a population with Gaussian distribution and unknown variance V*. The likelihood ratio for H_0 and H_1 can be written as

$$L = \frac{L_1}{L_0} \tag{2-86}$$

taking the logarithm of both sides of equation (2-76) yields:

$$\log L = \log L_1 - \log L_0 \,. \tag{2-87}$$

Before substituting for L_1 and L_0 from equations (2-83) and (2-85) into equation (2-87), the following definitions are adopted.

$$S_1 \triangleq V^{-1} \tag{2-88}$$

and

$$S_2 \triangleq V^{*-1} . \tag{2-89}$$

Using the above definitions the determinants of S_1 and S_2 can be expressed in terms of $|V|$ and $|V^*|$ as follows

$$|S_1| = |V|^{-1} \tag{2-90}$$

and

$$|S_2| = |V^*|^{-1} . \tag{2-91}$$

Now using equations (2-83) through (2-91), equation (2-87) can be rewritten as:

$$\text{Log } L = \frac{k}{2} \log|S_2| - \frac{1}{2} \sum_{j=1}^{k} r^T(j) S_2 r(j) - \frac{1}{2} k \log|S_1| + \frac{1}{2} \sum_{j=1}^{k} r^T(j) S_1 r(j). \tag{2-92}$$

Since V^* is unknown, then it must be estimated before log L can be evaluated. This is accomplished by maximizing log L with respect to S_2 (see Appendix C). This results in

$$\hat{S}_2 = k \left[\sum_{j=1}^{k} r(j) r^T(j) \right]^{-1} \tag{2-93}$$

Prior to substitution of equation (2-93) into equation (2-92) it is advantageous to use the following equivalent form:

$$\sum_{j=1}^{k} r^T(j) S_2 r(j) = \text{Tr} \left[S_2 \sum_{j=1}^{k} r(j) r^T(j) \right] \tag{2-94}$$

in equation (2-92) and then substitute $\hat{S}_2$ for S_2, this yields

$$L(k) = 2 \log L = -k \log|S_1| - k \log\left|\sum_{j=1}^{k} r(j)r^T(j)\right|$$

$$+ \mathrm{Tr}S_1 \sum_{j=1}^{k} r(j)r^T(j) - kg + k \log k \, . \qquad (2\text{-}95)$$

Anderson (Ref. 5) shows that under null hypothesis the ratio in equation (2-93) follows an asymptotic central chi-square distribution with $g(g + 1)/2$ degrees of freedom. That is, as $k \to \infty$ the distribution of $L(k)$ approaches a chi-squared with $g(g + 1)/2$ degrees of freedom. Based on the knowledge of the distribution of $L(k)$ a threshold ε can be selected and if $L(k)$ exceeds this threshold then a soft failure is declared. The selection of ε is accomplished by assigning a small probability α to the event of rejecting the true null hypothesis (type I error).

The above development does not provide any information regarding the failure time. If the knowledge of the failure time is needed, the formulation in equation (2-92) can be modified to furnish such information. For this purpose, note that $V^* = V$ before a failure occurs at time t then equation (2-92) can be modified as

$$\log L = \frac{(k - t)}{2} \log|S_2| + \frac{(t - k)}{2} \log|S_1| - \frac{1}{2} \sum_{j=t}^{k} r(j)S_2r^T(j)$$

$$+ \frac{1}{2} \sum_{j=t}^{k} r(j)S_1r(j) \, . \qquad (2\text{-}96)$$

The estimate of S_2 in this case becomes

$$\hat{S}_2 = (k - 1)\left[\sum_{j=t}^{k} r(j)r^T(j).\right]^{-1} \tag{2-97}$$

Utilizing equation (2-94) and substituting $\hat{S}_2$ for S_2 (from eq. (2-97)) in equation (2-96) yields

$$L(k) = 2 \log L = (-k + t)\log|S_1| - (k - t)\log\left|\sum_{j=t}^{k} r(j)r^T(j)\right|$$

$$+ \mathrm{Tr}S_1 \sum_{j=t}^{k} r(j)r^T(j) - (k - t)g + (k - t)\log(k - t). \tag{2-98}$$

In equation (2-98) the time of the failure, t, is unknown, hence, it has to be estimated before L(k) can be computed. Again, by maximizing L(k) with respect to t, an estimate of failure time is calculated that can be used in calculation of L(k). Maximization of L(k) with respect to t requires computation of L(k) in equation (2-98) for each possible value of t. It follows then that the burden of computation will grow rapidly as the number of observations grows. To circumvent this, an interval can be selected to restrict t as $k - M \leq t \leq k - N$ where M,N are the limits of the interval. In selecting these limits, consideration should be given to the fact that only the asymptotic distribution of L(k) is known. Hence, M should be selected such that the number of observations used in computing L(k) will be sufficiently large.

The brief development of a soft failure detection procedure in this Section indicates that the proposed detection scheme (illustrated

in Fig. 2.2) can also be utilized for soft failure detection. A full treatment of soft failure analysis is beyond the scope of this dissertation, however, the development in this section can serve as a basis for future research in this area. To conclude this chapter, a summary and discussion of the results developed in this chapter is given in the next section.

2.7 Summary and Discussion

The problem of detecting a hard failure in a linear dynamic system was addressed in this chapter. A new failure detection scheme was proposed (Section 2.2) that is applicable to both linear time-varying and time-invariant systems. The proposed method is based on testing the residuals of a system model. The basic underlying assumptions of the proposed method are that when no failure exists in the system the model residual is zero mean white Gaussian noise process and when a failure occurs the mean of the residual will deviate from zero while the Gaussian property is retained. Therefore, detecting a deviation in the mean value of the residuals is equivalent to detecting a failure in the system. To test the residuals, three modes of failure, namely hard-over actuator, brief disturbance in the actuator, and hard-over sensor failures are considered. Three pairs of hypotheses corresponding to these modes of failure are formed and in each case the null and the alternate hypotheses are assigned to a no-failure and a failure mode, respectively. The null hypothesis is tested against the alternate hypothesis by forming the ratio of the corresponding likelihood functions (eq. (2-32)). This yields a scalar function (referred to as GLR index). A decision regarding the occurrence of a failure is made by comparing the GLR index with a thres-

hold ε. If the GLR index exceeds ε then a failure is declared. The type of the failure can be identified by selecting the type corresponding to the maximum value of the GLR indices. The estimate of the time of the failure is chosen as the failure time resulting in the maximum value of GLR indices. The failure vector, ν, can be estimated (eq. (2-37)) by utilizing the $C_i(k,\hat{t})$ and $D_i(k,\hat{t})$ matrices corresponding to the detected type of failure i and the estimated time of failure $\hat{t}$.

The computation of the GLR indices is simplified by assuming that the linear system under study is time-invariant. This is the case in most of the practical applications. The simplifications are due to the fact that for time-invariant systems $G_i(d)$ is dependent on $d = k - t$ only and, hence, $C_i(d)$ is also a function of d only. This property of $G_i(d)$ and $C_i(d)$ also allows the off-line computation of these matrices. In situations, such as a jet engine application, where the computation time is critical, $G_i(d)$ and $C_i(d)$ can be computed off-line and stored for on-board utilization. In those cases where on-line calculation is possible the recursion relations for calculation of $G_i(d)$ simplify the computation of $C_i(d)$ and ultimately $L_i(d,t)$ (see Table 2.3).

It follows from the above discussion that the proper detection of a failure depends on the value of the threshold ε. The procedure for selection of ε will be discussed in the next chapter. Also in the next chapter various statistical and computational properties of the proposed detection plan will be discussed. This will include topics such as the probability of correct detection, false alarm, wrong-time detection, and detectability of a failure.

The concept of GLR can also be applied to the problem of soft failure detection in time-invariant systems. Similar to the case of hard failure, the GLR decision rule is comprised of comparing the likelihood ratio with a threshold, ε. The threshold ε is selected based on the probability of type I error. In conclusion, the derivation of the GLR technique using model residuals for sensor soft failure in this chapter demonstrates the applicability of the proposed detection plan (Fig. 2.2) to the problem of soft failure. Further development in this area is needed and the results of this chapter can serve as a basis for such efforts.

CHAPTER III

STATISTICAL ANALYSIS OF DETECTION TECHNIQUE

3.1 Introduction

The proposed Generalized Likelihood Ratio (GLR) failure detection decision rule, developed in Chapter II, requires a comparison of the GLR index (eq. (2-41)) with a threshold ε. In order to select a proper threshold ε, various detection probabilities such as probability of correct failure, false alarm, etc. should be determined. In this chapter these probabilities are developed. The derivation of these probabilities parallels the work of Chow in reference 3. The main difference between the results in this chapter and those of reference 3 is that the derivations in this chapter are based on using a plant model rather than the Kalman-Bucy filter in the detection scheme.

The organization of the materials presented in this chapter is as follows. The probability distribution of the GLR index is developed in the next section. After the probability distribution of GLR index is identified, the proper level of threshold ε can be established by examining the detection probabilities. These include the probability of correct detection, false alarm, cross detection, and wrong time which are derived in Sections 3.3 and 3.4. Following the derivation of the detection probabilities the question of failure detectability is addressed in Section 3.5. In Section 3.6 the asymptotic behavior of $C_i(d)$ (eq. (2-66)) is studied to determine the effect

of the number of observations on the detectability of failures. Finally, in Section 4.6 a summary and discussion of the results of this chapter is presented.

3.2 Probability Distribution of GLR

In the first part of this section the probability distribution for the GLR is derived without restricting the direction of the failure vector, ν. In Section 3.2.1, the failure vector is restricted to a single vector ν_0 and the distribution of the simplified GLR is derived. To develop the GLR distribution in a general form, assume that a GLR detector hypothesizes the occurrence of a type i failure at time t_i while actually a type j failure has occurred at time t_j. Since a type j failure has occurred the residuals are given by

$$r(k) = r_1(k) + G_j(k,t_j)\nu \tag{3-1}$$

where k is the observation number, t_j is the time of the failure, $r_1(k)$ is a zero mean white Gaussian noise process, $G_j(k,t_j)$ reflects the effect of type j failure on the residual, and ν is the failure vector. The GLR index was given in equation (2-48) as

$$L(k,t_i) = D^T_{i/j}(k,t_i)C_i^{-1}(k,t_i)D_{i/j}(k,t_i) \tag{3-2}$$

where $C_i(k,t_i)$ is the same as in equation (2-35) and $D_{i/j}(k,t_i)$ is given by

$$D_{i/j}(k,t_i) = \sum_{m=t_i}^{k} G_i^T(m,t_i)V^{-1}(m)r(m) \tag{3-3}$$

In equation (3-3) $V(m)$ is the covariance matrix of the residual of equation (3-1) and the subscript of $D_{i/j}(k,t_i)$ denotes the occurrence of type j failure while type i is hypothesized. To simplify the

presentation of mathematical relations in this chapter the following notation is adopted

$$C_{i/j}(k,t_i/t_j) = \sum_{m=t_i}^{k} G_i^T(m,t_i)V^{-1}(m)G_j(m,t_j) \tag{3-4}$$

Hence, for $i = j$ and $t_i = t_j$:

$$C_{i/i}(k,t_i/t_i) = C_i(k,t_i) = \sum_{m=t_i}^{k} G_i^T(m,t_i)V^{-1}(m)G_i(m,t_i) \tag{3-5}$$

which is the same as (2-35).

Consider $C_i(k,t_i)$ in (3-5). Since $V^{-1}(m)$ is positive definite and symmetric then $C_i(k,t_i)$ is also symmetric and positive semidefinite. Therefore, $C_i(k,t_i)$ can be transformed to a diagonal matrix by a similarity transformation as follows:

$$\Lambda_{i/i}(k,t_i/t_i) = S^{-1}C_i(k,t_i)S \tag{3-6}$$

where S is an orthonormal matrix and $\Lambda_{i/i}(k,t_i/t_i)$ is a diagonal matrix with eigenvalues of $C_i(k,t_i)$ as its elements. Utilizing equation (3-6) the GLR index in equation (3-2) can be written as

$$L_i(k,t_i) = h_{i/j}^T(k,t_i)\Lambda^{-1}(k,t_i/t_i)h_{i/j}(k,t_i) \tag{3-7}$$

where

$$h_{i/j}(k,t_i) = S^T D_{i/j}(k,t_i) \tag{3-8}$$

In order to determine the distribution of $L_i(k,t_i)$ it is necessary to identify the distribution of the random vector $h_{i/j}(k,t_i)$. The vector $h_{i/j}(k,t_i)$ in (3-8) is a Gaussian random vector and it can be completely identified by its mean and variance. The mean of

$h_{i/j}(k,t_i)$ can be computed as:

$$E\left[h_{i/j}(k,t_i)\right] = S^T E\left[D_{i/j}(k,t_i)\right] \tag{3-9}$$

substituting for $D_{i/j}(k,t_i)$ from (3-3) and taking the expectation yields

$$E\left[h_{i/j}(k,t_i)\right] = S^T \sum_{m=t_i}^{k} G_i^T(m,t_i)V^{-1}(m)G_j(m,t_j)\nu \tag{3-10}$$

Now using the notation introduced in (3-4), equation (3-10) can be written as

$$F\left[h_{i/j}(k,t_i)\right] = S^T C_{i/j}(k,t_i/t_j)\nu \tag{3-11}$$

The covariance of $h_{i/j}(k,t_i)$ can be calculated in the following manner:

$$E\left[h_{i/j}(k,t_i)\, h_{i/j}^T(k,t_i)\right] = S^T E\left\{\left[\sum_{m=t_i}^{k} G_i^T(m,t_i) \times V^{-1}(m)r(m)\right]\left[\sum_{m=t_i}^{k} G_i^T(m,t_i)V^{-1}(m)r(m)\right]^T\right\} S \tag{3-12}$$

Substituting for $r(m)$ from (3-1) and taking the expected value results in

$$E\left[h_{i/j}(k,t_i)h_{i/j}^T(k,t_i)\right] = S^T C_i(k,t_i)S + E\left[h_{i/j}(k,t_i)\right]\; E\left[h_{i/j}(k,t_i)\right] \tag{3-13}$$

The first term on the right-hand side of equation (3-13) is $\Lambda_{i/i}(k,t_i/t_i)$ (see eq. (3-6)), hence the variance of $h_{i/j}(k,t_i)$ is equal to $\Lambda_{i/i}(k,t_i/t_i)$. Since $\Lambda_{i/i}(k,t_i/t_i)$ is a diagonal matrix it follows that the elements of $h_{i/j}(k,t_i)$ are independent of one another.

Consider the GLR index in equation (3-7), the expression for GLR index can be written as:

$$L_i(k,t_i) = \sum_{q=1}^{g} \frac{h_q^2(k,t_i)}{\lambda_q} \tag{3-14}$$

where $h_q(k,t_i)$ and λ_q are qth elements of $h_{i/j}(k,t_i)$ vector and $\Lambda_{i/i}(k,t_i/t_i)$ matrix respectively, and g is the number of system outputs. Examination of (3-14) reveals that $L_i(k,t_i)$ is the sum of squares of the Gaussian random variables with mean of $\bar{h}_q(k,t_i)/\sqrt{\lambda_q}$, where $\bar{h}_q(k,t_i)$ is the mean of the qth element of the $h_{i/j}(k,t_i)$ vector. The variance of $h_q(k,t_i)/\sqrt{\lambda_q}$ is unity because λ_q is the variance of $h_q(k,t_i)$. Since the elements of $h_{i/j}(k,t_i)$ are independent of one another with a Gaussian distribution, then the GLR index has a noncentral chi-squared distribution with g degrees of freedom and noncentrality parameter δ^2 given by

$$\delta^2 = \sum_{q=1}^{g} \frac{\bar{h}_q^2(k,t_i)}{\lambda_q} \tag{3-15}$$

(Ref. 61). It is useful to write δ^2 in matrix form for the calculation of detection probabilities which will be presented later. Specifically,

$$\delta^2 = \nu^T C^T_{i/j}(k,t_i/t_j)\ S\ \Lambda^{-1}_{i/i}(k,t_i/t_i)\ S^T\ C_{i/j}(k,t_i/t_j)\ \nu \qquad (3\text{-}16)$$

Using the orthonormal property of matrix S, i.e., $S^T = S^{-1}$ equation (3-16) can be written as

$$\delta^2 = \nu^T C^T_{i/j}(k,t_i/t_j)\ C^{-1}_{i/i}(k,t_i/t_i)\ C_{i/j}(k,t_i/t_j)\ \nu \qquad (3\text{-}17)$$

This concludes the derivation of the probability distribution for the GLR index. Since no assumption regarding i,j,t_i,t_j and ν was made, various probabilities regarding failure detection can be computed as special cases of the general derivation of this Section. One special case of interest is to restrict the failure vector to a single known vector, ν_o, i.e., the case of Simplified GLR. For this case the distribution of the SGLR index is a Gaussian distribution and its derivation is presented in the next Section.

3.2.1 Probability Distribution of Simplified GLR

Consider the Simplified Generalized Likelihood Ratio (SGLR) index in equation (2-46). If an SGLR detector hypothesizes the occurrence of a type i failure at time t_i while a type j failure has actually occurred at time t_j the equation (2-46) can be rewritten as

$$L(k,t_i) = 2\nu_0^T\left[\sum_{m=1}^{k} G_i(m,t_i)V^{-1}(m)r_1(m)\right] + 2\nu_0^T\left[\sum_{m=1}^{k} G_i^T(m,t_i)V^{-1}(m)\right.$$

$$\left.\times\ G_j(m,t_j)\right]\nu - \nu_0^T\left[\sum_{m=1}^{k} G_i^T(m,t_i)V^{-1}G_i(m,t_i)\right]\nu_0 \qquad (3\text{-}18)$$

The equation (3-18) follows directly from (2-46) by substituting for r(m) from equation (3-1). Since $r_1(m)$ in (3-18) is a white Gaussian noise process then $L(k,t_i)$ is a sum of independent Gaussian random variables. Thus, the probability distribution of $L(k,t_i)$ for SGLR is Gaussian. The mean of $L(k,t_i)$ is given by

$$E\left[L(k,t_i)\right] = 2\nu_0^T\left[\sum_{m=1}^{k} G_i^T(m,t_i)V^{-1}(m)G_j(m,t_j)\right]\nu - \nu_0^T\left[\sum_{m=1}^{k} G_i^T(m,t_i)V^{-1}G_i(m,t_i)\right]\nu_0 \qquad (3\text{-}19)$$

Using the notation introduced in (3-4), equation (3-19) becomes

$$E\left[L(k,t_i)\right] = 2\nu_0^T C_{i/j}(k,t_i/t_j)\nu - \nu_0^T C_i(k,t_i)\nu_0 \qquad (3\text{-}20)$$

The variance of $L(k,t_i)$ can be calculated as follows:

$$E\left\{L(k,t_i) - E\left[L(k,t_i)\right]\right\}^2 = 4\nu_0^T\left[\sum_{m=1}^{k} G_i^T(m,t_i)V^{-1}(m) \times G_i(m,t_i)\right]\nu_0 \qquad (3\text{-}21)$$

or

$$E\left\{L(k,t_i) - E\left[L(k,t_i)\right]\right\}^2 = 4\nu_0^T C_i(k,t_i)\nu_0 \qquad (3\text{-}22)$$

This concludes the derivation of the distribution of the SGLR index. Next, the distribution of the GLR and the SGLR indicies will be utilized to determine four important detection probabilities, namely, the probability of correct detection, false alarm, cross detection, and wrong time failure.

3.3 Detection Probabilities

Based on the GLR decision rule, established in Section 2.3.3, if a GLR index corresponding to a type i failure exceeds a selected threshold ϵ then a failure is declared. It is possible, however, that the GLR index corresponding to a failure of type i exceeds the threshold ϵ while a failure of type j has actually occurred. It is, therefore, essential to establish the probability for various detection modes. Four important detection modes are correct detection, false alarm, cross detection, and wrong time.

Probability of Correct Detection

The probability of correct detection is a measure of reliability of the detection technique. It can be defined as:

$$P_D(k,i,t,\nu) \triangleq \text{Prob.}(L_i(k,t) > \epsilon / i,t,\nu) \tag{3-23}$$

that is the probability that the GLR index, $L_i(k,t)$, for a type i failure at time t exceeds the threshold ϵ given that a failure ν of type i has actually occurred at time t. This probability can be computed from the distribution of the GLR index which was developed in Section 3.2. For the case of correct detection the noncentrality parameter δ^2 (eq. (2-17)) for the GLR distribution is given by

$$\delta^2 = \nu^T C_i(k,t)\nu. \tag{3-24}$$

Equation (3-24) is derived from equation (3-17) by substituting $i = j$ and $t_i = t_j$ and using the notation defined in (3-5).

False Alarm

The false alarm probability indicates the consistency of the detector. It is the probability that the GLR index exceeds a

threshold ϵ given that no failure has occurred. Expressing this definition in symbols yields:

$$P_F(k,i,t) \triangleq \text{Prob.}(L_i(k,t) > \epsilon / \nu = 0) \tag{3-25}$$

The noncentrality parameter δ^2 (eq. (3-17)) for this case is zero because $\nu=0$. Thus, the distribution of the GLR index for this case is a central chi-squared with g degrees of freedom.

Cross Detection

The probability of cross detection provides a measure of the capability of the GLR technique in selecting the true type of failure. The probability of cross-detection can be defined as:

$$P_{CD}(k,i,j,t,\nu) \triangleq \text{Prob.}\ (L_i(k,t) > \epsilon / j,t,\nu) \tag{3-26}$$

which is the probability that GLR index for type i failure will exceed the threshold ϵ while a failure ν of type j has actually occurred. The noncentrality parameter for probability distribution of $L_i(k,t)$ for this case (from eq. (3-17)) is given by

$$\delta^2 = \nu^T C_{i/j}(k,t/t) C_i^{-1}(k,t) C_{i/j}(k,t/t) \nu \tag{3-27}$$

since $i \neq j$ and $t_i = t_j = t$.

Wrong Time

Correct estimation of the failure time is important for two reasons. First, the estimate of the failure vector is directly dependent on the estimate of the failure time. The second reason is that the estimate of failure time is often required when using the variable accommodation technique. The probability of wrong time detection is defined as the probability that the GLR index of type i failure at time t exceeds the threshold ϵ given that the failure has actually

occurred at time t_c. This can be expressed in mathematical symbols as:

$$P_{WT}(k,i,t,\nu,t_c) \triangleq \text{Prob.}(L_i(k,t)>\varepsilon/i,t_c,\nu) \tag{3-28}$$

Using equation (3-28) the noncentrality parameter for GLR probability distribution in this case is given by

$$\delta^2 = \nu^T C_{i/i}(k,t/t_c)C_i^{-1}(k,t)C_{i/i}(k,t/t_c)\nu \tag{3-29}$$

since $i=j$ and $t\neq t_c$. A summary of the above results for the four detection probabilities is presented in Table 3.1.

Derivation of the four detection probabilities for simplified GLR follows the same procedure as above. In the case of SGLR, however, the distribution of the SGLR index is Gaussian and instead of the non-centrality parameter, the mean and the variance of the distribution should be determined for each of the four cases. The variance of the Gaussian distribution for all four modes remains constant (see eq. (3-22)) while the mean varies. In the case of correct detection $i=j$, $t_i=t_j$ and $\nu=\nu_0$ the mean becomes

$$E\left[L_i(k,t_i)\right] = \nu_0^T C_i(k,t_i)\nu_0 \tag{3-30}$$

The above procedure repeats for the remaining three modes and a summary of the corresponding means is given in Table 3.2. The development of the detection probabilities in this section has been for time varying systems. In the next section the detection probabilities for the special case of time-invariant systems will be discussed.

3.4 Failure Detection Probabilities for Time-Invariant Systems

In many practical applications of control theory the system

TABLE 3.1

SUMMARY OF NONCENTRALITY PARAMETERS

FOR FOUR DETECTION MODES

Correct Detection:

$$\delta^2 = \nu^T C_i(k,t_i)\nu$$

Remarks: $i=j$ and $t_i=t_j$

False Alarm:

$$\delta^2 = 0$$

Remarks: $\nu=0$ and $i=j$

Central chi-squared distribution for GLR

Cross Detection:

$$\delta^2 = \nu^T C_{i/j}(k,t/t)C_i^{-1}(k,t)C_{i/j}(k,t/t)\nu$$

Remarks: $t_i=t_j=t$

Wrong Time:

$$\delta^2 = \nu^T C_{i/i}(k,t/t_c)C_i^{-1}(k,t)C_{i/i}(k,t/t_c)\nu$$

Remarks: $i=j$ and $t\neq t_c$

Also $t < t_c < k$ or $t_c < t < k$

TABLE 3.2

SUMMARY OF SGLR GAUSSIAN DISTRIBUTION MEANS

FOR FOUR MODES OF DETECTION

Correct Detection:

Mean = $\nu_0^T C_i(k,t_i)\nu_0$

Remarks: $i=j$ and $\nu=\nu_0$

False Alarm:

Mean = $-\nu_0^T C_i(k,t_i)\nu_0$

Remarks: $i=j$ and $\nu=0$

Cross Detection:

Mean = $2\nu_0^T C_{i/j}(k,t_i/t_i)\nu - \nu_0^T C_i(k,t_i)\nu_0$

Remarks: $i\neq j$, $\nu\neq\nu_0$ and $t_i=t_j$

Wrong Time:

Mean = $2\nu_0^T C_{i/i}(k,t_i/t_c)\nu_0 - \nu_0^T C_i(k,t)\nu_0$

Remarks: $t\neq t_c$, $i=j$, and $\nu=\nu_0$

Also $t<t_c<k$ or $t_c<t<k$

under study is assumed to be time-invariant. It is, therefore, important to study the probability of various modes of detection, namely, correct detection, false alarm, cross detection, and wrong time for such systems. In this section detection probabilities are developed for the three types of failure which were discussed in Chapter 2. The key elements in establishing these probabilities are the corresponding noncentrality parameters. Therefore δ^2 of the four detection probabilities are derived for each of the three failure types. Before proceding with the derivation, it should be noted that in case of false alarm the probability distribution of the GLR index reduces to central chi-squared, thus the corresponding noncentrality parameter is zero for all three failure types.

3.4.1 State-Step Failure

Consider the general formulation of the noncentrality parameter for correct detection, given in equation (3-24). The $C_i(k,t)$ for a state-step failure for the time-invariant system is given by

$$C_i(k,t) = \sum_{m=0}^{d} \left[H \sum_{x=0}^{m} \phi^{(m-x)} \right]^T V^{-1} \left[H \sum_{x=0}^{m} \phi^{(m-x)} \right] \qquad (3\text{-}31)$$

where $d = k - t$. The equation (3-31) is derived by substituting equation (2-56) in the expression for $C_i(d)$ in equation (2-66). Now by substituting equation (3-31) in equation (3-24) the noncentrality parameter δ^2 for this case becomes

$$\delta^2 = \nu^T \left\{ \sum_{m=0}^{d} \left[\sum_{x=0}^{m} \phi^{(m-x)} \right]^T (H^T V^{-1} H) \left[\sum_{x=0}^{m} \phi^{(m-x)} \right] \right\} \nu \qquad (3\text{-}32)$$

The noncentrality parameter for cross detection is given in its general form in equation (3-27). The $C_{i/j}(k,t/t)$ for state-step failure is given by

$$C_{i/j}(k,t/t) = \sum_{m=0}^{d} \left[\sum_{x=0}^{m} \phi^{(m-x)} \right]^T H^T V^{-1} G_j(m) \qquad (3\text{-}33)$$

where $d = k - t$. Equation (3-33) is the direct result of substituting equation (2-55) into equation (3-4). The matrix $C_i(k,t)$ is given by equation (3-31). Hence the δ^2 for cross detection can be written as

$$\delta^2 = \nu^T \left\{ \sum_{m=0}^{d} \left[\sum_{x=0}^{m} \phi^{(m-x)} \right]^T H^T V^{-1} G_j(m) \right\}^T$$

$$\times \left\{ \sum_{m=0}^{d} \left[\sum_{x=0}^{m} \phi^{(m-x)} \right]^T (H^T V^{-1} H) \left[\sum_{x=0}^{m} \phi^{(m-x)} \right] \right\}^{-1}$$

$$\times \left\{ \sum_{m=0}^{d} \left[\sum_{x=0}^{m} \phi^{(m-x)} \right]^T H^T V^{-1} G_j(m) \right\} \qquad (3\text{-}34)$$

The noncentrality parameter for wrong time detection can be derived from the general equation for this mode of failure in equation (3-29). Utilizing equation (2-55), $C_{i/j}(k,t/t_c)$ for state-step failure yields

$$C_{i/j}(k,t/t_c) = \sum_{m=t}^{k} \left[H \sum_{q=t}^{m} \phi^{(m-q)} \right]^T V^{-1} \left[H \sum_{q=t_c}^{m} \phi^{(m-q)} \right] \qquad (3\text{-}35)$$

and $C_i(k,t)$ remains the same as in equation (3-31). Thus δ^2 for wrong time detection for state-step failure becomes

$$\delta^2 = \nu^T \left\{ \sum_{m=t}^{d} \left[\sum_{x=t}^{m} \phi^{(m-x)} \right]^T (H^T V^{-1} H) \left[\sum_{x=t_c}^{m} \phi^{(m-x)} \right] \right\}^T$$

$$\times \left\{ \sum_{m=0}^{d} \left[\sum_{x=0}^{m} \phi^{(m-x)} \right]^T (H^T V^{-1} H) \left[\sum_{x=0}^{m} \phi^{(m-x)} \right] \right\}^{-1}$$

$$\times \left\{ \sum_{m=t}^{k} \left[\sum_{x=t}^{m} \phi^{(m-x)} \right]^T (H^T V^{-1} H) \left[\sum_{x=t_c}^{m} \phi^{(m-x)} \right] \right\} \nu \qquad (3\text{-}36)$$

This concludes the derivation of noncentrality parameter for state-step failures. The equations (3-32), (3-34), and (3-36) provide the necessary information for evaluating the performance of a GLR detector set to detect state-step failures in a time-invariant system. Specifically,

equation (3-32) provides a measure of detectability of failures as for a constant threshold ε, larger δ^2 results in higher probability of correct detection. Similarly, the equations (3-34) and (3-36) for δ^2 enable one to compute the probabilities of cross detection and wrong time detection, respectively. Next the noncentrality parameters for state-jump failure will be developed.

3.4.2 State-Jump Failure

The noncentrality parameter for correct detection of this failure mode can be calculated from the general form of δ^2 in equation (3-24). The $C_i(k,t)$ in equation (3-24) for state-jump failure becomes

$$C_i(k,t) = \sum_{m=0}^{d} \left(\phi^m\right)^T (H^T V^{-1} H) \phi^m \tag{3-37}$$

where $d = k - t$. Equation (3-37) is derived by substitution from equation (2-62) into the equation for $C_i(d)$ given in equation (2-66). Now substituting equation (3-37) in equation (3-24) yields δ^2 for state-jump failure as:

$$\delta^2 = \nu^T \left[\sum_{m=0}^{d} \left(\phi^m\right)^T (H^T V^{-1} H) \phi^m \right] \nu \tag{3-38}$$

The derivation of the noncentrality parameter for cross detection of state-jump failures can be accomplished by substituting the corresponding expressions for $C_{i/j}(k,t/t)$ and $C_i(k,t)$ for this mode of failure in equation (3-27). The expression for $C_i(k,t)$ is given in equation (3-37) and $C_{i/j}(k,t/t)$ can be calculated by substituting $G_i(m)$ from equation (2-62) into equation (3-4) which yields

$$C_{i/j}(d) = \sum_{m=0}^{d} \left(\phi^m\right)^T H^T V^{-1} H G_j(m) \tag{3-39}$$

Hence δ^2 for cross detection can be written as

$$\delta^2 = \nu^T \left[\sum_{m=0}^{d} \left(\phi^m\right)^T H^T V^{-1} H G_j(m)\right]^T \left[\sum_{m=0}^{d} \left(\phi^m\right)^T (H^T V^{-1} H)\phi^m\right]^{-1} \times \left[\sum_{m=0}^{d} \left(\phi^m\right)^T H^T V^{-1} H G_j(m)\right] \nu \tag{3-40}$$

The calculation of δ^2 for wrong-time detection is accomplished by substituting proper values of $C_{i/i}(k,t/t_c)$ and $C_i(k,t)$ in equation (3-29). The expression for $C_i(k,t)$ is given in equation (3-37) and $C_{i/i}(k,t/t_c)$ can be derived by substituting for $G_i(m,t)$ and $G_i(m,t_c)$ in equation (3-4) from equation (2-61). Thus

$$C_{i/i}(k,t/t_c) = \sum_{m=t}^{k} \left(\phi^{m-t}\right)^T (H^T V^{-1} H)\left(\phi^{m-t_c}\right) \tag{3-41}$$

therefore

$$\delta^2 = \nu^T \left[\sum_{m=t}^{k} \left(\phi^{m-t}\right)^T (H^T V^{-1} H)\left(\phi^{m-t_c}\right)\right]^T \times \left[\sum_{m=0}^{d} \left(\phi^m\right)^T (H^T V^{-1} H)(\phi^m)\right]^{-1} \times \left[\sum_{m=t}^{k} \left(\phi^{m-t}\right)^T (H^T V^{-1} H)\left(\phi^{m-t_c}\right)\right] \nu \tag{3-42}$$

This completes the derivation of the noncentrality parameters for state-jump failure. Equation (3-38) provides the essential information for calculation of the probability of correct detection when a failure has actually occurred. Similarly equations (3-40) and (3-42) give the necessary information for evaluating probabilities of cross detection and wrong-time detection, respectively. In the next section the noncentrality parameters for sensor-step failure will be calculated.

3.4.3 Sensor-Step Failure

The calculation of δ^2 for correct detection can be achieved by substituting for $C_i(k,t)$ in equation (3-24) from equation (2-79), which yields

$$\delta^2 = (1 + d)\nu^T V^{-1}\nu \tag{3-43}$$

where $d = k - t$.

For cross detection, δ^2 is calculated from equation (3-27) by substituting for $C_{i/j}(k,t/t)$ from the following expression

$$C_{i/j}(k,t/t) = \left[\sum_{m=0}^{d} V^{-1}G_j(m)\right] \tag{3-44}$$

Equation (3-44) is derived by substituting equation (2-64) in equation (3-4). Hence δ^2 is given by

$$\delta^2 = \nu^T \left[\sum_{m=0}^{d} V^{-1}G_j(m)\right]^T \left(\frac{V}{1 + d}\right) \left[\sum_{m=0}^{d} V^{-1}G_j(m)\right] \tag{3-45}$$

Finally δ^2 for wrong time failure can be derived from equation (3-29) by substituting the following expression for $C_{i/i}(k,t/t_c)$

$$C_{i/i}(k,t/t_c) = \left(\sum_{m=t}^{k} V^{-1}\sigma_{m,t_c}\right) \tag{3-46}$$

where σ_{m,t_c} is a unit step function defined in equation (2-4). Equation (3-46) is derived by substituting equation (2-64) into equation (3-4). The expression for $C_i(k,t)$ is the same as in equation (2-79). Then δ^2 can be written as:

$$\delta^2 = \nu^T\left(\sum_{m=t}^{k} V^{-1}\sigma_{m,t_c}\right)^T \left(\frac{V}{d+1}\right)\left(\sum_{m=t}^{k} V^{-1}\sigma_{m,t_c}\right)\nu \tag{3-47}$$

This concludes the derivation of the noncentrality parameters for the three modes of failure. The main utility of the relations developed in this section is to provide the necessary information for evaluation of reliability (correct detection) and consistency (false alarm) of the GLR detector, capability of selecting the true failure type, and correct estimation of the failure time. To continue the study of the characteristics of the GLR detectors, the next section is devoted to the detectability of failures.

3.5 Failure Detectability

In the course of development of any failure detection technique, it is essential to determine what failures can not be detected. The GLR technique utilizes the deviation of the residual mean from zero, in case of a failure, to detect various modes of failure. Therefore any failure which does not effect the mean of the residuals can not be detected. It follows that any failure in the unobservable space of the system under study can not be detected. An important question can be

raised immediately: is it possible to establish detectability conditions for the proposed GLR technique?

To investigate the answer to this question consider the general expression for the GLR index at kth observation

$$L_j(k,t) = D_i^T(k,t)C_i^{-1}(k,t)D_i(k,t) \tag{3-48}$$

It can be seen from equation (3-48) that the calculation of $L_i(k,t)$ depends on the invertibility of $C_i(k,t)$ matrix. Although it is difficult to establish the conditions for invertibility of $C_i(k,t)$ in case of actuator failures, it is possible to show that $C_i(k,t)$ is always invertible for sensor failures.

In order to establish invertibility of $C_i(k,t)$ for sensor failures consider $C_i(k,t)$ for a sensor-step failure

$$C_i(k,t) = \sum_{j=1}^{k} V^{-1}(j) \tag{3-49}$$

where $V(j)$ is the covariance matrix of the model residual. According to the assumption that model residuals are white Gaussian noise processes then the matrix $V(j)$ is a positive definite diagonal matrix. Therefore, $V^{-1}(j)$ is also positive definite. It can be shown that $C_i(k,t)$ in equation (3-49) is also positive definite (see the proof in Appendix B). Hence, $C_i(k,t)$ is always invertible which proves that all sensor step failures are detectable. In the case of time-invariant systems the conditions of invertibility of $C_i(k,t)$ matrix can be established for actuator failures. Before proceeding to develop these conditions it should be mentioned that the proof of the invertibility

of $C_i(k,t)$ for sensor failures is general, thus it is also valid for time-invariant systems.

3.5.1 Detectability of State-Step Failure in Time-Invariant Systems

It was shown in Chapter 2, Section 2.4, that for the time-invariant system $C_i(k,t)$ matrix becomes a function of $d = k - t$ where k is the number of observations and t is the failure time. Consider the general formulation of $C_i(d)$ for time-invariant systems

$$C_i(d) = \sum_{j=0}^{d} G_i^T(j) V^{-1} G_i(j) \tag{3-50}$$

where V is the covariance matrix of the residuals and $G_i(j)$ for $i = 1,2,3$ is given in Table 2.2. Equation (3-50) can also be written in the following form

$$C_i(d) = \left[G_i^T(0) \mid G_i^T(1) \mid \cdots \mid G_i^T(d) \right]$$

$$\times \begin{bmatrix} V^{-1} & & & 0 \\ & V^{-1} & & \\ & & \ddots & \\ 0 & & & V^{-1} \end{bmatrix} \begin{bmatrix} G_i(0) \\ \hline G_i(1) \\ \hline \vdots \\ \\ \vdots \\ \\ G_i(d) \end{bmatrix} \tag{3-51}$$

or

$$C_i(d) = \gamma_i^T \Omega \gamma_i \tag{3-52}$$

The matrix Ω is composed of V^{-1} matrices as diagonal blocks. Since

V^{-1} is positive definite then for $C_1(d)$ to be invertible, the matrix γ_1 must be also positive definite. Before proceeding to establish the conditions for invertibility of $C_1(d)$, it should be stated that equation (3-52) is valid for all failure modes in time-invariant systems because no restriction was imposed on i, the type of the failure.

For state-step failure the $\gamma_1(d)$ matrix is given by

$$\gamma_1(d) = \left[H \mid H + H\phi \mid \cdots \mid H \sum_{j=0}^{d} \phi^j \right] \tag{3-53}$$

Equation (3-53) is derived by substituting equation (2-56). For $C_1(j)$ for $j = 0,1,\ldots,d$. Equation (3-53) can be written as

$$\gamma_1(d) = \begin{bmatrix} I & & & & \\ I & I & & 0 & \\ \cdot & & \cdot & & \\ \cdot & & & \cdot & \\ \cdot & 0 & & & \cdot \\ I & & \cdot & \cdot & \cdot \; I \end{bmatrix} \begin{bmatrix} H \\ H\phi \\ \cdot \\ \cdot \\ \cdot \\ H\phi^d \end{bmatrix} \triangleq \Gamma\beta(d) \tag{3-54}$$

The lower block triangular matrix on the right-hand side of equation (3-54) is of full rank. Thus if $\beta(d)$ matrix is of full rank then $\gamma_1(d)$ will be positive definite and $C_1(d)$ will be invertible. The $\beta(d)$ matrix is identical to the matrix used to test the observability of a system. Thus a detectability test resulting from the above discussion can be stated as: a state-step failure is detectable if $\beta(d)$ is of full rank. Furthermore if $\beta(d)$ is not invertible in $n-1$ steps, where n is the dimension of the system, it will never be invertible. This fol-

lows from a property of linear constant systems that if an n dimensional linear constant system is not completely observable in $n - 1$ steps it will never be completely observable.

As a result of this finite-step detectability property a guideline may be established for selecting the observation window size that was introduced in Section 2.3.3. In that section the range of the failure time was restricted to $k - M \leq \hat{t} \leq k - N$ where $\hat{t}$ is the estimate of the failure time and N and M are window limits. The window of observation can be written as $N \leq k - t \leq M$, which is suitable for establishing the limits on $d = k - t$. Since the invertibility of $C_i(d)$ will not be effected by $d > n - 1$ then N may be selected to be $N \leq n - 1$. In summation the invertibility of $C_i(d)$ for state-step failures is related to the observability of the system under study. Hence, if the n dimensional system is not completely observable in $n - 1$ steps then the state-step failure in that system is not detectable either. The derivation of these conditions forms a basis for establishing the detectability criterion for state-jump failure in the next section.

3.5.2 Detectability of State-Jump Failure in Time-Invariant Systems

The general form of the $C_i(d)$ matrix in equation (3-52) is also valid for state-jump failure. In this case, however, the matrix $\gamma_2(d)$ is given by

$$\gamma(d) = \begin{bmatrix} I & & & \\ & I & & 0 \\ & & \ddots & \\ & 0 & & \ddots \\ & & & & I \end{bmatrix} \begin{bmatrix} H \\ H\phi \\ \vdots \\ \vdots \\ \vdots \\ H\phi^d \end{bmatrix} \qquad (3\text{-}55)$$

The block diagonal matrix on the right-hand side of equation (3-55) is of full rank and the second matrix is identical to the one derived for state-step failure in equation (3-54). Thus the conclusions of the previous section are also applicable to state-jump failure case as well.

It follows from the discussions in Sections 3.3 through 3.5 that the $C_i(d)$ matrix (see Table 2-2) has an important effect on the successful detection of a failure. The effect of the $C_i(d)$ matrix can be summarized as follows. First, to calculate the GLR index, equation (3-48), it is necessary that $C_i^{-1}(d)$ be invertible. The second effect of $C_i(d)$ is that the noncentrality parameter, δ^2, of correct detection is a function of $C_i(d)$ (see eq. (3-24)). Since the larger δ^2 is the higher the probability of correct detection will be then $C_i(d)$ has a direct influence over the probability of correct detection. Finally it can be shown that $C_i(d)$ is the covariance matrix of the failure vector estimate, $\hat{\nu}$(proof is presented in Appendix D). Hence, the accuracy of the failure vector estimate depends on $C_i(d)$. Therefore, it is important to study the behavior of $C_i(d)$ as the number of observations increases. For this purpose the next section is dedicated to the discussion of the asymptotic behavior of the $C_i(d)$ matrix.

3.6 Asymptotic Behavior of C-Matrix in Time-Invariant Systems

In this section the behavior of $C_i(k,t)$ (defined in eq. (2-35)) for time-invariant systems as the number of observations, k, increases will be studied. It was shown in Section 2.4 that for time-invariant systems the matrix $C_i(k,t)$ becomes a function of $d = k - t$, i.e., $C_i(d)$. Since t, the failure time, is constant, then the study of the behavior of $C_i(d)$ as a function of d is equivalent to studying the behavior of $C_i(d)$ as a function of k. The behavior of $C_i(d)$ for each of the three modes will be considered separately.

1. State-Step Failure

Consider the general form of the $C_i(d)$ for time-invariant systems

$$C_i(d) = \sum_{j=0}^{d} G_i^T(j) V^{-1} G(j) \tag{3-56}$$

Since V, the covariance matrix of the residuals, is constant then the asymptotic behavior of $C_i(d)$ depends on $G_i(j)$. For a state-step failure

$$G_1(j) = H \sum_{s=0}^{j} \phi^{j-s} \tag{3-57}$$

Equation (3-57) was initially derived in equation (2-56). Expanding the matrix series in equation (3-57) results in

$$G_1(j) = H\left[\phi^j + \phi^{j-1} + \phi^{j-2} + \ldots + I\right] \tag{3-58}$$

or

$$G_1(j) = H \sum_{s=0}^{j} \phi^s \qquad (3\text{-}59)$$

post multiplication of equation (3-59) by ϕ yields

$$G_1(j)\phi = H \sum_{s=0}^{j} \phi^{s+1} \qquad (3\text{-}60)$$

Subtracting equation (3-60) from equation (3-59) and rearranging terms results in

$$G_1(j) = H(I - \phi^{j+1})(I - \phi)^{-1} \qquad (3\text{-}61)$$

The $C_1(d)$ matrix can then be written as

$$C_1(d) = \sum_{j=0}^{d} \left[H(I - \phi^{j+1})(I - \phi)^{-1}\right]^T V^{-1} \left[H(I - \phi^{j+1})(I - \phi)^{-1}\right] \qquad (3\text{-}62)$$

Rearranging the terms inside the summation yields

$$C_1(d) = (I - \phi)^{-T} \left[\sum_{j=0}^{d} \left(I - \phi^{j+1}\right)^T (H^T V^{-1} H)(I - \phi^{j+1})\right] (I - \phi)^{-1} \qquad (3\text{-}63)$$

Since only the terms inside the brackets are functions of d, the behavior of these terms will effect $C_1(d)$. Thus consider

$$B(d) = \left[\sum_{j=0}^{d} \left(I - \phi^{j+1}\right)^T V_1 (I - \phi^{j+1})\right] \qquad (3\text{-}64)$$

where V_1 is defined as

$$V_1 = H^T V^{-1} H \tag{3-65}$$

Equation (3-64) can be written

$$B(d) = \sum_{j=0}^{d} V_1 + \sum_{j=0}^{d} \left(\phi^{j+1}\right)^T V_1 \phi^{j+1}$$

$$- \left[\sum_{j=0}^{d} \left(\phi^{j+1}\right)^T V_1 + \sum_{j=0}^{d} V_1 \phi^{j+1} \right] \tag{3-66}$$

The last two terms in equation (3-66) can be written in closed form by following the same procedure used to derive equation (3-61); thus equation (3-66) can be rewritten as

$$B(d) = (1 + d)V_1 + \sum_{j=0}^{d} \left(\phi^{j+1}\right)^T V_1 \phi^{j+1} - (I - \phi)^{-T}\left(I - \phi^{j+1}\right)^T$$

$$\times \phi^T V - V\phi(I - \phi^{d+1})(I - \phi)^{-1} \tag{3-67}$$

Now as $d \to \infty$ then ϕ^{d+1} approaches zero because the system under study is assumed to be stable, hence, all the eigenvalues of ϕ are within the unit circle. Hence, the limit of $B(d)$ as $d \to \infty$ can be written as

$$\lim_{d \to \infty} B(d) = \lim_{d \to \infty} (1 + d)V_1 + \lim_{d \to \infty} \sum_{j=0}^{d} \left(\phi^{j+1}\right)^T V_1 \phi^{j+1}$$

$$- (I - \phi)^{-T} \phi^T V - v\phi(I - \phi)^{-1} \tag{3-68}$$

It can be seen from equation (3-68) that as $d \to \infty$ the elements of $B(d)$ and thus the elements of $C_1(d)$ will grow larger. Thus at least some eigenvalues of $C_1(d)$ will grow as the number of observations increases.

The increase in the eigenvalues of $C_1(d)$ improves the probability of correct detection of state-step failures that lie in the direction of the corresponding eigenvectors. This can be seen easily by examining the noncentrality parameter for

$$\delta^2 = \nu^T C_i(d)\nu \tag{3-69}$$

As δ^2 increases in value the probability of correct detection improves. Hence, the failure vectors which lie in the direction of eigenvectors corresponding to growing eigenvalues have a higher probability of being detected as k increases.

2. State-Jump Failure

As in the case of state-step failure, the behavior of $C_i(d)$ matrix depends on the behavior of $G_i(j)$ matrix. The $G_i(j)$ matrix for a state-step failure is given by

$$G_2(j) = H\phi^j \tag{3-70}$$

Taking the norm of equation (3-70) yields

$$||G_2(j)|| = ||H\phi^j|| \tag{3-71}$$

It can be shown that (see Appendix B)

$$||G_2(j)|| \leq ||H||\ ||\phi^j|| \tag{3-72}$$

Now since the system under study is assumed to be stable the eigenvalues of ϕ are within the unit circle. Hence, as $j \to \infty$ the matrix ϕ^j becomes a null matrix, thus $||\phi^j|| \to 0$ as $j \to \infty$. It follows that

$$\lim_{j\to\infty} ||G_2(j)|| = 0 \tag{3-73}$$

The above results will be used to show that the sequence $\{C_2(1), C_2(2), \ldots, C_2(d)\}$ forms a Cauchy sequence, thus it converges to a constant matrix as $d \to \infty$. To accomplish this consider the following definition

$$\Delta C(d,q) \triangleq \sum_{j=d+1}^{q} G_2^T(j) V^{-1} G_2(j) = C_1(q) - C_2(d) \tag{3-74}$$

where $q > d$. To establish that the sequence $\{C_2(1), C_2(2), \ldots, C_2(d)\}$ forms a convergent Cauchy sequence, it should be proved that the norm of $\Delta C(d,q)$ approaches zero as $q \to \infty$. Now to prove this consider $G_2(j)$ for state-jump failure in equation (3-70) and $\Delta C(d,q)$ in equation (3-74). Substituting for $G_2(j)$ in equation (3-74) from equation (3-70) yields

$$\Delta C(d,q) = \sum_{j=d+1}^{q} \phi^{jT} H^T V^{-1} H \phi^j \tag{3-75}$$

Taking the norm of both sides and using the properties of the matrix norm yields

$$||\Delta C(d,q)|| \leq \sum_{j=d+1}^{q} ||\phi^{jT} H^T V^{-1} H \phi^j||$$

$$\leq \sum_{j=d+1}^{q} ||V^{-1}||\ ||H||^2\ ||\phi^{2j}||$$

or

$$||\Delta C(d,q)|| \leq (q - d - 1)||V^{-1}||\ ||H||^2\ ||\phi^{2d}|| \tag{3-76}$$

Now as $d \to \infty$ the term $||\phi^{2d}||$ approaches zero, thus the left-hand side of the inequality in equation (3-76) vanishes as $d \to \infty$. Therefore $||\Delta C(d,q)|| \to 0$ as $d \to \infty$ which proves that the sequence $\left\{C_2(1), C_2(2), \ldots, C_2(d)\right\}$ forms a convergent Cauchy sequence. This result indicates that δ^2 (eq. (3-69)) for state-jump failure approaches a constant limit as $d \to \infty$. Hence, the probability of correct detection for state-jump failure does not change after d becomes sufficiently large. This also has the implication that the estimate of the failure vector will not significantly improve after $C_2(d)$ has reached its limit. As Chow (Ref. 3) suggests the rate of convergence of $C(d)$ to its limit may be used in establishing the length of window $N \leq d \leq M$ for detection. That is, the value of M can be selected based on how fast the corresponding $C_1(d)$ approaches its limit. Next the asymptotic behavior of $C_1(d)$ matrix for sensor-step failures will be developed.

3. Sensor-Step Failure

In order to study the asymptotic behavior of the $C_1(d)$ matrix for sensor-step failures consider the formulation of $C_1(d)$ for this type of failure (initially derived in eq. (2-79)):

$$C_3(d) = (d + 1)V^{-1} \tag{3-77}$$

It can easily be seen from equation (3-77) that as $d \to \infty$, the elements of $C_3(d)$ will grow. Therefore, at least some of the eigenvalues of $C_3(d)$ will increase as $d \to \infty$. This has the implication that for actual failures in the direction of eigenvectors corresponding to growing eigenvalues the probability of correct detection improves as $d \to \infty$.

Also the accuracy of the estimate of a failure vector, $\hat{\nu}$, improves as $d \to \infty$ because $C_1^{-1}(d)$, the covariance matrix of $\hat{\nu}$, becomes smaller as $d \to \infty$. This can be easily verified by computing $C_3^{-1}(d)$ from equation (3-77) as

$$C_3^{-1}(d) = \frac{1}{d+1} V \tag{3-78}$$

Another important conclusion which follows from equation (3-78) is that if the variances of the residuals are large then more observations are needed to improve the estimate of the failure vector, $\hat{\nu}$.

3.7 Summary and Discussion

The results developed in this chapter can be summarized under three main topics. These topics are the probability distribution of the GLR index, failure detectability, and the asymptotic behavior of the $C_1(d)$ matrix. The probability distribution of the GLR index was determined to be a noncentral chi-squared when a failure actually occurs. On the other hand when no failure has occurred the probability distribution of the GLR index is a central chi-squared distribution. It was established that when the direction and magnitude of the failure vector is restricted to a known vector, ν_o, the simplified GLR index will be distributed as a Gaussian random variable. Identifying the distribution of the GLR index leads to the calculation of four important detection probabilities. These detection probabilities are probability of correct detection, false alarm, cross detection, and wrong-time detection. Calculation of these probabilities furnishes a guideline for selection of a threshold for GLR decision rule. For instance by utilizing the probability of false alarm a threshold can be selected such that a low number of false alarms would result.

Another major utility of the detection probabilities is that they offer a way of evaluating the performance of the GLR detector. In this regard, the probability of correct detection provides a measure of confidence in the overall result of detection and isolation while false alarm probability gives an indication of the consistency of the detector. The probability of cross detection can be used to evaluate the isolation capability of the detector and the probability of wrong-time detection offers a way of measuring the accuracy of the failure time estimate.

After identifying various probabilities associated with the GLR technique, it is essential to determine what failures can be detected. It was established that the detectability of a failure is dependent on the invertability of the $C_i(k,t)$ matrix. Based on this result it was shown that sensor-step failures are always detectable. For the time-invariant systems detectability of actuator failures is related to system observability and failures which fall into the unobservable subspace are not detectable. In addition it was shown that if $C_i(d)$ for actuator failures is not invertible in $n - 1$ steps then it will never be invertible.

Failure detectability can also be examined by comparing the probabilities of correct detection and false alarm. It was shown in Section 3.3 that the noncentrality parameter, δ^2, for false alarm is zero. However, the noncentrality parameter for correct detection is nonzero and is given by

$$\delta^2 = \nu^T C_i(k,t)\nu \tag{3-79}$$

Now if $C_i(k,t)$ has an eigenvalue which is very close to zero then any

failure along the eigenvector corresponding to the small eigenvalue drives δ^2 close to zero. Thus the probability of correct detection becomes very close to the probability of false alarm. This confirms the previous result that if the $C_i(k,t)$ is not invertible (i.e., $C_i(k,t)$ has at least one zero eigenvalue) then not all failures are detectable. From a similar argument it can be concluded that the probability of correct detection of failure vectors lying in the direction of eigenvectors corresponding to large eigenvalues is higher. It follows from the above discussion that $C_i(d)$ plays an important role in successful detection of a failure. Since $C_i(d)$ is a function of the number of residuals observed then it is important to study its behavior as more observations are taken.

The significance of studying the asymptotic behavior of $C_i(d)$ matrix is twofold. First, the invertibility of $C_i(d)$ determines the detectability of failures. The second reason for such study is that the $C_i^{-1}(d)$ is the covariance matrix of the estimate of the failure vector, hence it is a measure of the estimate accuracy. The results of studying the asymptotic behavior of $C_i(d)$ for the three modes of failure are as follows. For state-step and sensor-step failures $C_i(d)$ will have some eigenvalues which grow as $d \to \infty$. On the other hand $C_i(d)$ for state-jump failures converges to a constant matrix. Thus the corresponding GLR index, $L_i(k,t)$, will also approach a constant value.

The elements of $C_i(d)$ for sensor-step failure (eq. (3-77)) grow as $d \to \infty$; hence both the failure detection probability and the accuracy of the failure vector estimate improve as $d \to \infty$. If $C_i(d)$ in this case is a diagonal matrix then $C_i^{-1}(d)$ is also a diagonal matrix which implies that the elements of the failure vector estimate are

mutually independent. This is a desirable feature of the proposed detection technique because the estimate of each sensor failure is not affected by a failure in another sensor. This facilitates the isolation of failed sensors as they are associated with the elements of the failure vector which are significantly different from zero.

The study of the statistical properties of the proposed GLR technique provides substantial information regarding the reliability of the detection and isolation. Furthermore, a simple condition for detectability of failures can be established and finally the study of asymptotic behavior of $C_i(d)$ furnishes a guideline for the necessary number of observations. In the next Chapter the application of the proposed detection technique to a jet engine will be presented.

CHAPTER IV

PERFORMANCE EVALUATION OF GLR TECHNIQUE

In this chapter the application of the proposed GLR detection technique to sensor/actuator failures in a turbofan jet engine will be presented. The objective is to evaluate the performance of the technique when it is applied to a realistic problem. The study provides more insight into the problems and capabilities associated with the on-line implementation of the technique. This study is performed by simulating the sensor/actuator failures of a jet engine in a nonlinear digital simulation of the engine. Then the effect of sensor/actuator failures on the output measurements is used in the GLR detection routine to detect and isolate the failures.

The description of this study and the associated results are presented in the following order. In Section 4.1 a brief description of the engine and the nonlinear simulation is given. In Section 4.2 the digital simulation of the sensor/actuator failures is described. Then in Section 4.3 the performance of the GLR technique is tested by utilizing the digital simulation program. The results of Section 4.3 are based on using the full-scale nonlinear engine simulation as the engine model (Fig. 3.2) for generating model residuals. To evaluate the effect of model accuracy, in Section 4.4 the nonlinear simulation is replaced with a linear engine model derived from the nonlinear simulation. Finally in Section 4.5 a summary and discussion of the chapter is presented.

4.1 Turbofan Jet Engine

A turbofan jet engine developed by General Electric Company under

contract to the National Aeronautics and Space Administration was selected for the application of the proposed GLR technique. The engine is referred to as Quiet Clean Short-Haul Experimental Engine, QCSEE. Two models of QCSEE for Over The Wing (OTW) and Under The Wing (UTW) utilization were developed. For the purpose of this study the UTW model was used. A schematic diagram of the UTW model is given in Figure 4.1.

The fundamental objective of the QCSEE development has been to develop an advanced engine for short-haul commercial aircraft having Short-Takeoff-Or-Landing (STOL) capability and producing less noise and atmospheric pollution than current aircraft. Another specific technical objective of the QCSEE program was to develop a digital control system for the engine to be evaluated in a simulated flight environment. To achieve these objectives, a turbofan jet with special design features evolved. Some of these design features are: a composite high Mach inlet; a variable-pitch fan with composite blades; a variable geometry exhaust nozzle; an advanced core and low pressure turbine; and a treated fan duct with an acoustic splitter. Also a digital control system was designed and incorporated in the engine to perform the overall engine computation and evaluate the engine command. The digital control monitors the engine sensors and generates signals for manipulating fuel flow, fan pitch angle, and fan nozzle area. Fault indication and corrective action is also incorporated in the digital control system.

As it was discussed in Chapter 1, the detection techniques using analytical redundancy are mainly suitable for engines with digital control systems. Since QCSEE provides a digital control system it is an appropriate choice for the performance evaluation of the proposed detection technique. In addition the sensors and actuators of QCSEE are de-

signed to be compatible with the digital control, therefore the corresponding failure study will be realistic and applicable.

QCSEE has four input controls which can be used to control the engine response. These input controls are fuel flow, fan nozzle area, fan pitch angle, and compressor stator position. The compressor stator position is controlled indirectly by the hydromechanical control backup system; hence, it is not used for this study. The fuel flow to the combustor is controlled by an electrohydraulic servovalve. The fan nozzle actuator adjusts the position of four interlocking flaps of the nozzle as a function of flow and pressure from an electrohydraulic servovalve. For the variable-pitch fan the actuator is a ball-spline system. The mechanical rotation for this system is provided by a hydromechanical motor. The digital control corrects the position of the blades by sending a signal to the servovalve controlling the fluid flow to the hydromechanical motor.

Engine sensors are designed to be compatible with the digital control system. Pressure, temperature, and speed sensors are utilized in QCSEE. Three types of temperature sensors are utilized. A thermocouple is used to measure the compressor discharge temperature and a platinum wire-wound resistance-type device is used to monitor the fan inlet temperature. To measure the core engine inlet temperature a zirconium gas-filled coil is used. Application of different temperature sensors is based on the range, response time, accuracy, and sensitivity of the sensor. For measuring fan speed a magnetic pickup system is used while for compressor speed voltage from alternator windings is employed. All absolute and relative pressures in the engine are monitored by thin-film strain gauge bridge transducers. More detailed information re-

garding QCSEE sensors and actuators is available in reference 48.

4.1.1 QCSEE Simulati :

In order to evalute the performance of QCSEE, NASA initiated a program for studying QCSEE performance in a STOL flight environment. A manned flight simulator was used to study engine performance. Details of the QCSEE simulation program and some results of the flight simulation program are given in reference 49. A main requirement of this program was a reasonably detailed engine simulation which would provide realistic engine response with acceptable execution time. For this simulation study a digital QCSEE simulation was selected. The execution time for QCSEE simulation must be such that the overall flight simulation could be accomplished in real time. To meet the time requirement, the high frequency elements of the engine were not included in the development of the simulation for the engine.

The simulation was derived from the real QCSEE propulsion system. This simulation represents the engine and control system dynamics. Since the high frequency elements were excluded, only rotor dynamics and compressor and turbine capacitances are included. To represent accurately the operation of the high Mach inlet engine all major engine components for the bypass duct and core are included in the model. Inlet throat and duct performance are also included in the model. Similarly, the fan and compressor are modeled using pressure and temperature ratio maps. The combustor was modeled by relations which include pressure drop and heat rise. Combustor dynamics were not included. The engine turbines were represented by flow and enthalpy drop maps as functions of pressure ratio and corrected speed.

The simulation of QCSEE engine control consisted of two parts,

digital and hydromechanical controls. In the digital part the fan speed, inlet Mach number, and engine pressure ratio controls were modeled. The hydromechanical segment represented core speed, acceleration, and deceleration controls.

The simulation had four engine states, four iterative loops. four control sensor states, and four actuator states. For programming the model, a computationally efficient curve fitting technique was used to represent various multivariable functions. Model dynamic equations were solved using a modified Euler integration technique. The resulting digital engine simulation program is accurate, stable, and runs faster than real time.

The QCSEE digital simulation model was selected to be used in evaluation of the performance of the proposed GLR failure detection technique. Specifically, two duplicates of the simulation program were employed to represent the actual engine and the engine model (see Fig. 4.3). Then sensor/actuator failures were introduced in the program representing the engine and the resulting residuals were tested for failure. Although the proposed GLR technique is developed for linear systems, using nonlinear models of the engine provides a more realistic measure of the GLR performance. Following this evaluation, the nonlinear simulation program representing the model of the engine was replaced with a linear model of the engine. These simulation studies provide a measure of the effects of model inaccuracies on failure detection. The proposed GLR technique, however, requires a linear state space representation of QCSEE. The derivation of the state space matrices for QCSEE is discussed in the next section.

4.1.2 QCSEE Linear Model

For evaluating the performance of the GLR technique a linear state space model representation of QCSEE at the 62.5% engine power level was generated. The linear model was generated from the QCSEE digital simulation and is briefly described in this section.

Consider the schematic diagram of the QCSEE engine in Figure 4.2. In order to develop a linear model it is necessary to select the engine states. The following engine variables were selected as engine states:

P12 - Fan inlet duct total pressure

P13 - Fan discharge total pressure

P4 - Compressor discharge pressure

P8 - Core nozzle total pressure

NL - Fan speed

NH - Compressor speed

T3 - Compressor discharge temperature

T4 - Combustor discharge temperature

Three inputs are given as follows:

XMV - Fuel metering valve setting

X18 - Fan nozzle area actuator position

THETAI - Fan pitch mechanism drive motor position

The set of output variables includes different types of measurements:

PS11 - Engine inlet static pressure

P13 - Fan discharge total pressure

P4 - Combustor pressure

P8 - Core nozzle total pressure

NL - Fan rotor speed

NH - Compressor speed

T41C - Calculated turbine temperature

FN - Net thrust

Based on the above selection of state variables and the given input-output variables, a linear model of the engine using a small signal perturbation technique is developed (Ref. 47). The corresponding A, B, C, and D matrices for the linear model representing a 62.5% power level condition are presented in Appendix E. The dynamics of the engine control are not included in the linear model because only the detection of engine sensor or actuator failure is of interest.

To develop the GLR detectors for QCSEE it is necessary to discretize the system matrix, A, of the linear model. This is accomplished by using standard discretization techniques (see, e.g., Ref. 53). The computation of the discrete system matrix, ϕ, completes the essential information for the development of the GLR detection program. Utilizing the detection program, the performance of the GLR technique will be evaluated by failure simulations. The failure simulations will be discussed in the next section.

4.2 GLR Simulation Program

In this section a description of the digital simulation program for evaluating the performance of the GLR detection technique is presented. In the first part two duplicates of the nonlinear QCSEE simulation program are used to represent the engine and the model of the engine as shown in Figure 4.3. The objective in this part is to evaluate the performance of the detection technique when the model follows the engine perfectly. Sensor/actuator failures in this case are simulated in the program representing the engine. In the second part the nonlinear QCSEE simulation program representing the engine model is replaced with

the linear model described in Section 4.1.2. This will result in a discrepancy between the engine output and the linear model as the model does not follow the engine perfectly. Thus this study will provide insights into the effect of the degree of model accuracy on the behavior of the GLR detectors. The configuration for this simulation is illustrated in Figure 4.4.

4.2.1 Failure Simulation Under Perfect Modeling

Consider the GLR simulation arrangement in Figure 4.3. Three main elements of this configuration are the two nonlinear QCSEE digital simulations and the GLR detection program. The nonlinear QCSEE simulations represent the engine and the engine model. The inputs to both the engine and engine model are the same. These inputs are: fuel metering valve position, XMV; fan nozzle actuator position, X18; and fan pitch mechanism. As it is shown in Figure 4.3, the outputs of the engine model are subtracted from those of the engine to compute the model residual. The six output selected for residual calculations are:

PS11 - Engine inlet static pressure

NL - Fan rotor speed

NH - Compressor speed

P12 - Fan inlet duct total pressure

P4 - Combustor pressure

P8 - Core nozzle pressure

The residuals computed from the above outputs are transmitted to the GLR detection program for sensor/actuator failure detection.

Using identical QCSEE digital simulations for the engine and engine model representations allows studying the performance of GLR in the presence of perfect modeling. In this case when no failure has occurred

the difference between the engine output and the model output is the engine sensor noise. The QCSEE simulation program does not incorporate the engine sensor noise. Therefore to generate realistic engine outputs, the sensor noise characteristics must be added to the outputs of the QCSEE program representing the engine.

4.2.2 QCSEE Sensor Noise Characteristics

Due to the unavailability of QCSEE sensor noise characteristics the noise characteristics of an F-100 engine were used. This is justified on the basis that comparable sensors are used for pressure, speed, and temperature measurements in the QCSEE and the F-100 engines. Thus actual sensor measurements from an F-100 jet engine altitude test (Ref. 22) were utilized to compute the sensor noise characteristics. For this purpose, 100 samples of engine pressure, temperature, and speed measurements were used to calculate the variance for the three types of sensors. This process was repeated for two engine operating points and the resulting variances were averaged over the two points. The sensor variances computed in this fashion are the elements of the diagonal sensor noise covariance matrix which is shown in Appendix F.

Using the computed noise covariance matrix, zero mean independent Gaussian variables were generated and were added to the output of the QCSEE simulation representing the engine. Addition of the noise to the engine output, completes the measures necessary for computing the residuals required by the GLR detection program.

4.2.3 GLR Detection Program

The GLR detection program is designed to detect failures in time-invariant systems. The program is not restricted to QCSEE applications and can be utilized for any time-invariant system.

The inputs to the GLR detection program are: the discrete system matrix ϕ; the output matrix H; the model residual vector sequence r(k); residual variance V; the input and output dimensions of the system; the failure threshold ε; the first detection test observation number; the failure time sliding window limits M and N; and the maximum number of residuals. In addition the number of observation at which the first detection test is to be performed should also be specified in the program. The logical structure of the GLR program is divided into three parts. In the first part the matrices $G_i(d)$ and $C_i(d)$ (see Table 3.2) for the three failure types are computed and stored. Since these matrices remain unchanged they may be computed and stored off line and then retrieved for GLR computations. In the second part the GLR indices, $L_i(k,t)$, (Table 3.2) for the three failure types, i, and for all possible values of failure time, t, inside the interval $k - M \leq t \leq k - N$ are calculated. Then, for each type of failure, $L_i(k,t)$ is maximized over the values of t. These maximum values of the GLR indices are compared with each other and the largest value is selected. This two-step maximization for the failure type, i, (i = 1,2,3) and the failure time, t, ($k - M \leq t \leq k - N$) can be expressed as

$$L_{\hat{i}}^{*}(k,\hat{t}) = \left[\max_{i} \max_{t} L_i(k,t)\right] \tag{4.1}$$

If the maximum GLR index computed in this fashion exceeds the threshold ε then the program declares a failure of type $\hat{i}$ at time $\hat{t}$. The threshold ε is chosen such that the probability of false alarm will be less than 0.001. Since the false alarm probability is distributed

as a central chi-squares, then ε can be selected directly from the chi-squared distribution tables (e.g., see Ref. 46). For the QCSEE simulation there are six output residuals, therefore there will be six degrees of freedom associated with the GLR index. The threshold was selected approximately twice the average of the maximum GLR index under a no-failure condition, or $\varepsilon = 34$. For six degrees of freedom this results in a false alarm probability of less than 0.001 for each of the three GLR detectors.

Finally, in the last part of the program the estimate of the failure vector, ν, is computed and sensor failure isolation is accomplished. The calculation of the estimate of the failure vector is achieved by employing the maximum likelihood estimator for ν in equation (3-32). Sensor failure isolation calculation logic is derived from the constrained GLR (CGLR) technique which was described in Section 3.3.3. Specifically, a set of vectors are associated with possible sensor failures. Each vector in this set has all zero elements except unity at the position corresponding to the failed sensor. In the QCSEE simulation, for single failure isolation the vector set contains six vectors of dimension 6. As an example the failure vector associated with the fourth sensor has the form of:

$$f_4 = \begin{pmatrix} 0 \\ 0 \\ 0 \\ 1 \\ 0 \\ 0 \end{pmatrix} \qquad (4.2)$$

Application of CGLR leads to selection of the vector associated with the failed sensor and thus isolates the failed sensor. The detection deci-

sion rule for CGLR is derived as follows. The CGLR indices for sensor-step failure are computed from equation (3-37) and maximized with respect to failure time, t, and constrained vector directions, f_j. The maximum value of CGLR selected in this fashion is compared with threshold ϵ for failure detection. This comparison can be used as a cross check for the detection results of GLR. At the same time, the failure vector direction associated with the maximum value of the CGLR is utilized to isolate the failed sensor. The failure time, t, associated with the maximum value of CGLR can also be used as a cross check for the estimate of failure time, $\hat{t}$, which is computed in the second part of the program. A flow diagram of the complete program logic is given in Figure 4.5.

4.3 GLR Performance Tests

To evaluate the performance of the proposed GLR technique for the case of perfect modeling three categories of failure simulation tests were performed: (1) No failure, (2) Single sensor or actuator failure, and (3) Multiple sensor/actuator failure. The no-failure tests evaluate the consistency of the detection technique and establish a baseline of performance.

4.3.1 Consistency Test

The consistency of the GLR technique is tested by applying the GLR technique to model residuals when no failure has occurred. For this purpose two noise sequences for the six sensors of QCSEE are generated by utilizing the same covariance matrix (given in Appendix F) but with two different seed numbers. Then two consistency test runs are made by employing these noise sequences. For each run, the noise sequence is added to the output of the QCSEE program representing the engine (Fig. 4.3). Then without inducing any failure in the engine the model

residuals are computed. It should be mentioned that in this case the model residuals are identical to the output sensor noise. Since no failure has occurred the GLR indices over the sliding detection window must be smaller than the threshold ($\varepsilon = 34$). Application of the GLR technique to the model residuals in this case yields the expected results. That is the maximum GLR index, $L_i^*(k,\hat{t})$, is substantially smaller than the threshold ε. These results are shown in Figures 4.6 and 4.7. In each of these figures the maximum GLR index, $L_i^*(k,\hat{t})$, is plotted versus the observation time, k. The limits of the sliding window in this case are $N = 3$ and $M = 13$ and the total number of observations is $k = 30$. The length of sampling interval for this test and all the subsequent tests is 0.08 second. Figures 4.6 and 4.7 are useful in providing more insight into the relationship between the probability of false alarm and the selected value of the threshold, ε. For example consider Figure 4.6, it can be seen from this figure that for $\varepsilon < 18$ there will be at least one false alarm. The probability of false alarm for $\varepsilon = 18.0$ is approximately 0.0065 which is 6.5 times larger than the probability of false alarm when $\varepsilon = 34$. Finally, the plots of the GLR indices in Figures 4.6 and 4.7 indicate that the GLR results are highly consistent. Next the capability of the GLR technique in detecting single sensor failures will be examined in the following section.

4.3.2 Single Sensor Failure Tests (Using Sensor Set A)

In this category of tests performance of the GLR (under a perfect modeling assumption) in detecting a single sensor/actuator failure is studied. For the single sensor failure study a step failure is introduced in each sensor separately. The magnitude of the failure for all sensor failure simulations was selected to be larger than the tolerable

sensor inaccuracies (normally three standard deviations of the sensor noise). Specifically, the failure size was selected to be equal to five standard deviations of the noise. Then, the failure sizes in pressure, speed, and temperature sensors are, respectively, 0.5%, 0.19%, and 0.55% of the nominal value of the corresponding sensor measurements. The normalized covariance matrix for sensor noise and the nominal values are given in Appendix F.

Two distinct groups of single sensor failure tests are performed. For this purpose two sets of sensors are utilized, namely set A and set B. Each set contains six sensors. Specifically, the sensors in set A are the same as in Section 4.2.1. The sensors in set B are the same as in set A except P8 is replaced with T3. The results of single sensor failure tests using set A are given in Table 4.1. The actual failure time for the results in Table 4.1 is at the fifth (5) observation and the window limits for failure time are $M = 23$ and $N = 3$. The total number of observations in these runs is 30 and the first detection test is performed at the tenth (10) observation. The time of the first detection test was selected somewhat arbitrarily. The results in table 4.1 indicate that all of the sensor failures are properly detected and the failure times are correctly estimated. Also the isolation of the failed sensors in all six runs is successfully achieved. The estimate of the failure time computed from the CGLR section of the program is in agreement with the estimate from the GLR detection calculation.

The estimate of failure size for two typical output sensors, namely PS11 and NL, are plotted in Figures 4.8 and 4.9. These plots indicate that the estimate of failure size in both pressure and speed sensors are very close to the actual value of the failure size. It is shown in

TABLE 4.1

SIMULATION RESULTS FOR SINGLE SENSOR FAILURE

(Using Sensor Set A)

Sensors	PS11	NL	NH	P12	P4	P8
Detection						
Detected type	3	3	3	3	3	3
Detected failure time	5	5	5	5	5	5
Actual failure time	5	5	5	5	5	5
Isolation*	C	C	C	C	C	C
Failure time from isolation calculation	5	5	5	5	5	5
Simulation inputs	Number of outputs = 6 Initial detection test observation = 10 Total observations = 30 M = 23, N = 3 ϵ = 34					

*C is used to indicate correct isolation.

Appendix G that the accuracy of the failure size estimate improves as the number of observations increases. Examining the plots in Figures 4.8 and 4.9 reveals that as k becomes larger the estimates of failure size tend toward the actual values of failure sizes. The remaining difference between the estimates and the actual failure size is due to sensor noise characteristics. That is, if the mean of the noise sequence is not truely zero, then the estimate of failure size will not converge to the exact value of the failure size. This is shown to be true for all failure types in general in Appendix G.

4.3.3 Single Actuator Failure Tests (Using Sensor Set A)

In this section single actuator failure tests are discussed. The output sensor measurements utilized for these tests are the same as before, namely, P311, NL, NH, P12, P4, and P8. Likewise the threshold and the limits of the sliding window are unchanged. The failure size for actuator step failures is set to 5% of the nominal value of the actuator input at 62.5% power level (these nominal values are given in Appendix F). For jump failures, the failure size is selected to be equal to 20% of the nominal input values. The jump and step failures in the fan nozzle actuators are induced in the negative direction because the fan nozzle area at 62.5% power level is fully open (i.e., the nominal value for X18 is the same as the maximum value of X18).

The results of the single actuator failure runs are presented in Table 4.2. Each column of this table represents a simulation run. The results in this table indicate that the GLR technique has detected the failure type properly. Multiple estimates of the failure time for step failure in X18 and THETAI resulted. The evolution of these failure

TABLE 4.2

SIMULATION RESULTS FOR SINGLE ACTUATOR FAILURE

(Using Sensor Set A)

	Step failure			Jump failure		
Actuators	XMV	X18	THETAI	XMV	X18	THETAI
Detection						
Detected type	1	1	1	2	2	2
Actual failure time	5	5	5	5	5	5
Detected failure time	5	5 6 7	4 5 6	5	5	5
Simulation inputs	Number of outputs = 6 First detection test observation number = 10 Total observations = 30 M = 23, N = 3 ε = 34					

time estimates are plotted in Figures 4.10 and 4.11, respectively.

4.3.4 Single Sensor Failure Tests (Using Sensor Set B)

The second group of single failure simulation runs are made using sensor set B. Specifically, the core nozzle pressure, P8, is replaced with the compressor discharge temperature, T3. The reasons for replacing this output are as follows. The GLR detection technique utilizes the effect of sensor/actuator failures on the residuals for detection. Since the effect of actuator failures on various outputs is different then the GLR response will be different depending on the outputs used to compute the model residuals. Another reason for replacing P8 with T3 is that in the first group no temperature sensor was included. Hence the new output set contains all three types of sensors, namely, pressure, temperature, and speed sensors.

For the simulations using sensor set B the first detection test is performed before the failure occurs. This is in contrast to the simulation tests using sensor set A in Section 4.3.3. In that section the first detection test was performed after the failure occurs. This change in the time of the first detection test provides more information about the performance of the technique. One such extra measure of performance is to count the number of observations (after the failure occurs) required until one of the GLR indices exceeds the threshold, ϵ. This is referred to as "time to detection." In situations when no information about the type of failure is available (i.e., any of the three failure types are possible) another measure of performance can be defined as "time to correct type." This measure is defined as the total number of observations (after the occurrence of the failure) until the

GLR program identifies the correct type of failure. To describe the concept of these performance measures consider the plots of maximum GLR indices for a hypothetical sensor failure in Figure 4.12. The first detection test is performed at the fifth (5) observation while the sensor failure occurs at the tenth (10) observation. However, it can be seen that none of the GLR indices exceeds the threshold until the thirteenth (13) observation. Thus the time to detection for this example is three. It can be seen from the figure that the GLR index corresponding to state-step failure continues to be the largest index until the sixteenth (16) observation. Then at the sixteenth (16) observation the GLR index corresponding to correct failure type (sensor step) becomes the largest index. Therefore, the time to correct type is 6. Now assume that the failure time is still not estimated correctly (as 10) and will not be until the eighteenth (18) observations. Hence the total detection time is 8. It is noted that these performance measures are defined to be compatible with the GLR decision rule which was described in Section 4.2.3. It is possible, however, that these measures of performance be defined differently. For example, the time to detection may be defined as the total number of observations before the GLR index corresponding to the actual failure type exceeds the threshold ε (rather than any of the three indices).

Simulation results for single sensor failures of this set of outputs are given in Table 4.3. As in the previous case each column in the table represents one simulation run. All failures in this group are detected properly and the isolation of the failed sensors is also achieved successfully. Two measures of GLR response time, namely time to detection and time to correct type are also shown in the table. It

TABLE 4.3

SIMULATION RESULTS FOR SINGLE SENSOR FAILURE

(Using Sensor Set B)

Sensors	PS11	NL	NH	P12	P4	T3
Detection						
Detected type	3	3	3	3	3	3
Detected failure time	10	10	10	10	10	10
Actual failure time	10	10	10	10	10	10
Isolation*	C	C	C	C	C	C
Failure time from isolation calculations	10	10	10	10	10	10
Time to detection	0	1	0	2	2	2
Time to correct type	2	9	4	2	3	4
Total detection time	3	9	4	3	3	4
Simulation inputs	Number of outputs = 6 First detection test observation = 5 Total observations = 20 M = 23, N = 3 ε = 34					

*C indicates correct isolation.

follows from these results that all failures are detected in two observations or less. However, identifying the correct failure type requires more observations. The maximum time to correct detection of the failure type for the simulation tests in Table 4.3 is nine observation interval periods. Another useful measure of detection speed is total time required for correct identification of the failure type and time. In Table 4.3 and the subsequent tables this is referred to as: total detection time.

The evolution of the estimate of failure size, α, for PL11, NH, and T3 sensor failures is shown in Figures 4.13, 4.14, and 4.15, respectively. The observation number in these plots start with the time at which the failed sensor is properly identified. It should be noted, however, that the correct estimation of the failure time requires at least three observations after the failure occurs. This is due to setting the upper limit of the failure time window ($k - M \leq t \leq k - N$), N, to three. This delay can be better understood by examining the maximum GLR index, $L_{\hat{i}}^{*}(k,\hat{t})$, in equation (4-1). Note that the GLR indices are only computed and extremized over the values of t inside the window $k - M \leq t \leq k - N$. Now if a failure occurs at the current observation, k, the GLR index corresponding to this failure time will not be computed until N observations later. Therefore, the correct estimation of the failure time would not be possible until N observations later.

Plots of the maximum GLR index, $L_{\hat{i}}^{*}(k,\hat{t})$, corresponding to single sensor failure detection in PS11, NH, and T3 are plotted in Figures 4.16, 4.17, and 4.18, respectively. In these figures the values of $L_{\hat{i}}^{*}(k,\hat{t})$, from the first detection test at the fifth (5) observation are plotted. The time of the actual failure is marked with a vertical

dotted line and the value of threshold, $\epsilon = 34$, is shown by a horizontal solid line. The limits of the failure time window for these plots are $M = 23$ and $N = 3$.

It follows from the examination of these plots that as soon as the failure occurs the $L_i^*(k,\hat{t})$ starts to increase. This increase occurs even before the actual failure time enters the window. The reason for the rise in $L_i^*(k,\hat{t})$ is that while the calculation of $L_i^*(k,\hat{t})$ is restricted to the observations inside the sliding window, the residuals used in the calculation include the most recent observation. Hence as soon as the residual carrying the effects of a failure is encountered the $L_i^*(k,t)$ will rise. This GLR property is especially desirable when only the detection of a failure is of interest and the estimate of the failure time is not utilized.

The effect of the value of threshold on the time to detection can be examined from the plots of $L_i^*(k,\hat{t})$. Lower values of threshold, ϵ, yield faster detection of a failure in the system but increase the required number of observations (after the detection) for identifying the correct failure type. This may be easily verified from Figures 4.16 through 4.18. The increase in false alarm rate due to a low value of threshold, ϵ, can be assessed from the same figures. Specifically the values of $L_i^*(k,\hat{t})$ before a failure occurs can be compared with ϵ. Alternatively increasing the value of threshold delays the detection but reduces the rate of false alarm and improves the identification of correct failure type. Therefore, an alternative method of establishing the threshold, ϵ, is to use the time to detection as a criteria. Care should be exercised in using this criteria as fast detection increases the rate of false alarm.

4.3.5 Single Actuator Failure Tests (Using Sensor Set B)

Corresponding to the set B of output sensors (i.e., PS11, NL, NH, P12, P4, and T3) a series of single actuator failure simulation runs are made. The results of these runs are summarized in Table 4.4. Two modes of failures are simulated in each actuator. The step failure size is selected to be 5% of the nominal value of the corresponding input at 62.5% power level. For the actuator jumps the failure size is selected to be 20% of the nominal value of the inputs. For X18 the failures are introduced by subtracting the failure size from the input while for the other two actuators the respective failure sizes are added to the inputs. The failures are introduced at the thirteenth (13) observation and the first failure detection test is made on the tenth (10) observation. A total of 30 observations are tested. The failure time window limits at $N = 3$ and $M = 23$ and the threshold ε is kept at 34. It is remarked that the value of N assures the invertibility of $C_i(d)$ matrix and the value of M provides a reasonable range for $C_i(d)$ convergence (see Sections 3.5 and 3.6).

The results in Table 4.4 indicate that all failures are properly identified and the failure time is estimated with good accuracy. The estimates of failure time for all jump failures are correctly determined while failure time estimates for step failures are accurate to one observation. Also the results in Table 4.4 reveal that actuator failures are detected immediately following the failures. Identifying correct failure type, however, requires more observations after the failure occurs. The maximum number of observations required for identifying the correct failure type is eight observation intervals. Alternatively, determination of the correct failure time requires at least three obser-

TABLE 4.4

SIMULATION RESULTS FOR SINGLE ACTUATOR FAILURE

(Using Sensor Set B)

	Step failure			Jump failure		
Actuator	XMV	X18	THETAI	XMV	X18	THETAI
Detection						
Detected type	1	1	1	2	2	2
Actual failure time	13	13	13	13	13	13
Detected failure time	13	**12 13	12 13	13	13	13
Time to detection	0	0	0	0	0	0
Time to correct type	8	0	0	1	3	1
Total detection time	8	3	3	3	3	3
Simulation inputs	Number of outputs = 6 First detection test observation number = 10 Total observations = 30 M = 23, N = 3 ϵ = 34					

**Only at one observation point failure time estimate is 12.

vations because the upper limit of the failure-time window ($k - M \leq t \leq k - N$) N is three.

The evolution of the maximum GLR index, $L_i^*(k,\hat{t})$ corresponding to the step failure in XMV and jump failure in X18 are plotted in Figures 4.19 and 4.20, respectively. The values of $L_i^*(k,\hat{t})$ for actuator failures become very large after the failures occur. This is due to small value of the sensor noise variance as compared to the effect of the actuator failures on the model residuals.

The presentation of the results of single actuator failures corresponding to the second group of outputs concludes the simulation of single failures under a perfect modeling assumption (Fig. 4.3). In summary two sets of output sensors were selected and for each set three modes of failure were studied. In these simulations the failures were introduced separately in sensors and actuators. In the simulations corresponding to sensor set A (see Tables 4.1 and 4.2) the failure occurs prior to the first detection test and in the case of set B the failure occurs after the initial detection test. This provides insight into the behavior of the GLR for various failure times. In the next section detection of multiple failures will be explored. The objective is to evaluate the capability of the GLR technique in detecting multiple failures under perfect modeling.

4.3.6 Multiple Sensor Failure Simulation

During jet engine operation it is possible that two or more sensor/actuator failures will occur simultaneously. The occurrence of two or more simultaneous sensor/actuator failures is referred to as a multiple failure. It is logical to expect that the detection of multiple failures will be easier. The reason for such an expectation is as follows.

Any single sensor/actuator failure causes the mean of the residuals to deviate from zero. Thus the cumulative effects of multiple failures increase the deviation of the residual mean from zero further.

Although detection of multiple sensor failures may be easier, isolation of such failures poses a problem. This is true since the extension of the constrained GLR (CGLR) technique to the multiple failure case is not straightforward. This is due to the following reasons. The CGLR for single failure was derived by restricting the failure vector, ν, to αf_j where α is the failure size and f_j is the jth vector direction. When CGLR is employed for single sensor failure isolation, f_j has all zero elements except unity in the jth position (e.g., see eq. (4-2)). Therefore, for single failures the number of possible failure directions is equal to the number of sensors. But in the multiple failure case the number of possible failure directions can grow very rapidly. Another difficulty is the unequal size of failures in the failed sensors. That is, if the failure size is not the same in the failed sensors then the failure vector, ν, can not be represented by αf_j.

An alternative approach to the problem of multiple sensor isolation is to use the estimate of the failure vector (eq. (2-37)). The elements of failure vector estimate associated with the failed sensors are substantially different from zero. Thus the failed sensors can be isolated easily.

To evaluate the performance of the proposed GLR technique in a multiple failure application, multiple sensor failure simulation tests for QCSEE were performed. For these tests perfect modeling was assumed (Fig. 4.3) and several combinations of sensor failures involving

at least two or more sensors were simulated. To achieve the desired results multiple sensor failures were induced in the nonlinear simulation program representing the engine and the resulting residuals were fed into the detection program. Since in the development of the GLR program no assumptions regarding the maximum number of failed sensors was made the program can be directly utilized. It should be noted that in all cases the failures were introduced simultaneously. The results of these simulations are summarized in Table 4.5. The six sensors used to generate these results are PS11, NL, NH, P12, P4, and T3. The total number of observations for each run is 26. The magnitude of the failure in each failed sensor is five times the standard deviation of the corresponding noise sequence. The first detection test in all cases is performed at the tenth (10) observation. The limits of the window around the failure time are $N = 3$ and $M = 23$.

The results of Table 4.5 indicate that all multiple sensor failures are detected and the failure type is also identified successfully. For multiple failures which occur at the fifth (5) observation, the occurrence of the failure is detected immediately after the first detection test. For these failures total detection time reflects the number of observations from the first detection test until the time and type of the failure is correctly determined.

The values of the GLR index for multiple failure in PS11 and NL are plotted in Figure 4.21. Comparing this figure with Figure 4.22 (a single failure in PS11) reveals that the level of the GLR index for the multiple failure case is higher as was expected. It was remarked before that CGLR may not be applicable for isolation in the multiple failure case. It was also indicated that the estimate of the failure size

TABLE 4.5

MULTIPLE SENSOR FAILURE SIMULATION RESULTS

Sensor number	1,2	1,2,3	1,3,4,6	1,2,3,4,5	1,2,3,4,5,6
Detected type	3	3	3	3	3
Actual failure time	5	5	10	5	12
Detected failure time	5	5	10	5	12
Time to detection	---	---	0	---	0
Time to correct type	**1	**1	2	**0	2
Total detection time	**1	**1	3	**0	3
Sensors	PS11 = 1, NL = 2, NH = 3, P12 = 4, P4 = 5, T3 = 6				
Simulation inputs	Number of outputs = 6 First detection test performed at tenth observation Total number of observations = 26 Window limits M = 23, N = 3 ε = 34				

**Number of observations after the first detection test.

may be used for the multiple failure isolation. The vector ν (eq. (2-37)) provides an estimate of the failure size in the sensors corresponding to its various elements. Plot of these estimates for PS11, NH, and T3 when multiple failures in PS11, NH, P12, and T3 have occurred are shown in Figures 4.23 through 4.25, respectively.

An interesting observation can be made regarding these failures. It is evident that the estimate of the size of the failure in the speed sensor, NH, is more accurate than the estimates for PS11 and T3 sensors. The reasons for such a difference are as follows. It can be seen from the covariance matrix of the sensor noise sequences (see Appendix F) that the variance of the speed sensor is approximately 10 times smaller than the variance of the other sensors. Since this covariance matrix is used to generate the noise sequences for all three sensors, the pressure and temperature sensor residuals will have more inherent variation around the mean and thus a less accurate estimate of the failure sizes.

Alternatively, it is shown in Appendix G that the GLR estimate of the failure vector is unbiased. Therefore, as more observations are taken the estimate of the failure vector will approach the true failure vector. The rate by which the estimate will approach the true vector can be assessed by the variance of the failure vector estimate. It was shown in Appendix D that the covariance of the failure vector estimate is $C^{-1}(k,t)$. In the proposed GLR, $C^{-1}(k,t)$ has a simple form for sensor failures in time-invariant systems,

$$C_i^{-1}(d) = \frac{1}{d+1} V \qquad (4-3)$$

Equation (4-3) was originally derived in Chapter II (eq. (2-79)). It

follows from equation (4-3) that as $d = k - t$ grows the variation in the failure vector estimate will be reduced. Since in this case V, the covariance matrix of sensor noise sequences, is diagonal the rate of convergence of each element in the estimate vector is independent of the other elements. The rate of convergence for each element, however, is dependent on the noise variance of the corresponding sensor. Hence the convergence for sensors with smaller noise variances will be faster. Specifically, the estimate of the failure size in NH will converge approximately 10 times faster than the estimates for PL11 and T3.

4.3.7 Multiple Actuator Failure Simulation

The capability of the proposed GLR detection technique for detecting multiple actuator failures was also tested by simulation. For this purpose both multiple jump and multiple step actuator failures were simulated. The results of these simulation runs are summarized in Table 4.6. In each case the magnitude of the failure is equal to 5% of the nominal value of the corresponding actuators. The failures are introduced simultaneously and the resulting residuals are passed to the detection program. Perfect modeling is assumed (i.e., configuration of Fig. 4.7) and a total of 26 residual observations are examined for failure detection. The failure time window limits are $N = 3$ and $M = 23$. The outputs used to generate the residuals are PS11, NL, NH, P12, P4, and T3. The first detection test is performed at the tenth (10) observation and the corresponding threshold is the same as before, namely $\varepsilon = 34$.

The results in Table 4.6 indicate that all failures are detected and the correct type of failure is identified. The detection and identification of the failures in all cases requires five (5) or less

TABLE 4.6

SIMULATION RESULTS FOR MULTIPLE ACTUATOR FAILURES

Failed actuators	XMV X18	XMV X18 THETAI	XMV X18	XMV X18 THETAI
Detected type	1	1	2	2
Detected failure time	10	10	10	10, *12, *13
Actual failure time	10	10	10	10
Time to detection	0	0	0	0
Time to correct type	1	1	5	0
Total detection time	3	3	5	3

*Indicated as failure time only once in 17 estimates computed.

observations. The correct estimate of the failure time is obtained in all cases except when jump failures are induced in all three actuators. In this case, however, each of the two wrong estimates occurs only once in the total of 17 GLR tests performed.

To illustrate the increase in magnitude of the GLR index for multiple actuator failures, plots of $L_j^*(k,\hat{t})$ for step and jump failures in XMV, X18, and THETAI are plotted in Figures 4.26 and 4.27, respectively. Comparing these figures with Figures 4.19 and 4.20, respectively, confirms that the values of $L_i^*(k,\hat{t})$ for multiple failures are higher than $L_i^*(k,\hat{t})$ for a single failure.

This completes the study of GLR performance under a perfect modeling assumption. The results can be summarized in two parts. First, single failures were simulated in sensors and actuators separately. Two different sets of output sensors were tested. Second, multiple failures were simulated to assess the capability of the proposed GLR technique in detecting multiple failures.

The overall results of all simulations indicate excellent GLR performance. Failures were detected in all cases and the proper failure types were determined. Specifically, for sensor failures not only were failures detected and isolated properly in all cases but also failure times were estimated without any error. However, for step failures in X18 and THETAI (and for multiple failures involving these actuators) small inaccuracies in estimating the time of the failure are encountered. It should be noted that the proposed GLR technique is developed for linear systems but the residuals used in the above cases are generated from nonlinear engine models. Although such an arrangement represents a realistic situation in which the proposed GLR technique is applied

to the jet engine, the results will not be perfect because of the nonlinearity of the residuals. Hence, the inaccuracies in the estimate of the failure time is attributed to these nonlinear effects in the residuals.

The main restriction in the above simulations was that the engine model follows the engine perfectly. In the next section a linear model is employed to replace the nonlinear simulation representing the engine model in Figure 4.3. The resulting configuration will be identical to Figure 4.4. The objective will be to evaluate the effect of model degradation on the overall performance of the GLR technique, specifically when a linearized model of the engine is used to generate the residual. Since the linear model does not follow the engine exactly, the discrepancy between the simulation model and the linearized model can be viewed as model degradation.

The study of the effect of model inaccuracies on the performance of the GLR tests is also useful because storage requirements and the overall computation time requirements for an on-line GLR detection may often be severe. Since a complete simulation of the engine often requires large storage and high computation time, a simplified engine model can be used to reduce computational requirements. A linear model of the engine is one of the simplest forms of the engine model. The linear model will not model the engine perfectly however. Thus, it is important to investigate the impact of these modeling errors on the performance of the GLR technique.

4.4 GLR Simulation with Model Degradation

In this section the effect of model degradation on the performance of the GLR technique is studied. For this purpose the nonlinear simula-

tion program representing the engine model is replaced by a linear state space model of the engine. Specifically the simulation results of this section are generated from a configuration identical to the configuration in Figure 4.4. The linear model used in this configuration is generated from the QCSEE nonlinear simulation (see Appendix E). Since the linear engine model does not follow the nonlinear simulation of QCSEE perfectly, the discrepancy between the model and the simulation can be viewed as the model degradation.

To study the performance of the proposed GLR under model degradation, single and multiple sensor/actuator failures were simulated using the linear model. However, the model residuals calculated by subtracting the linear model output from the output of the nonlinear simulation model are no longer zero mean white Gaussian. This is due to the discrepancy between the linear model and nonlinear simulation of the engine. In this case application of the proposed GLR detection technique to the model residuals (when no failure has occurred) resulted in declaring a failure. This occurs because the bias in the residuals caused by modeling inaccuracies is indistinguishable from the bias due to a sensor failure. Therefore, for studying the performance of the GLR under model degradation, the sensitivity of the detection technique to the model discrepancies should be reduced.

The sensitivity of the detection technique can be reduced by two methods. The first approach is to increase the value of threshold to a level that GLR indices computed from the model residuals with no failure would not exceed the threshold. This approach, while simple, is not always desirable because it is difficult to establish a guideline for increasing the level of threshold, c. Specifically, it is difficult

to establish a level for ϵ which will reduce the sensitivity of the detection technique uniformly. That is, when the level of threshold is raised then the GLR corresponding to output sensors which have higher discrepancies will exceed the threshold faster than the sensors with lower discrepancies. If the effect (magnitude) of model degradation is approximately the same in all outputs then of course this approach can be utilized.

The second approach is to increase the elements of the covariance matrix artificially. That is, to enter a covariance matrix for model residuals into the detection program that has larger elements than the true covariance of the residuals. This method is more attractive than the previous approach because each element of the covariance matrix may be increased individually. Changing individual elements of the covariance matrix allows compensation of different levels of output discrepancies. Another advantage of this method is that the amount of increase in each covariance matrix element can be estimated from the respective output discrepancy caused by the linear model. Following this approach the discrepancies between the linear model and the nonlinear simulation of QCSEE at steady state were determined. For this purpose identical inputs were applied to the linear model and the nonlinear simulation. The respective outputs were subtracted from each other to compute the discrepancies. Each steady state discrepancy was approximately 10^3 times larger than the standard deviation of the corresponding sensor noise level. This indicates that the lowest number by which the covariance matrix should be multiplied to avoid false alarms (due to model degradation) is approximately 10^6. Hence, the covariance matrix must be multiplied by a larger number to provide a greater margin between

the GLR index and the threshold. This is necessary to avoid high false alarm rate as larger elements of the generated noise sequence together with imperfect modeling effects cause the GLR index to exceed the threshold. Thus the normalized covariance matrix was multiplied by 5×10^{6}.

The residuals computed according to the covariance matrix which was described above were tested by the GLR detection program (with no failure effect in the residuals). The plot of the GLR indices corresponding to this test is shown in Figure 4.28. Although the value of GLR index over the observation sequence does not exceed the threshold ε, it shows an increasing trend in the indices. Comparing the pattern of the GLR indices in Figure 4.28 with plots of the GLR indices in Figures 4.5 and 4.6 reveals the existing pattern more vividly. This trend is due to the model degradation effects on the residuals. Experience from several trial simulation runs indicate that increasing the value of the covariance matrix elements reduces the magnitude of GLR indices but does not remove the increasing pattern. This is indeed due to the fact that degradation in the model forces the mean of the residuals to deviate from zero and increasing the value of the element in the covariance matrix only reduces the sensitivity of the detection technique. However, the reduction in the sensitivity of the GLR does allow performing the simulation of various failure modes without a forced false alarm due to model degradation. In the next section the simulation results for sensor failures are presented.

4.4.1 Sensor-Step Failure Simulation

To evaluate the performance of GLR in detecting sensor failures when model degradation occurs, simulation tests involving single and

multiple sensor failures were made. Specifically, single failures were introduced in the pressure sensor (PS11), the speed sensor (NL), and the temperature sensor (T3) separately. The same six outputs (i.e., PS11, NL, NH, P12, P4, and T3) as before were used to generate the residuals. The total number of observations used for these runs was 30 and the window limits for failure time are $M = 23$ and $N = 3$. The threshold ε was kept at 34 and the covariance matrix used in the detection program was computed as in Section 4.4. The failure size in the sensors is five times the standard deviation of its noise.

The results of these simulation runs are summarized in Table 4.7. The results of single sensor failures indicate that the step failures in pressure and temperature sensors are detected and identified properly. However, the step failure in speed sensor, NL, is not properly identified. Although the type of the failure is not correctly identified the occurrence of the failure is detected and the estimate of failure time is also correctly estimated in six (6) observations.

When model degradation occurs the estimate of the failure size (computed by constrained GLR) is a combination of the estimate of failure size and the output degradation effect on the sensor. For example the average estimate of failure size in PS11 over 14 estimation tests results is 5.142 and the actual failure size is 5.098; thus the difference is 4.4×10^{-3}. The average effect of model degradation on the PS11 sensor calculated from residuals is 5.55×10^{-2}. The estimates of the failure size in PS11 are plotted in Figure 4.29.

The speed of failure detection can be measured by time to detection. From the results in Table 4.7 can be seen that although occur-

TABLE 4.7

SIMULATION RESULTS FOR SENSOR FAILURES

(With Linear Model)

Failed sensor	PS11	NL	T3	NH P12 T3	PS11 NL NH	P12 P4 T3
Detected type	3	1,3	3	3	3	
Detected failure time	12	12	12	12	12	
Actual failure time	12	12	12	12	12	
Isolation*	C	--	C	--	--	
Failure time from isolation	12	--	12	--	--	
Time to detection	5	3	2	2	1	
Time to correct type	5	--	15	2	2	
Total detection time	5	--	15	3	3	

*C correct isolation.

rence of a failure is detected rapidly more observations are required before the correct type of failure is identified. A comparison between the number of required observations to correct type for single sensor failures and multiple failures indicates that multiple failures are detected more rapidly than single failures. These results are similar to the results obtained under perfect modeling. Higher speed and accuracy of detection and estimation of multiple failures are attributed to the more intensive effect of the multiple failures on the residuals. The multiple failure simulation results in Table 4.7 show accurate estimation of the failure time. To illustrate the evolution of the GLR index for single and multiple failures the indices for a single sensor failure in PS11 and multiple sensor failures of all six sensors are plotted in Figures 4.30 and 4.31, respectively. Again the index in the multiple failure case rises more rapidly. Next, detection of actuator failures under model degradation is discussed.

4.4.2 Actuator Failure Simulation

The performance of the GLR detection technique with imperfect modeling was evaluated by simulating single and multiple actuator failures. The results of these simulation tests are presented in Tables 4.8 and 4.9, respectively. The failure size for these tests are 5% of the input for step failures and 20% of the input for jump failures. Each simulation is performed over a total of 30 observations and the window limits for failure time are set as $N = 3$ and $M = 23$. The level of threshold c is maintained at 34 but the covariance matrix of the residuals is computed according to the same procedure that was explained in Section 4.2.

Consider the results of single actuator failure simulations in

TABLE 4.8

SIMULATION RESULTS FOR ACTUATOR FAILURE

(Linear Model)

	Step failure			Jump failure		
Failed actuator	XMV	X18	THETAI	XMV	X18	THETAI
Detected type	1	1	1	2	2	1,2
Detected failure time	12	12	11,12	12	11	11,12
Actual failure time	12	12	12	12	12	12
Time to detection	0	3	0	0	3	0
Time to correct type	10	7	0	1	3	--
Total detection time	10	7	--	3	--	--

TABLE 4.9

SIMULATION RESULTS FOR MULTIPLE ACTUATOR

(Linear Model)

	Step failure		Jump failure	
Failed actuators	XMV THETAI	XMV X18 THETAI	X18 THETAI	XMV X18 THETAI
Detected type	1	1	2	2
Detected failure time	9,10,11,12	10,11,12	12	12
Actual failure time	12	12	12	12
Time to detection	0	0	0	0
Time to correct type	0	0	1	1
Total detection time	--	--	5	3

Table 4.8. For these simulations the type of the failure is accurately determined except for the jump failure in THETAI. However, for this case the number of times that the failure type is correctly determined as a jump failure by far exceeds the number of times that the failure type is erroneously identified. Specifically, from the total of 18 detection tests performed, 14 test results indicated that the failure is a jump failure.

The estimate of the failure time is accurately determined for all cases. The largest error in the estimate of failure time is one observation. In the case of a step failure in THETAI only four out of 16 failure time estimates were incorrectly estimated as 11. The remaining 12 were correctly estimated. Exactly the same results were obtained for a jump failure in THETAI.

The actuator failures are detected rapidly in all cases. Maximum delay in detecting the failure is three (3) observations. Identification of the type of the failure, however, requires more observations. Finally, it should be mentioned that when a failure type or time is not correctly estimated then no number appears in the boxes corresponding to the time to correct type or detection time. The plots of GLR indices for step and jump failures in THETAI are shown in Figures 4.32 and 4.33.

Consider the results of multiple failure simulations in Table 4.9. The failure type has been detected successfully in all cases. The estimate of the failure time for step failures are not as accurate as in the case of no model degradation. Specifically, for the case of multiple failures in XMV and THETAI the failure time is estimated as 9 and 10 once and as 11 twice in the total of 16 estimates. Similarly, for step

failure in all three actuators the time of failure is estimated as 10 once and as 11 three times. Nonetheless, in both cases the majority of the failure time estimates are equal to the actual failure time.

Due to more intensive effects of multiple failures on the model residuals the time to detection for multiple failues is less than the time to detection for single failures. The evolution of the GLR indices for multiple step and jump failure in all three actuators are plotted in Figures 4.34 and 4.35, respectively. Comparing the plots in Figures 4.34 and 4.35 with the plots in Figures 4.32 and 4.33, respectively, reveals the increase and rapid rise of the GLR indices for multiple failures.

The study of performance of the GLR detection technique under model degradation is concluded at this point. In this study the performance of the GLR technique for single and multiple sensor/actuator failures was evaluated. For this purpose various performance measures such as correct failure type detection, estimate of the actual failure time, time to detection, and total detection time were used. Tables 4.7 through 4.9 provide a summary of the complete results of the performance evaluation tests. Next a summary and discussion of the results of this chapter will be presented.

4.5 Summary and Discussion

Simulation tests were conducted to evaluate the performance of the GLR detection technique in a realistic and practical environment. Specifically, the GLR technique was applied to a Quiet Clean Short-Haul Experimental Engine, QCSEE. The simulation studies were carried out by utilizing a reasonably detailed nonlinear digital simulation of the QCSEE engine. The QCSEE digital simulation was developed by NASA for utiliza-

tion in a flight simulator for STOL flight tests. The simulation program has been tested against a highly detailed digital model of the engine and the results match very well. For failure detection simulation studies a linear discrete state space representation of the engine and engine sensor noise characteristics are required.

The linear model of the engine was generated from the engine simulation (see Appendix E) and the sensor noise characteristics were extracted from actual engine measurements of an F-100 engine. The use of F-100 sensor noise characteristics is justified on the basis that similar sensors are used for measuring comparable engine parameters in jet engines. Another main assumption in this regard is that the noise characteristics of sensors measuring analogous engine outputs are identical. For example, noise characteristics of all QCSEE pressure sensors are assumed to be the same.

To conduct the failure detection simulation tests, a digital computer program incorporating the GLR concept was developyd to examine the model residuals for failure detection. The program is capable of detecting a failure, identifying the type of the failure, and estimating the failure time. Isolation of single sensor failure inside the program is achieved by utilizing the concept of the constrained GLR. For multiple sensor failure isolation, the estimate of failure vector is used. The underlying idea for this approach is to associate the failed sensors with the nonzero elements of the failure vector. Incidently, estimates of failure vector are also useful for failure accommodation. The GLR program has been extensively tested by numerous simulation tests.

At first the consistency of the GLR program was examined by test-

ing the model residuals when no sensor/actuator failure was present. The results indicate that no false alarm was encountered. Specifically, it follows from Figures 4.6 and 4.7 that the level of threshold, ϵ, remained substantially higher than the maximum value of the GLR index over the observation range. Another interesting result from these figures is that lowering the level of ϵ increases the probability of false alarm. The consistency tests were carried out by utilizing model residuals generated from the simulation configuration of Figure 4.3. For easy reference this configuration is referred to as perfect modeling configuration or in short, perfect modeling.

After consistency tests the capability of the GLR technique in detecting sensor/actuator failure was tested. To conduct these tests the perfect modeling configuration was employed first. This configuration provided a realistic performance evaluation of the detection technique for situations in which the model follows the engine without any discrepancies. Alternatively, testing the GLR technique (which originally is developed for linear systems) with the nonlinear QCSEE simulation provides a more realistic evaluation of the performance of the technique. The results of failure detection tests with regular modeling configuration is referred to as the first test category. The second test category consists of failure simulations in the presence of some discrepancy between the model output and the engine (Fig. 4.4). This is referred to as imperfect modeling configuration.

Under perfect modeling two sets of single sensor and actuator failure tests were conducted. The summary of the results of these tests are reported in Tables 4.1 through 4.6. Examination of the results reveals an impressive performance by the GLR detection technique.

Particularly, all single sensor failures were correctly detected and isolated. Also the failure times in all sensor failure cases were correctly estimated. The speed of detection in all cases was high such that the failed sensor was completely identified in nine (9) observations or less. Here complete identification refers to the correct failure detection, isolation, and proper estimation of the failure time. The estimates of failure size in the sensors were also computed accurately. Similarly, all single actuator failures were detected and the correct failure types were identified. The estimates of failure time for all cases were also correctly determined except for step failure in the fan pitch angle and fan nozzle actuators. However, the inaccuracies in these estimates do not exceed two observations. In addition, the frequency of the correct estimates of failure time exceeds the frequency of incorrect estimates (see, e.g., Figs. 4.10 and 4.11).

Under perfect modeling the capability of the GLR technique in detecting multiple sensor/actuator failure was also examined. As expected the effects of multiple failures on the residuals were stronger and therefore the failure detection was accomplished faster. It should be mentioned that since any single actuator failure affects the output of all sensors, multiple sensor failure residuals might resemble the residuals of single actuator failure. As a result cross detection may occur. However, the results of multiple failure analysis for QCSEE indicate that the proposed detection technique successfully identified all the multiple sensor failures. In addition the failure time and size were correctly identified in all cases. Similarly, the performance of the detection technique in detecting multiple actuator

failures is impressive (see Table 4.6). The technique identified all the multiple actuator failures with a very short delay in detection (the maximum delay was five (5) observations). Estimates of failure time were accurately calculated in all cases except for multiple jump failures in three actuators. It should be noted, however, that each of the two wrong failure time estimates occurred only once in a total of 17 estimate calculations.

To evaluate the performance of the GLR technique further the second category of tests with model degradation were carried out. The objective of these tests was to study the role of the engine model in succesful detection of the sensor/actuator failures. To achieve this, a linear model of the engine was generated and substituted for the nonlinear simulation representing the engine model. The linear model was generated from the simulation program and it follows the simulation model closely. However, the model residuals generated from the linear model would no longer be zero-mean white noise. Therefore, the sensitivity of the detection program must be reduced to avoid false alarms due to model degradation biases. This sensitivity reduction was achieved by increasing the values of the elements of the sensor noise covariance matrix.

After reducing the sensitivity of the detection technique a series of simulation tests were conducted. The results of these tests are summarized in Table 4.7. These results indicate that even when a linear model is utilized the detection results are quite satisfactory. The sensor failure simulation results in this category indicate that with the exception of failure in the fan speed sensor all other failures were correctly detected. Several interesting observations can be made

by comparing the results of sensor failure simulation of perfect and imperfect modeling. For instance the results of failure tests for PS11 and T3 in Tables 4.3 and 4.7 reveals that in case of model degradation the failure detection is slower. However, this reduction in detection speed is due to lowering the sensitivity of the GLR detection program rather than model degradation. Alternatively it can be conjectured that increase in the delay to correct failure type is due to the model degradation effects. Specifically, the modifications of the covariance matrix in the GLR detection program effect the GLR indices of all three failure types equally. Similar comparison can be made between the simulation results of multiple failure of all sensors in Tables 4.5 and 4.7. It follows from this comparison that longer delay in detection under imperfect modeling was not encountered. Thus it follows that multiple failures accentuate the change in the residual mean and thus they compensate for the reduced sensitivity of the detection program.

The performance of the GLR in detecting single and multiple actuator step and jump failures with imperfect modeling was also evaluated. A summary of these results is in Tables 4.8 and 4.9. For single actuator failures all failures were successfully identified except the jump failure in THETAI. Comparing the results in Table 4.8 with the perfect modeling actuator failure simulation results in Table 4.4 indicates that longer delay in detection under imperfect modeling were encountered. This confirms the previous conclusion that longer time to detection is due to reduction in the sensitivity of the detection program. It also follows from the results in Table 4.9 that the estimates of

failure time contain small inaccuracies which do not exceed one sampling interval.

Multiple actuator failure results in Table 4.9 indicate that the intensive effects of multiple failure again eliminate the delay in failure detection. In addition the failure types are also correctly identified (no cross detection). The estimate of failure time, however, continues to show inaccuracies. Compared to the results in Table 4.6 the frequency of inaccurate failure time estimate, in Table 4.9, increased under imperfect modeling while the error range is the same for both test categories. Another comparison which can be made between the results in Tables 4.6 and 4.9 concerns total detection times. It can be seen that for jump failures the total detection time are equal for the two test categories.

It should be emphasized that even under imperfect modeling the GLR technique performs quite satisfactorily. These performance results warrant further investigation into the use of imperfect models in the proposed technique. The use of simpler but imperfect model can broaden the application of GLR to complex systems which require very detailed and complicated modeling for perfect reproduction of their dynamics.

In summary the GLR performance evaluation tests indicate that the proposed detection technique is a reliable, consistent, fast, and accurate method of detecting failures. In addition it provides all the necessary information regarding the size, time, and type of failures. The proposed GLR technique is also capable of isolating failed sensors and it furnishes the required information for accommodating the failure. The problem of failure accommodation is studied further in the next chapter.

CHAPTER V

FAILURE ACCOMMODATION

5.1 Introduction

The last phase of the proposed failure analysis, namely failure accommodation, is discussed in this chapter. As it was indicated in the first chapter, failure accommodation techniques are closely related to the system control design methodology. The accommodation technique, proposed in this Chapter, is based on the Multivariable Nyquist Array (MNA) technique. Hence, it is compatible with the proposed GLR failure detection and isolation techniques and completes the proposed failure analysis technique. The concept of failure accommodation and its relation to the MNA failure technique is described in Section 5.2. Also in Section 5.2 the concepts of the MNA technique that are utilized in the development of the proposed accommodation technique are discussed. Then in Section 5.3 the proposed accommodation procedure is described. Examples of the accommodation procedure for the QCSEE engine are presented in Section 5.4. Finally, in Section 5.5 a summary and discussion of the results are presented.

5.2 Failure Accommodation

The significance of sensors in successful control of jet engines was discussed in Chapter I (Section 1.3). It follows from the discussion that a sensor failure may degrade the overall performance of the engine. Thus, after a failure has been detected and isolated it is necessary to take corrective actions to minimize the performance

degradation (i.e. to accommodate the failure). Based on the proposed failure analysis technique (see Section 2.2), failure accommodation may be achieved in two alternative fashions. First, the control system remains unchanged and the lost measurement is replaced by the corresponding model output. In the second method the system control design is altered to minimize the performance degradation. The implementation of the first method is straightforward. However, the replacement (or reconstruction) of the lost measurements is not always practical. Therefore, the second accommodation technique must be developed. Such a development for the proposed failure analysis technique is based on the MNA design methodology. Therefore, it is helpful to review the MNA concepts essential to the development of the accomodation technique.

5.2.1 MNA Design Technique

The use of Nyquist stability criterion in classical control theory for single input single output systems is well established. In 1969, Professor H. H. Rosenbrock proposed an extension of the Nyquist criterion to multivariable systems (Ref. 17). In his paper, Rosenbrock utilized the concept of diagonal dominance for the linear system transfer function matrices in the inverse polar plane to develop the Nyquist stability theory for multivariable systems. Since the stability theory was developed for the inverse polar plane, it is referred to as the Inverse Nyquist Array (INA) method. The Nyquist stability theory for the direct polar plane was introduced by Rosenbrock in 1974 (Ref. 18). Likewise, this method is referred to as the Direct Nyquist Array (DNA) method.

Being natural extensions of the classical control techniques,

both INA and DNA have been examined by researchers (see, e.g., Refs. 19 to 21, 23, and 24). This has produced significant results which enhances the understanding and applicability of these techniques. One such result is due to Leininger (Ref. 24) who has shown that it is possible to achieve dominance in either the direct or inverse plane and complete the design in the opposite plane, thus unifying the INA and DNA under a single heading as the "Multivariable Nyquist Array" (MNA). In applying MNA to any system the main concern is to achieve dominance in either polar plane. Once dominance is obtained the design of individual feedback loops can proceed in the same fashion as in single input single output systems. Hence, it is of great importance to achieve dominance in a fast reliable fashion.

To understand the concept of dominance consider the system block diagram in Figure 5.1. In this diagram G(S) is the n × n system transfer matrix, and K(S) and L(S) are two n × n pre- and post-compensators, respectively. The n × n diagonal matrix F(S) represents the feedback gain matrix. The open-loop transfer function matrix, Q(S), in the direct polar domain is given by

$$Q(S) = L(S)G(S)K(S) \tag{5-1}$$

In the inverse polar plane the open-loop transfer matrix is given by

$$\hat{Q}(S) = \hat{K}(S)\hat{G}(S)\hat{L}(S) \tag{5-2}$$

where

$$\hat{G}(S) = G^{-1}(S)$$

$$\hat{Q}(S) = Q^{-1}(S)$$

$$\hat{K}(S) = K^{-1}(S)$$

$$\hat{L}(S) = L^{-1}(S)$$

note that

$$\hat{q}_{ij}(S) \neq q_{ij}^{-1}(S).$$

To proceed with the feedback gain design either $Q(S)$ or $\hat{Q}(s)$ must be diagonally dominant. The definition of the diagonal dominance can be expressed in a more unified and general fashion as follows. Let $P(S)$ represent the general open loop transfer function matrix, given as

$$P(S) = A(S)Z(S)B(S) \tag{5-3}$$

Where $A(S)$ and $B(S)$ are the pre- and post-compensators or their proper inverse depending on the plane in which the dominance is sought. Likewise $Z(S)$ represents either $G(S)$ or $\hat{G}(S)$ and $P(S)$ becomes $Q(S)$ or $\hat{Q}(S)$. Now using equation (5-3) the concept of diagonal dominance for rows and columns of $P(S)$ can be defined.

Definition: Let $P(S)$ be a rational polynomial matrix and θ_i^r and θ_i^c be determined for all $i = 1,2,\ldots,n$ by

$$\theta_i^r = \underset{S\in D}{\text{Max}} \sum_{\substack{j=1 \\ j\neq i}}^{n} \left|P_{ij}(S)\right| \Big/ \left|P_{ii}(S)\right| \tag{5-4}$$

and

$$\theta_i^c = \underset{S\in D}{\text{Max}} \sum_{\substack{j=1 \\ j\neq i}}^{n} \left|P_{ji}(S)\right| \Big/ \left|P_{ii}(S)\right| \tag{5-5}$$

Where D is the Nyquist contour. Then $P(S)$ is row dominant if for all $i = 1,2,\ldots,n$

$$\theta_i^r < 1 \tag{5-6}$$

and $P(S)$ is column dominant if for all $i = 1,2,\ldots,n$

$$\theta_i^c < 1 \qquad (5\text{-}7)$$

The functions defined in equations (5-4) and (5-5) are called row and column dominance levels, respectively.

For an MNA design to proceed row or column dominance in either direct or inverse plane is sufficient It follows from the above definition of diagonal dominance that there are twelve possible MNA design forms wherein A(S) or B(S) can be specified or varied to achieve dominance. Therefore, it is of interest to establish a relationship between the dominance in the direct and inverse polar plane. In the course of the research for this dissertation a new relationship between the dominance in the two polar planes is established. The theorem establishing this relationship utilizes a theorem provided by Rosenbrock (Ref. 52). For easy reference Rosenbrock's theorem is repeated here without the proof.

Theorem 5.1: Let the nxn complex matrix Q satisfy

$$\sum_{\substack{j=1 \\ j\neq i}}^{n} |q_{ij}| = \theta_i |q_{ii}| \qquad (5\text{-}8)$$

$$\left(\text{Respectively} \sum_{\substack{j=1 \\ j\neq i}}^{n} |q_{ji}| = \theta_i |q_{ii}| \right)$$

Where $0 < \theta_i \leq 1$ for $i = 1,2,\ldots,n$. Then Q has an inverse $\hat{Q} = Q^{-1}$ satisfying

$$|\hat{q}_{ji}| < \theta_j |\hat{q}_{ii}| \qquad (5\text{-}9)$$

$$\left(\text{Respectively } |q_{ij}| < \theta_j |q_{ii}| \right)$$

For $i = 1,2,\ldots,n$ and $j = 1,2,\ldots,i-1,i+1,\ldots,n$

Proof: See reference 52, Chapter 5, Section 6.1.

Now utilizing theorem 5.1 the dominance conditions in the direct and inverse plane can be linked by the following theorem.

Theorem 5.2: If an $n \times n$ transfer matrix $Q(S)$ is row (column) dominant then $\hat{Q}(S)$ is column (row) dominant if the sum of any $n-1$ of the dominance levels is less than unity.

Proof: Note that if $Q(S)$ is row dominant then equation (5-8) is satisfied for all S on the Nyquist contour, D. It follows from theorem 5.1 that the equation (5-9) is also valid for $S \in D$ Then the dominance levels of $Q(S)$ can be expressed in terms of θ_i as follows:

$$\theta_i^r = \max_{S \in D} \theta_i \tag{5-10}$$

$$\left(\text{Respectively } \theta_i^c = \max_{S \in D} \theta_i \right)$$

for $i = 1,2,\ldots,n$. Now consider the equation (5-9), adding the inequities for all possible $j \neq i$ yields

$$\sum_{\substack{j=1 \\ j \neq i}}^{n} |q_{ji}| < \sum_{\substack{j=1 \\ j \neq i}}^{n} \theta_j |q_{ii}| \tag{5-11}$$

$$\left(\text{Respectively } \sum_{\substack{j=1 \\ j \neq i}}^{n} |q_{ij}| < \sum_{\substack{j=1 \\ j \neq i}}^{n} \theta_j |q_{ii}| \right)$$

Note that from the conditions of the theorem

$$\sum_{j=1}^{n} \theta_j^r < 1 \tag{5-12}$$

$$\left(\text{Respectively} \quad \sum_{\substack{j=1 \\ j\neq 1}}^{n} \theta_j^c < 1 \right)$$

then it follows from (5-10) that

$$\sum_{\substack{j=1 \\ j\neq 1}}^{n} \theta_j < 1 \qquad (5\text{-}13)$$

Therefore, it can be seen from (5-11) that Q(S) is column (row) dominant.

Theorem 5.2 provides a method of testing for dominance in either direct or inverse polar plane after the dominance condition is satisfied in the opposite plane. It also follows from theorem 5.2 that the dominance levels satisfying the conditions of the theorem, automatically provide the freedom of completing the design in either of the polar planes. Having established the definition of diagonal dominance, the methods of achieving dominance can now be considered.

Three alternative methods of achieving dominance have been proposed by the researchers. Rosenbrock introduced the concept of pseudo diagonalization (Ref. 18) and Schafer and Sain developed (Ref. 54)a dominance seeking graphical technique, called CARDIAD plots. However, both these techniques emphasize the selection of compensator parameters by the designer through a trial and error procedure. Thus they require excessive time for obtaining dominance. The third approach introduced by Leininger (ref. 20) is based on a function minimization procedure. This method utilizes a conjugate direction function minimization technique to adjust the parameters of the compensators to obtain the dominance conditions (eqs. (5-6) and/or (5-7)). The function minimization technique has been successfully applied to numerous

practical problems (Ref. 19).

The function minimization method transfers the task of obtaining dominance to the computer and requires minimal intervention on the designer's part in achieving dominance, hence allowing the designer to devote more of his time to the design of the feedback gains. In addition, due to lack of need for continuous intervention by the designer, the technique can be implemented in a batch mode. These attractive features of the functional minimization technique are particularly useful for failure accommodation, as alternative design configurations can be generated faster.

One of the main assumptions in the development of the MNA technique is that the system under study has an equal number of inputs and outputs; namely the system is square. However, when a sensor/actuator failure occurs it may not be possible to utilize an equal number of inputs and outputs in the control design. Hence a procedure must be developed to make the MNA technique applicable to non-square systems. A procedure for this purpose is proposed in the next section.

5.3 Failure Accommodation Technique

In this section a method of failure accommodation based on the MNA design technique is developed. The main objective is to develop a procedure that will make the MNA design technique applicable to non-square systems. Since the MNA design technique is developed for square systems, the procedure entails converting the nonsquare systems to square configurations. This may be achieved by designing pre- and post-compensators of proper dimension so that the open-loop transfer

Q(S); however, an $n \times n$ Q(S) resulting from a G(S) of rank $n - 1$ cannot be made dominant. This can be seen by examining the rank of Q(S). Since the rank of Q(S) cannot be raised above the rank of G(S) through matrix multiplication, then the rank of Q(S) is at most $n - 1$. Therefore, the eigenvalues of Q(S) include at least one zero. Now, according to Greshgorin Theorem (Ref. 55) the union of Greshgorin discs for Q(S) (for any S) contain all the eigenvalues of Q(S). Therefore, for all values of S on the Nyquist contour the Greshgorin discs sweep out a band which contains all the eigenvalues of Q(S) (for S on D). This band is referred to as Greshgorin band. For the dominance conditions (eq. (5-6) or (5-7)) to be satisfied, the Greshgorin band must exclude the origin (Ref. 18). Hence, to obtain dominance the compensators should be selected such that the dimension of Q(S) will be equal to $n - 1$.

It follows from the above discussion that for failure accommodation the system transfer matrix should always be squared down to the lower dimension of G(S). Thus far it has been established that the INA design is not suitable for failure accommodation and the DNA design can only be carried out by squaring the system down to its lower dimension. Hence, it remains to develop a dominance-seeking procedure for DNA design that will yield a square system of dimension $n - 1$.

The method of function minimization is utilized to obtain dominance for nonsquare systems. To describe the technique, consider the open-loop transfer matrix in equation (5-1). Now suppose that a sensor has failed, then G(S) becomes an $(n - 1) \times n$ matrix. Thus, to obtain dominance L(S) should be an $(n - 1) \times (n - 1)$ matrix and K(S) must be an $n \times (n - 1)$. Note that depending on the type of dominance

(i.e. row or column) and whether K(S) and L(S) are specified or variable, there are six possible DNA design forms. The purpose of any of these designs is to obtain dominance levels (eq. (5-6) and (5-7)) below unity. It is remarked that the dominance levels for several of these forms can be adjusted by varying only one row (or column) of the compensators. For instance, consider the case of row dominance when K(S) is specified and L(S) is varied. It follows from equations (5-1) and (5-4) that the elements in the ith row of L(S) do not effect the dominance levels of the remaining rows. Based on this observation, two separate functions can be specified for the function minimization technique as

$$J_1 = \begin{cases} \theta_i^r & \text{(Row)} \\ \theta_i^c & \text{(Column)} \end{cases} \tag{5-14}$$

and

$$J_2 = \begin{cases} \underset{i}{\text{Max}} \ (\theta_i^r) & \text{(Row)} \\ \underset{i}{\text{Max}} \ (\theta_i^c) & \text{(Column)} \end{cases} \tag{5-15}$$

where θ_i^r and θ_i^c are given in equations (5-4) and (5-5) respectively. Equation (5-14) is used whenever the rows or columns of the unspecified compensator effect the corresponding dominance levels independently. Alternatively, equation (5-14) is utilized when such independence does not exist. Whenever J_1 can be used, the unknown parameters of individual rows or columns are computed to minimize J_1. Thus, at most n unknown parameters are computed to extremize J_1

for each dominance level. For the design corresponding to equation (5-15) all the unknown coefficients are adjusted to achieve low overall dominance levels. Therefore, the number of unknown parameters used in extremizing the dominance levels is at least $(n - 1)^2$ and at most $(n - 1)(2n - 1)$.

The optimization technique selected to minimize J_1 and J_2 is a conjugate direction technique developed by Zangwill and Powell (Refs. 56 and 57). The technique is particularly suitable for minimizing J_1 and J_2 functions because it does not require an explicit evaluation of the gradient, as the calculation of the gradient of these functions may pose some numerical problems. Additionally, Fletcher, in his comparative study of optimization techniques (Ref. 62) concludes that among the techniques which do not require the calculation of the gradient Powell's technique may be computationally the most efficient.

After minimizing the functions in (5-14) and (5-15), the resulting dominance levels are usually of different magnitude. Indeed, often the resulting dominance levels for certain rows (or columns) are less than unity and for the remaining rows (columns) exceed one. In this case the DNA design still cannot be completed until all the dominance levels are less than one. Leininger has shown (Ref. 24) that it is possible to share the dominance between rows (columns). The concept of dominance sharing can be described by examining the open-loop transfer function $Q(S)$ in (5-1). Suppose that it is desired to achieve column dominance for $Q(S)$, and the function minimization technique has been applied and the resulting

dominance levels are unequal. Then $Q(S)$ is premultiplied by a diagonal $T = \text{dig}(t_i)$ for $i = 1,2,\ldots, n-1$. The resulting matrix is given by

$$R(S) = TQ(S) = TL(S)G(S)K(S)$$

or

$$R(S) = \begin{bmatrix} q_{11}t_1 & q_{12}t_1 & \cdots & q_{1(n-1)}t_1 \\ q_{21}t_2 & q_{22}t_2 & \cdots & q_{2(n-1)}t_2 \\ \vdots & \vdots & & \vdots \\ q_{(n-1)1}t_{(n-1)} & q_{(n-1)2}t_{(n-1)} & & q_{(n-1)(n-1)}t_{(n-1)} \end{bmatrix} \tag{5-16}$$

It can be seen from the above equation that by selecting t_i for $i = 1,2,\ldots, n-1$ the dominance levels in $R(S)$ can be varied. It is also possible to establish a set of sufficient conditions that will provide a guideline for selecting t_i's such that the dominance is shared while it is still retained in the rows (columns) that are already dominant (Ref. 24). However, it is practically more feasible to employ the concept of function minimization technique to select the diagonal elements of the T matrix. This may be achieved by minimizing the following function

$$J_c = \underset{i}{\text{Max}} \left(\gamma_i^c\right) \quad i = 1,2,\ldots,n-1 \tag{5-17}$$

where γ_i^c is the column dominance level for $R(S)$. If the minimization of (5-17) is continued until the lowest value of J_c is obtained,

then γ_i^c for $i = 1,2,\ldots, n-1$ will become equal. Similarly, when row dominance is desired, the $Q(S)$ is postmultiplied by $T = \text{dig}(t_i)$, then, $R(S)$ in this case becomes

$$R(S) = Q(S)T = L(S)G(S)K(S)T$$

or

$$R(S) = \begin{bmatrix} q_{11}t_1 & q_{12}t_2 & \cdots & q_{1(n-1)}t_{(n-1)} \\ q_{21}t_1 & q_{22}t_2 & \cdots & q_{2(n-1)}t_{(n-1)} \\ \vdots & \vdots & & \vdots \\ q_{(n-1)1}t_1 & q_{(n-1)2}t_2 & & q_{(n-1)(n-1)}t_{(n-1)} \end{bmatrix} \tag{5-18}$$

To obtain dominance the following function is minimized

$$J_r = \max_i \left(\gamma_i^r \right) \quad i = 1,2,\ldots, n-1 \tag{5-19}$$

Where γ_i^r are the row dominance levels for $R(S)$ in (5-19).

Utilizing the failure accommodation technique developed in this section, a digital computer program capable of obtaining dominance for nonsquare systems was developed. The performance of the program was then tested by using the QCSEE linear model at 62.5% power. The results of these tests are reported in the following section.

5.4 Performance Evaluation of Failure Accommodation Technique

A digital computer program for implementation and evaluation of the preposed failure accommodation technique was developed. The main

purpose of the program was to provide the capability of obtaining dominance for nonsquare systems. However, the program is designed such that it can be utilized for square systems as well. In addition, various forms of MNA designs can be examined by the program for obtaining dominance. That is for square systems both INA and DNA row and column dominance can be examined.

For nonsquare systems, row and column dominance in the DNA mode can be tested. The dominance-seeking logic of the program is based on the function minimization technique that was described in the previous Section. In addition, the concept of dominance sharing is implemented in the program logic.

Although the main objective of the program development is to demonstrate the capability of obtaining dominance, the program has the capability of plotting Greshgorin and Ostrowski bands. These bands are used to complete the DNA design. Graphically the Greshgorin and Ostrowski bands are plotted by utilizing Crossley's (Ref. 63) envelope curves, hence saving a significant amount of time in plotting.

For performance evaluation the proposed accommodation technique was applied to the QCSEE with unequal number of inputs and outputs. Specifically, two categories of tests were conducted. In the first category the number of outputs is smaller than the number of inputs. This group of tests represent a case of sensor failure wherein the system must be reduced to the nonsquare system. The second category of tests examine the system with fewer inputs than outputs; they represent actuator failures. One example from each of the two test categories will be presented here.

For the case of a sensor failure, three inputs and two sensors are utilized. The inputs are XMV, THETAI, and X18 and the two sensors are NL and NH (for a description of inputs and outputs see Section 4.1.2 in Chapter IV). The dynamics of the sensor are neglected in this case. Column dominance is sought over the range of zero to 50 Rad/s divided into 100 equally spaced points. The initial pre- and post-compensators are

$$K = \begin{pmatrix} 1 & 0 \\ 0 & 1 \\ 1 & -1 \end{pmatrix} \tag{5-20}$$

and

$$L = \begin{pmatrix} 1 & 0 \\ 0 & 1 \end{pmatrix} \tag{5-21}$$

The dominance levels resulting from the above compensators are

$$\theta_1^c = 3.193$$

$$\theta_2^c = 54.259 \tag{5-22}$$

To obtain dominance, the post-compensator is kept constant and the elements of the pre-compensator are varied to get dominance. It is remarked that for this DNA design form, changing the elements in the column i of K for $i = 1,2$ effects only the ith dominance level of $Q(S)$.

After a single application of the function minimization program, the following values for the pre-compensator result.

$$K = \begin{pmatrix} 0.10157 & 0.31457 \times 10^{6} \\ 0.81920 \times 10^{3} & -0.67101 \times 10^{6} \\ 0.82020 \times 10^{3} & -1.0 \end{pmatrix} \tag{5-23}$$

and the associated dominance levels are

$$\begin{aligned} \theta_1^c &= 0.09582 \\ \theta_2^c &= 0.6125 \end{aligned} \tag{5-24}$$

It can be seen that although diagonal dominance is obtained with the new K, dominance level θ_2^c is six times larger than θ_1^c in (5-24). Using the dominance sharing option of the program, the following T matrix is computed

$$T = \begin{pmatrix} 0.49638 & 0.0 \\ 0.0 & 1.255 \end{pmatrix} \tag{5-25}$$

which results in

$$\begin{aligned} \theta_1^c &= 0.24227 \\ \theta_L^c &= 0.24226 \end{aligned} \tag{5-26}$$

Now if the post-compensator, L, in (5-21) is premultiplied by T in (5-25), a new post-compensator is obtained. Using the new compensator, the function minimization and dominance sharing is repeated twice and the following dominance levels result

$$\begin{aligned} \theta_1^c &= 0.099509 \\ \theta_L^c &= 0.099502 \end{aligned} \tag{5-27}$$

The corresponding T matrix is

$$T = \begin{pmatrix} 1.0012 & 0 \\ 0 & 1.0 \end{pmatrix} \tag{5-28}$$

and the K and L are

$$K = \begin{pmatrix} 6.5101 & 0.27307 \times 10^{5} \\ 404.09 & -0.96637 \times 10^{6} \\ 0.13446 \times 10^{7} & -0.12080 \times 10^{7} \end{pmatrix} \tag{5-29}$$

and

$$L = \begin{pmatrix} 0.50052 & 0.0 \\ 0.0 & 1.2545 \end{pmatrix} \tag{5-30}$$

Examining the T matrix in (5-28) reveals that the T matrix is almost an identity matrix; hence, multiplying L by T will not change L significantly. This implies that repeating the function minimization and dominance sharing will not change the dominance levels significantly. It is noted that very low values of dominance levels are obtained while both K and L are constant. This is desirable due in part to easy implementation of constant compensators in practice. The Greshgorin bands corresponding to the final compensators are plotted in Figures 5.2 and 5.3.

In the second test category, a nonsquare QCSEE transfer function matrix representing an actuator failure in THETAI was used. The outputs in this case were NL,NH, and P8 and the inputs were XMV, and X18. Column dominance for the nonsquare DNA design form was sought over the range of zero to 50 Rad/s divided into 100 equally spaced points. The initial pre- and post-compensator were

$$K = \begin{pmatrix} 1.0 & 0.0 \\ 0.0 & 1.0 \end{pmatrix} \tag{5-31}$$

and

$$L = \begin{pmatrix} 1.0 & 0.0 & 0.0 \\ -1.0 & -1.0 & 1.0 \end{pmatrix} \tag{5-32}$$

The dominance levels resulted from utilizing the above compensators are

$$\theta_1^c = 4.1969$$

$$\theta_2^c = 1.1281 \tag{5-33}$$

After a single application of the function minimization program, the following dominance levels were obtained

$$\theta_1^c = 0.98448$$

$$\theta_2^c = 0.30873 \tag{5-34}$$

The pre-compensator associated with the above dominance levels is

$$K = \begin{bmatrix} 1.0 & -1.2885 \\ 0.83886 \times 10^6 & 0.85 \end{bmatrix} \tag{5-35}$$

The post compensator elements were not varied. Using the dominance sharing technique and function minimization in an alternating fashion (as in the previous test category) twice, the T matrix approached the identify matrix and the following dominance levels were obtained

$$\theta_1^c = 0.58554$$

$$\theta_2^c = 0.58544 \tag{5-36}$$

The pre- and post-compensator corresponding to the dominance levels in (5-36) are

$$K = \begin{pmatrix} -0.85731 \times 10^{3} & -0.11644 \times 10^{10} \\ 0.83912 \times 10^{6} & 0.85 \end{pmatrix} \tag{5-37}$$

and

$$L = \begin{pmatrix} 1.522641 & 0.0 & 0.0 \\ -1.011035 & -1.011035 & 1.011035 \end{pmatrix} \tag{5-38}$$

The Greshgorin plots corresponding to this case are given in Figures 5-5 and 5-6. Finally, as in the previous case the dominance is obtained with constant pre- and post-compensators.

5.5 Summary and Discussion

In this chapter a new method for sensor/actuator failure accomodation was proposed. The proposed technique is based on Multivariable Nyquist Array (MNA) design methodology. Fundamentally, the technique provides for restructuring the MNA designed control system after the failure is detected and isolated. In order to restructure the control system after a sensor/actuator failure, it becomes essential to design the controls for unequal number of inputs and outputs. To meet this need it is essential to extend the MNA techniques to nonsquare system applications. The proposed failure accommodation technique is indeed such an extension.

In the development of the proposed technique, it was shown (Section 5.4) that obtaining dominance in the inverse plane for nonsquare systems is cumbersome. Alternatively, it was demonstrated that achieving dominance in the direct polar plane is feasible.

In addition, a set of new conditions relating the dominance in the direct and inverse plane was established. These conditions can be utilized to assess dominance in the inverse plane using the dominance levels in the direct plane. Hence, it follows that under these conditions (Theorem 5.2) it is possible to obtain dominance in the direct plane and complete the design in either plane.

The proposed accommodation technique calls for converting the nonsquare system to a square one; thus making standard MNA techniques applicable. It was shown (Section 5.3) that in general, dominance for converted square systems is only obtainable if the dimension of the converted system is equal to the lower dimension of the nonsquare system. Based on this result the concept of function minimization and dominance sharing are incorporated in the proposed technique to achieve dominance. Therefore, the compensator for converting the nonsquare system to a square one is selected such that the resulting square system will be dominant.

The performance of the proposed technique was tested by applying it to the QCSEE. Two types of tests involving sensor and actuator failure were conducted. The results of these tests were excellent, as in both cases high degree of dominance was obtained without having to employ dynamic compensators. Development of the accommodation technique in this chapter, together with failure detection and isolation in the previous chapters, complete all phases of the proposed failure analysis technique. In the next chapter a brief summary of the development of all three phases of the proposed failure analysis technique will be presented and certain recommendations for future research will be made.

CHAPTER VI

SUMMARY OF RESULTS AND CONCLUSIONS

It was established in Chapter I that future jet engines will rely on digital controls to meet high performance requirements. The design technique of these controls was indicated to be the modern control techniques in both the time and frequency domains. A major design requirement of digital control implementations in advanced aircraft engines is high system reliability. The reliability of the sensors and actuators used to implement the control are important aspects of this requirement. Improvements in this reliability can be achieved by utilizing analytical redundancy.

Techniques for detection and isolation of sensor/actuator failures utilizing analytical redundancy were closely related to engine control design. Specifically, it was indicated that failure analysis techniques compatible with the multivariable frequency domain control techniques had significant advantages as they did not require state estimation. Therefore, the main objectives of the research were to develop a failure analysis technique which utilized analytical redundancy and was compatible with the multivariable frequency domain control design techniques, and to develop a failure accommodation capability in the Multivariable Nyquist Array (MNA) technique.

In Chapter II, a new failure detection and isolation technique

based on the concept of Generalized Likelihood Ratio (GLR) was developed. The technique did not require multiple hardware redundancy and utilized the redundant information embedded in the model residuals. Development of the technique focused on three failure types; namely, state step, state jump, and sensor step. These failure types cover a wide range of possible physical sensor/actuator failures. The technique was derived for both time-varying and time-invariant linear systems. In addition to detection and isolation, the technique provided estimates of failure time, direction and magnitude. In the case of time-invariant systems a major portion of the computational burden of the technique could be accomplished off-line, hence facilitating the on-line implementation of the technique. For time-invariant systems, a set of recursion relations was derived that simplified the on-line implementation of the technique further. Finally, in Chapter II, it was demonstration that the GLR technique can also be utilized for soft sensor failure detection.

The results of Chapter III can be summarized under three main topics. These topics were: (1) probability distribution of the GLR index; (2) failure detectability of the GLR technique; and (3) asymptotic behavior of the $C_i(d)$ matrix. Under the first topic the probability distribution of the GLR index was found to have a noncentral chi-squared distribution in the case of a failure and a central chi-squared if no failure occurred. The knowledge of the probability distribution of the GLR index provided the capability of computing four important detection probabilities. The probabilities of correct detection, false alarm, cross detection, and wrong time were used to evaluate the confidence, consistency, isolation capability and failure

time estimate accuracy of the technique, respectively. Under the second topic, the detectability of the failures were examined. It was shown that the technique was always capable of detecting sensor failures in both the time-varying and time-invariant systems. The detectability of actuator failures was linked to the invertibility of the $C_i(k,t)$ matrix and it was established that for observable time-invariant systems $C_i(d)$ is always invertible. The significant impact of the behavior of $C_i(d)$ on both the detectability and the accuracy of failure vector estimate warranted the investigation of the asymptotic behavior of $C_i(d)$. Hence under the third topic the behavior of the $C_i(d)$ matrix was studied and this provided more insight into the effects of observation numbers on the detectability of failures and the accuracy of failure estimates.

The performance of the GLR technique was evaluated in Chapter IV by applying the technique to a Quiet Clean Short-Haul Experimental Engine (QCSEE). For this purpose a reasonably detailed nonlinear simulation of the engine was utilized. All other required programs for simulating single and multiple sensor/actuator failure in the QCSEE were developed. The programs included the implementation of the proposed GLR detection technique with its isolation capability derived from the constrained GLR (CGLR) technique. The performance evaluation studies were divided into two categories. In the first category perfect modeling of the engine was assumed while in the second category model degradations (imperfect modeling) were permitted. In the perfect modeling category single and multiple sensor and actuator failures were simulated. The performance of the proposed GLR technique in all test cases was excellent. Specifically, all

sensor and actuator failures were properly and rapidly detected. The isolation of the failed sensors and the estimation of the failure size and time were also successfully accomplished in all simulation tests. Small inaccuracies occurred in the estimates of failure time for actuators.

In the imperfect modeling tests, single and multiple sensor/actuator failures were simulated in the QCSEE. The results of these tests were also quite satisfactory. For these tests the technique continued to detect single sensor/actuator failures properly with small inaccuracies in identifying the failure types. It should be emphasized, however, that no difficulty was encountered in identifying multiple sensor and actuator failure types properly. Likewise, failure times were properly estimated for all sensor failures while for actuator failures, the estimates showed small inaccuracies. In addition, the estimates of the combined effects of sensor failures and model degradations were accurately determined.

A new failure accommodation technique was developed in Chapter V. The technique was based on the Multivariable Nyquist Array control design technique. Specifically, it utilized the MNA techniques to design the nonsquare systems resulting from the loss of a sensor or an actuator. It was shown that obtaining dominance for nonsquare systems in the inverse polar plane was cumbersome, thus dominance was sought in the direct polar plane. However, a set of new relations between dominance in the inverse plane and the direct plane was established. These relations could be used for deducing dominance in the inverse plane from the dominance levels in the direct plane. The accommodation technique called for converting nonsquare systems

to square ones. For this purpose a new general guideline applicable to nonsquare systems of any dimension was developed. Based on this guideline a suite of programs for handling nonsquare systems was developed. Using these programs the new accommodation technique was applied to the QCSEE for both sensor and actuator accommodation. The results of these tests were excellent, as high levels of dominance were obtained without having to utilize dynamic compensators.

In brief, the achievements of this research include:

1. The development of a new, fast, and reliable failure detection and isolation technique which is compatible with modern multivariable control design techniques and does not require hardware redundancy.

2. The development of general computer algorithims for application of the proposed detection and isolation technique to any linear time-invariant dynamic system.

3. The successful application of the proposed technique to an actual engineering system, namely the QCSEE.

4. The extension of MNA design techniques to nonsquare systems for sensor/actuator failure accommodation.

5. The derivation of a new relationship between the dominance levels in the direct polar plane and the inverse polar plane.

6. The development of a suite of programs for MNA design of nonsquare systems.

7. The successful application of the accommodation technique to the QCSEE.

From the results of this research it can be concluded that the proposed failure analysis technique provides a fast, reliable, and accurate method for sensor/actuator failure analysis of future jet

engines.

There are several areas in which further research could lead to significant results. First, although performance of the proposed detection technique under model degradation was investigated, more studies concerning the effects of model degradation are needed. Second, the study of the computational requirement of the GLR technique for on-line implementation is also very important. It is noted the results of the studies of model degradation effects are of fundamental importance for the computational requirement studies. If an imperfect model with a low computational requirement can still provide reliable detection, then the on-line implementation becomes more feasible. Another significant research area is the problem of cross detection, as wrong type detection could severely degrade engine performance.

For more long term future research, several significant areas can be identified as follows. It was demonstrated in Chapter II that the concept of GLR can be applied to the problem of soft failure. However, much work remains to be done to develop a complete failure analysis methodology parallel to the hard failure analysis in the previous chapters. Also of significant importance is the investigation of the simultaneous failures in sensors and actuators. Finally, the detection and isolation of several failures which occur in sequence is of great practical importance.

APPENDIX A

Figures Referenced in the Text

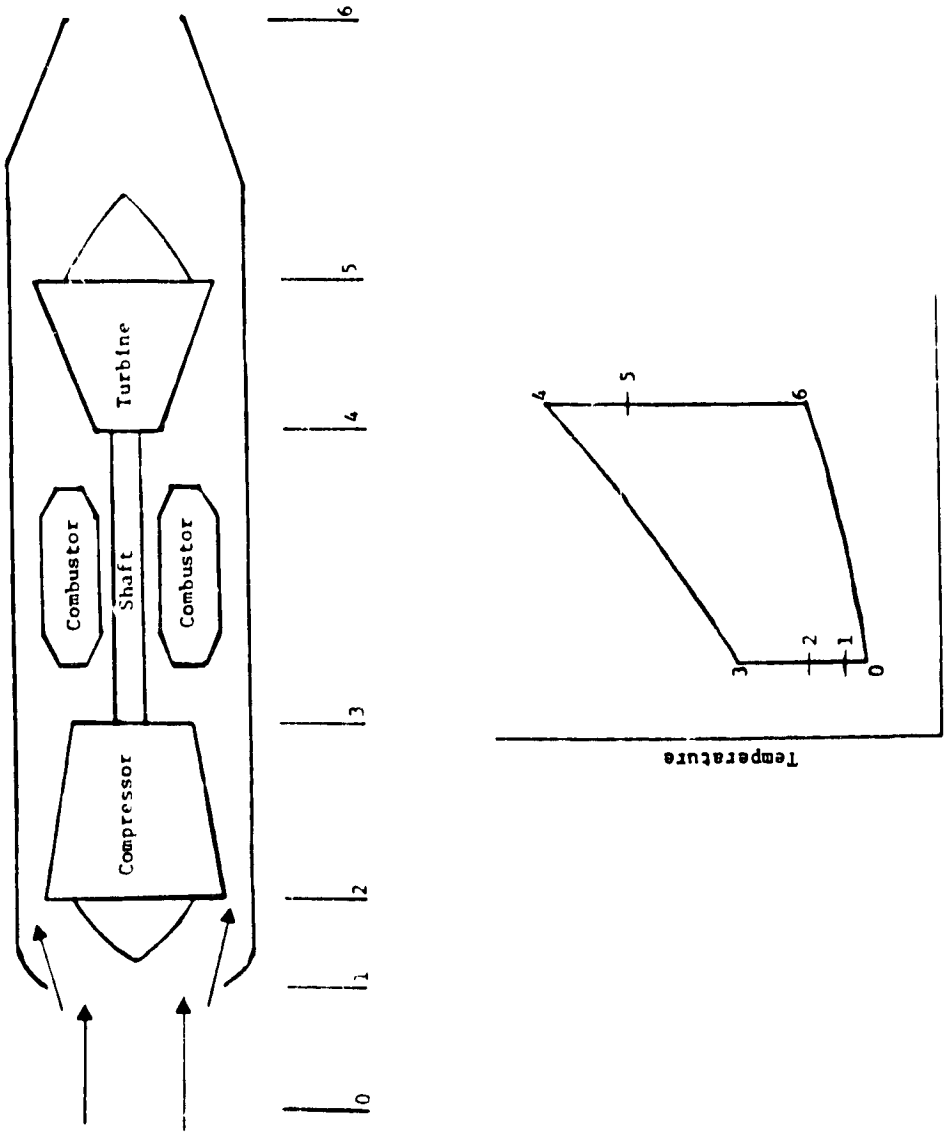

Figure 1.1. - Single spool jet engine and ideal fluid process cycle.

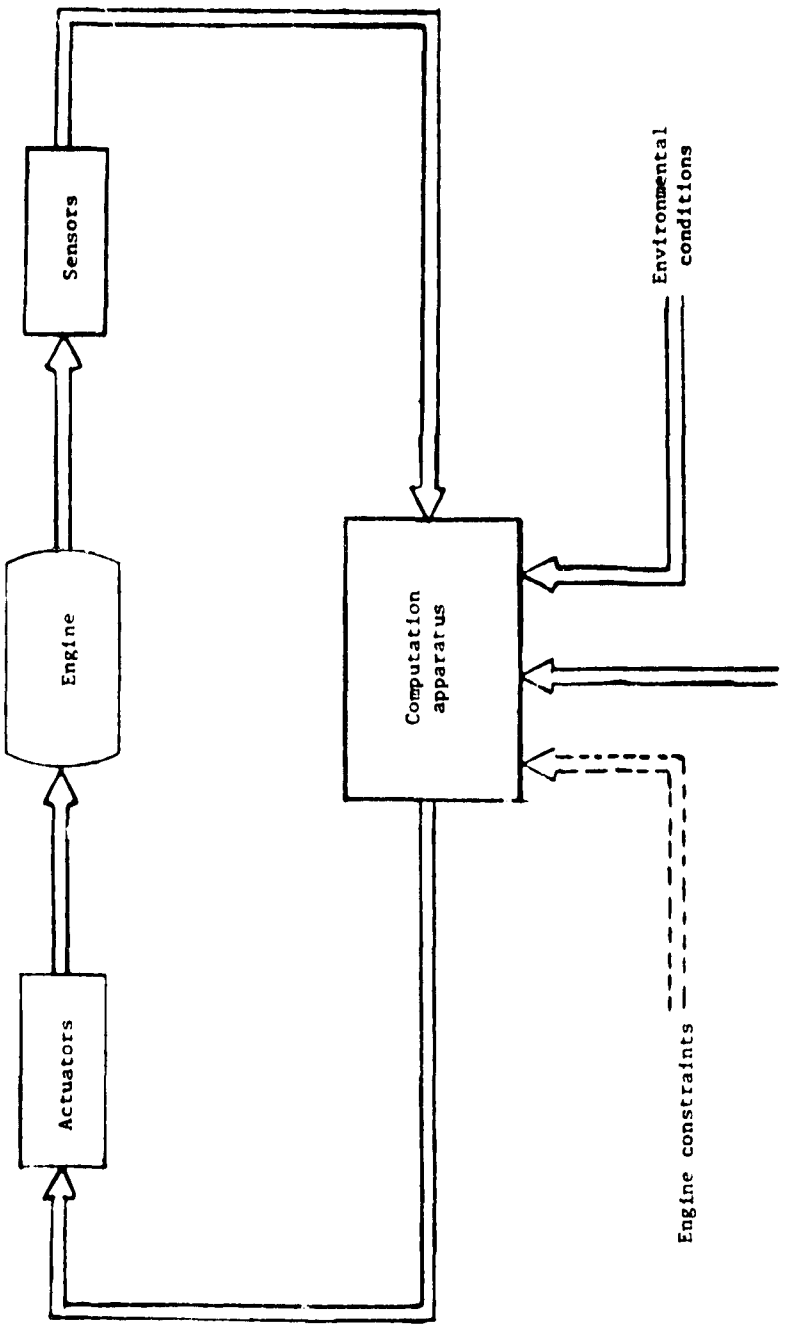

Figure 1.2. - Typical engine control configuration.

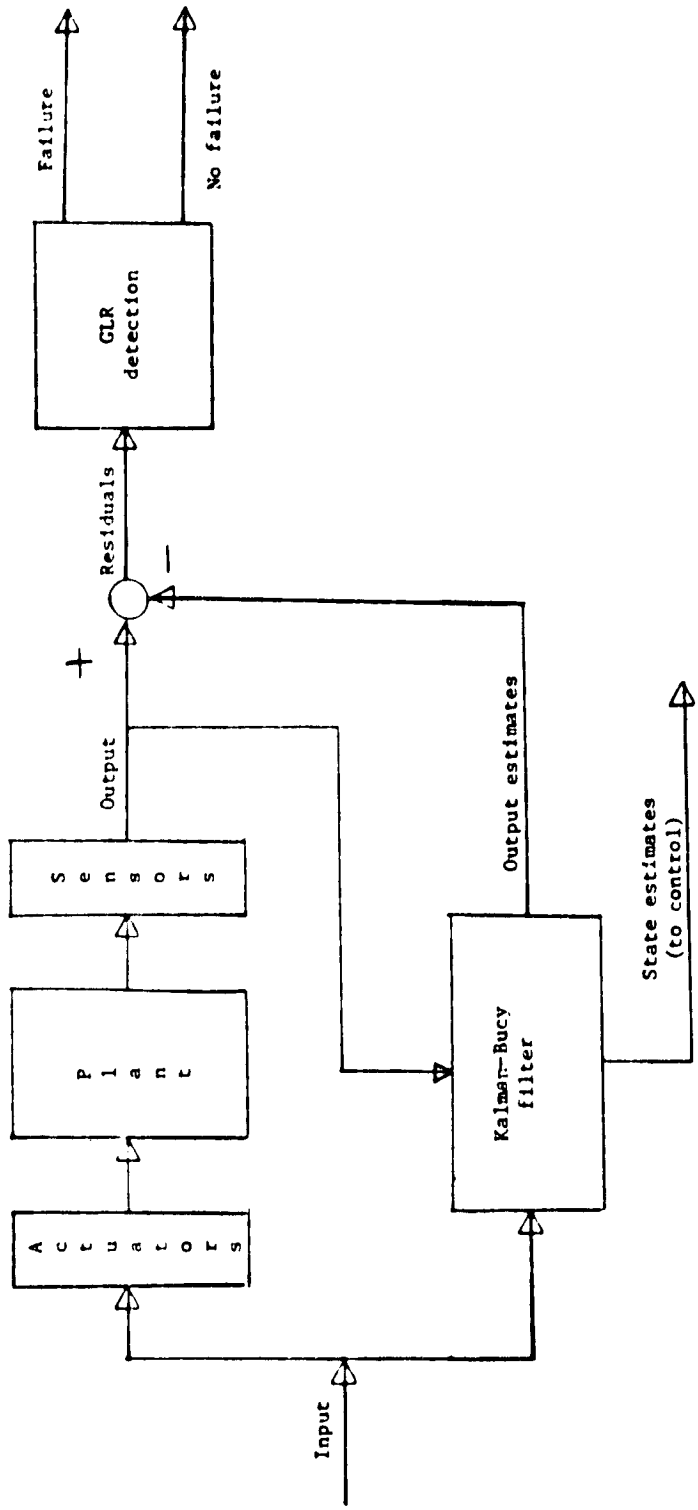

Figure 2.1. - Failure detection with Kalman-Bucy filter.

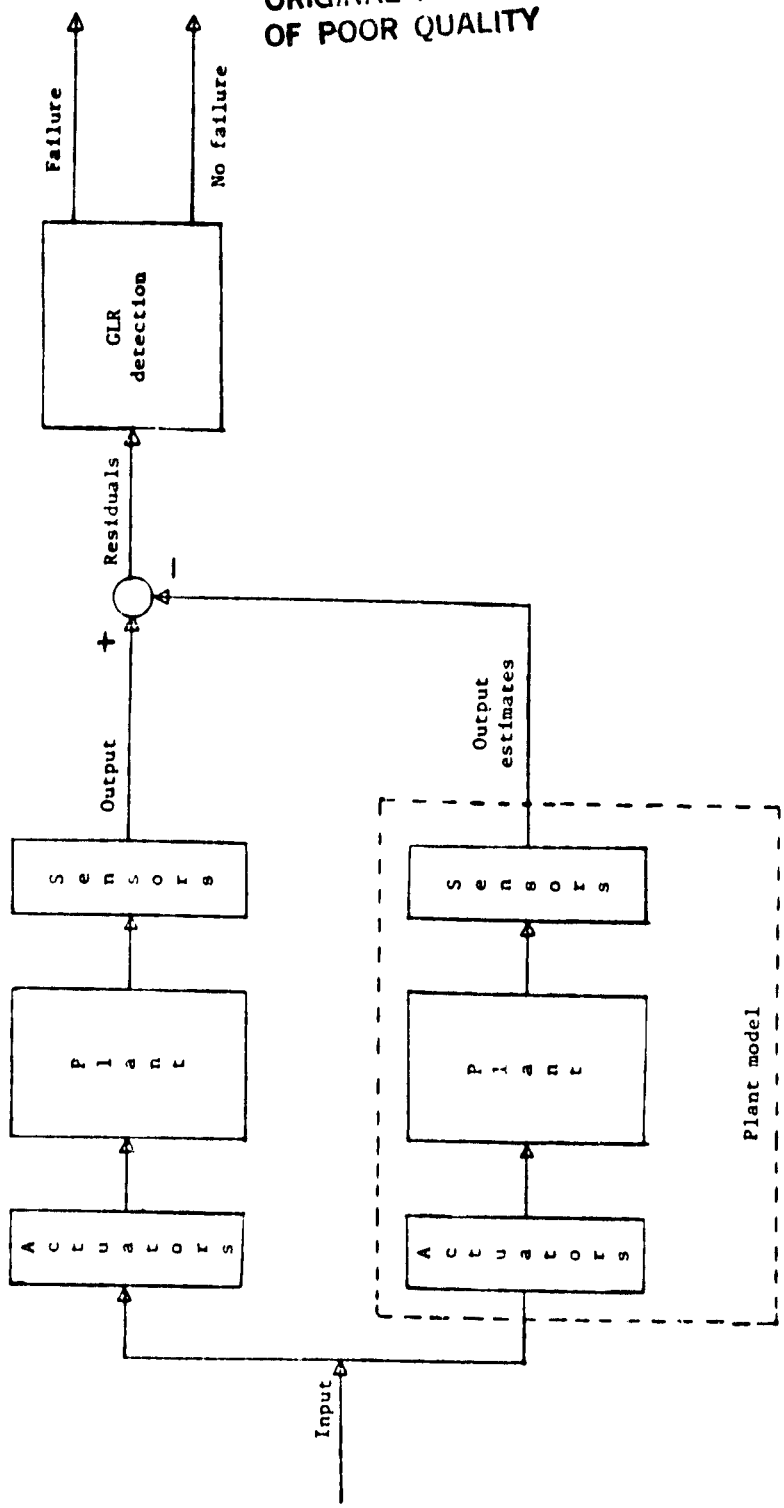

Figure 2.2. - Failure detection with plant model.

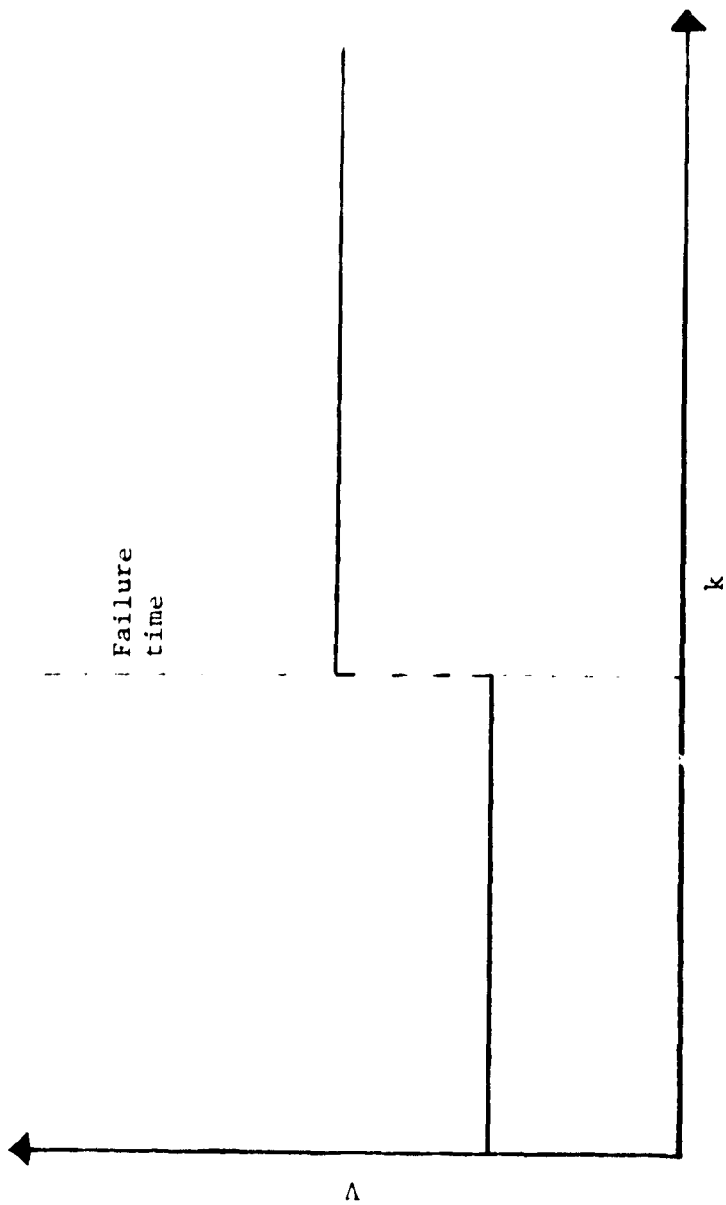

Figure 2.3. - Change in sensor noise variance due to a sensor soft failure.

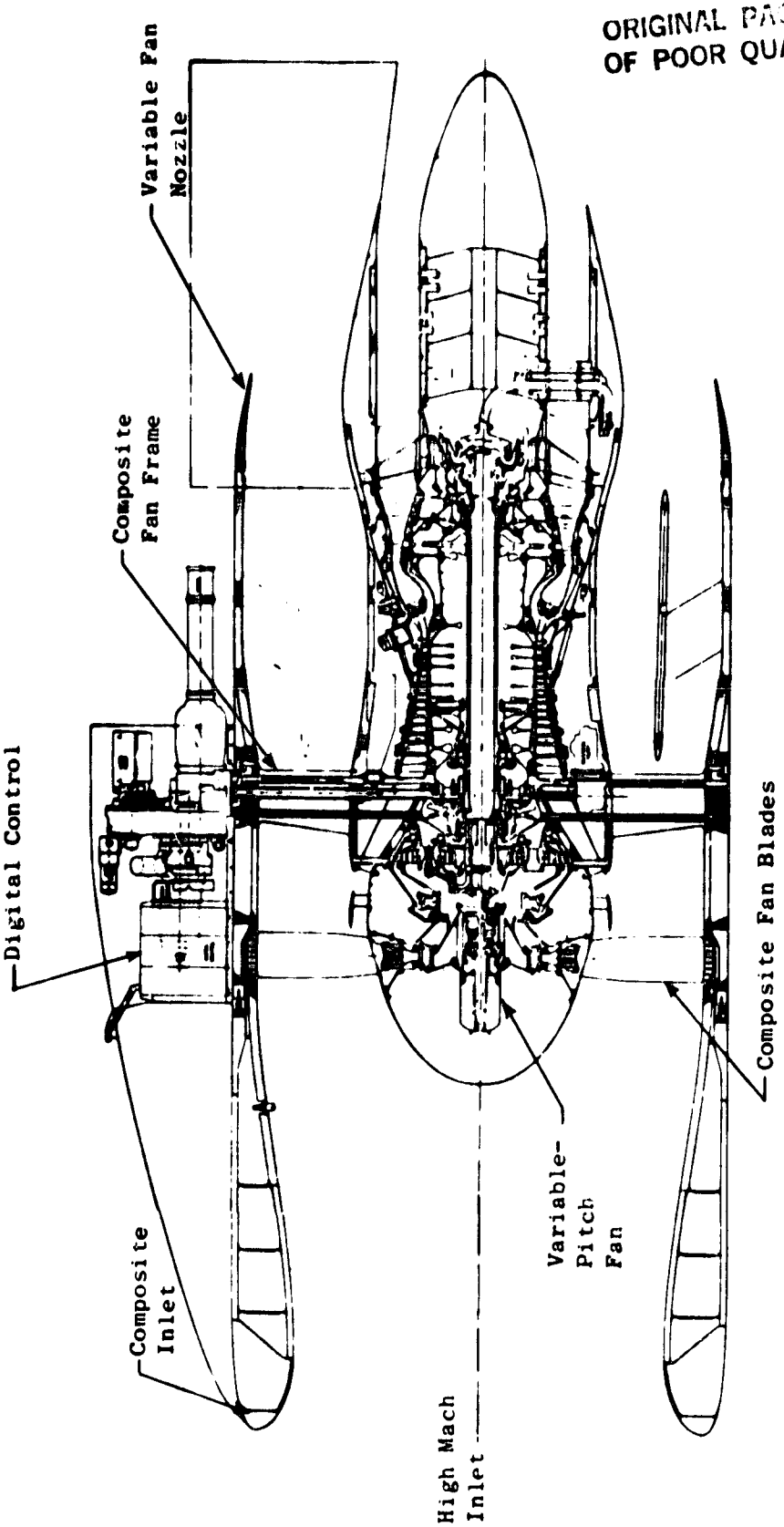

Figure 4.1. - UTW experimental propulsion system.

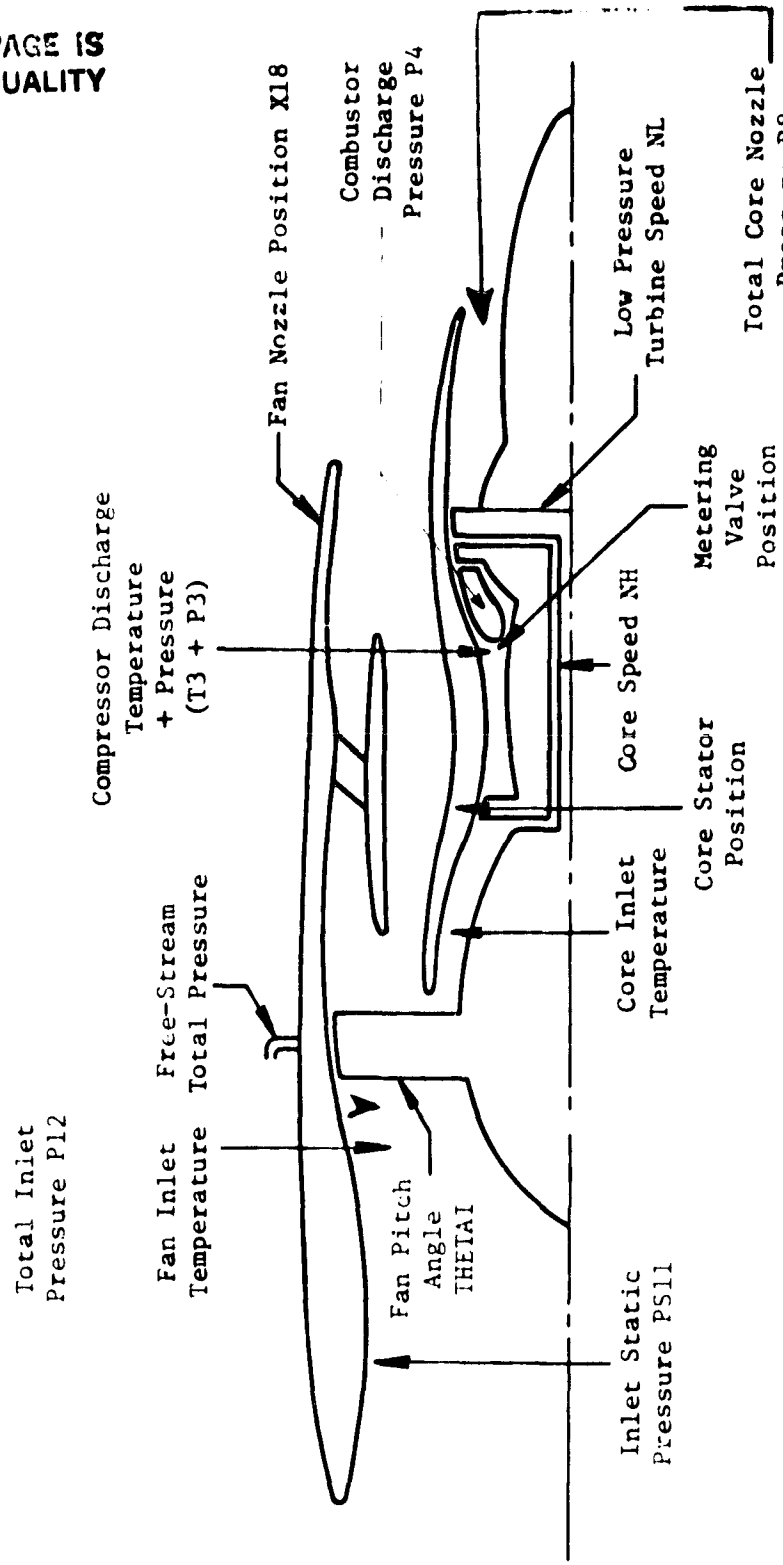

Figure 4.2. - Sensed engine and control variables.

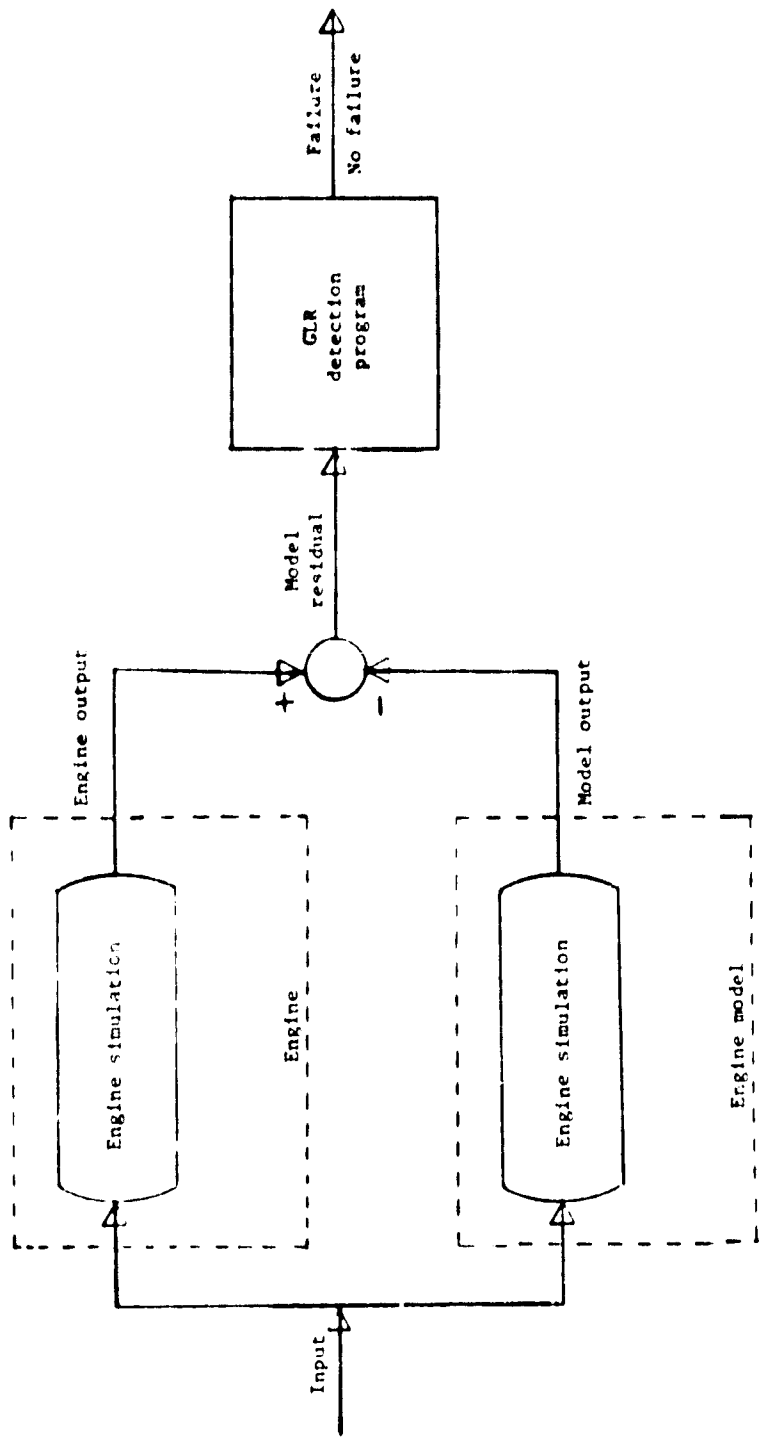

Figure 4.3. - QCSEE sensor/actuator failure detection plan using two nonlinear engine simulation programs.

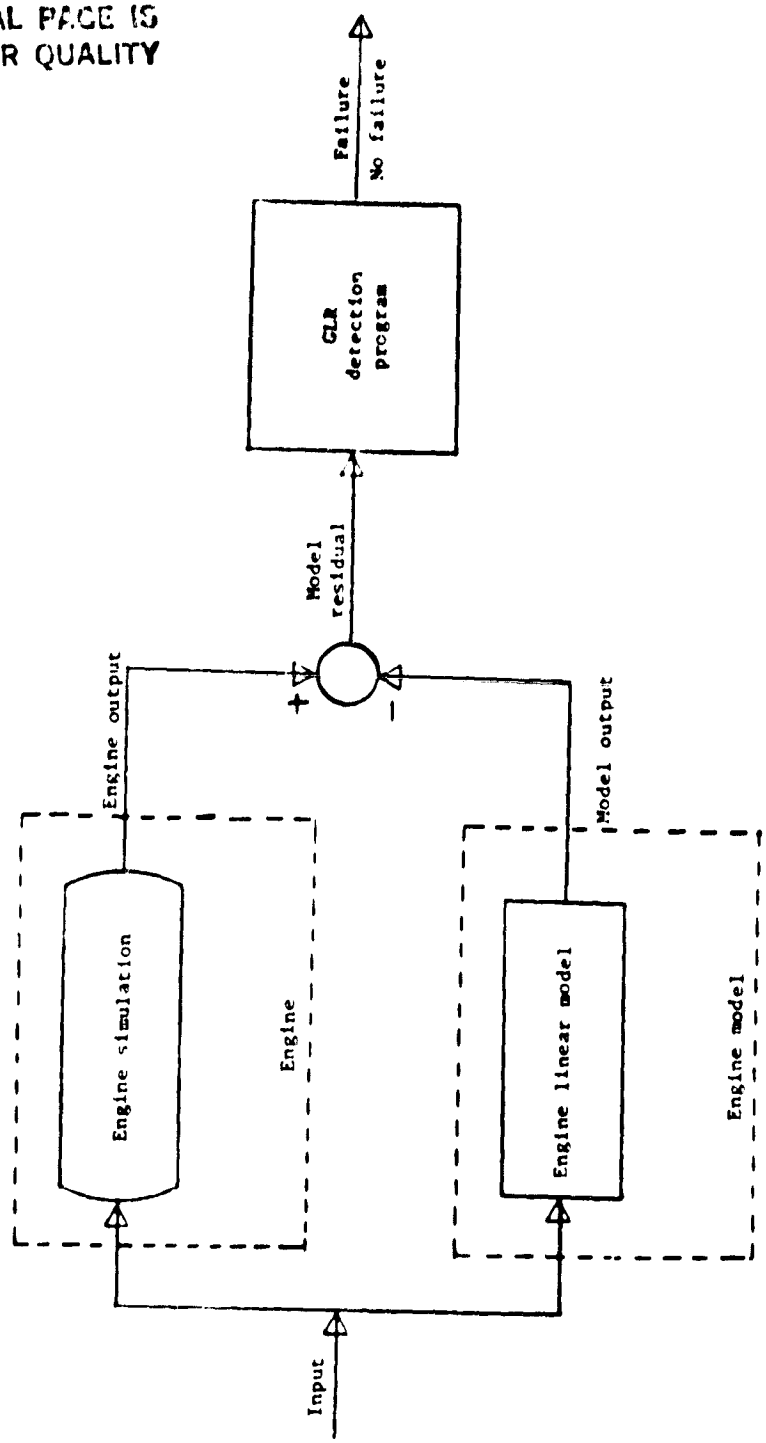

Figure 4.4. - QCSEE sensor/actuator failure detection plan using linear engine model.

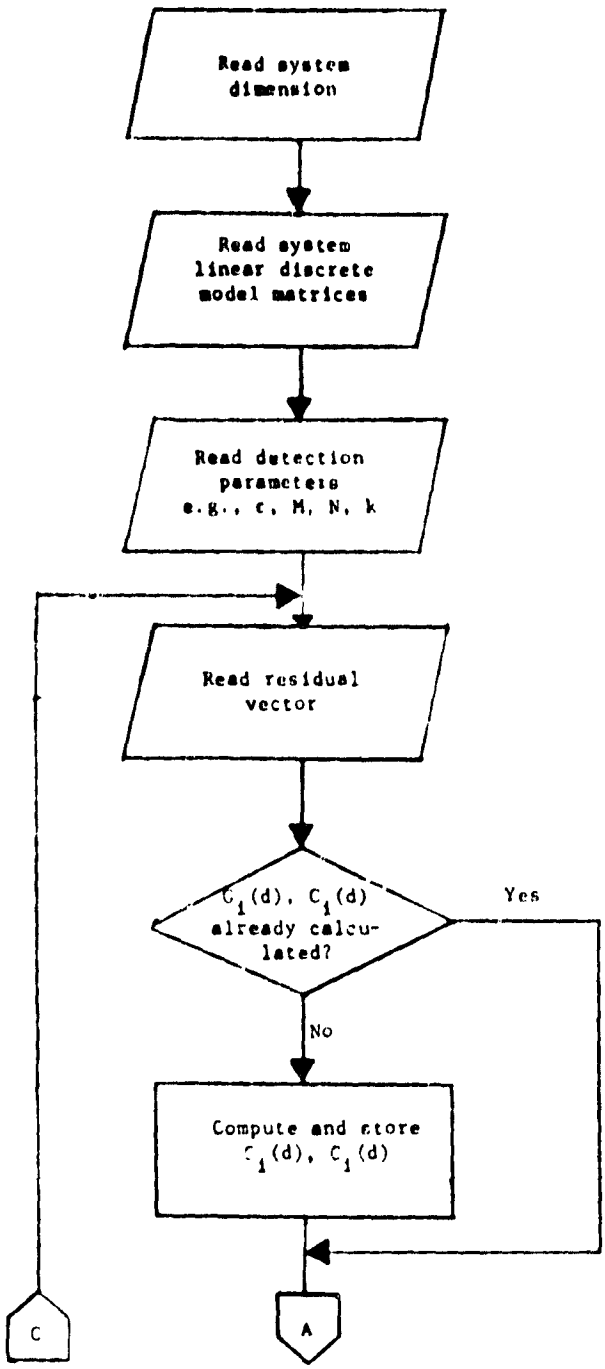

Figure 4.5. - Logic flow diagram for the GLR detection program.

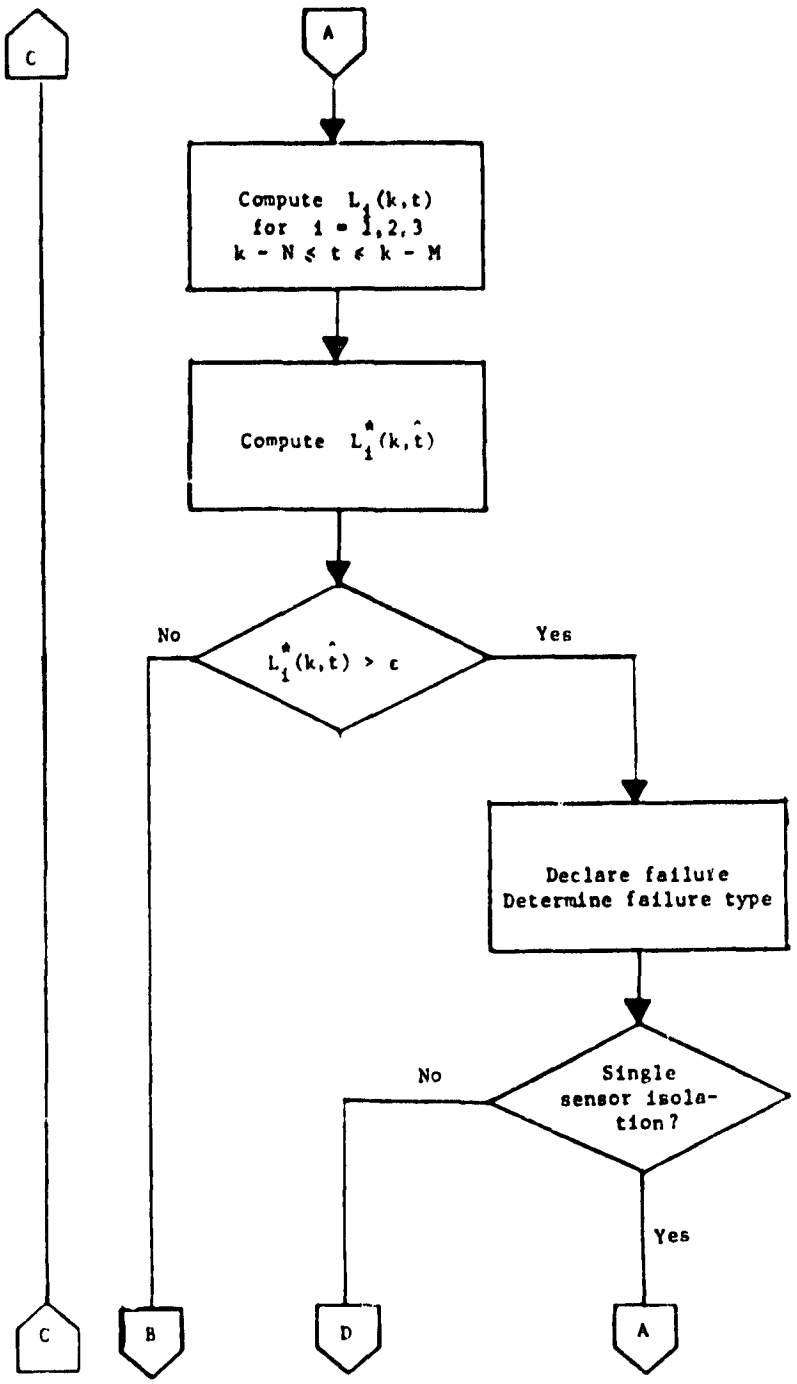

Figure 4.5 - Continued. Logic flow diagram for the GLR detection program.

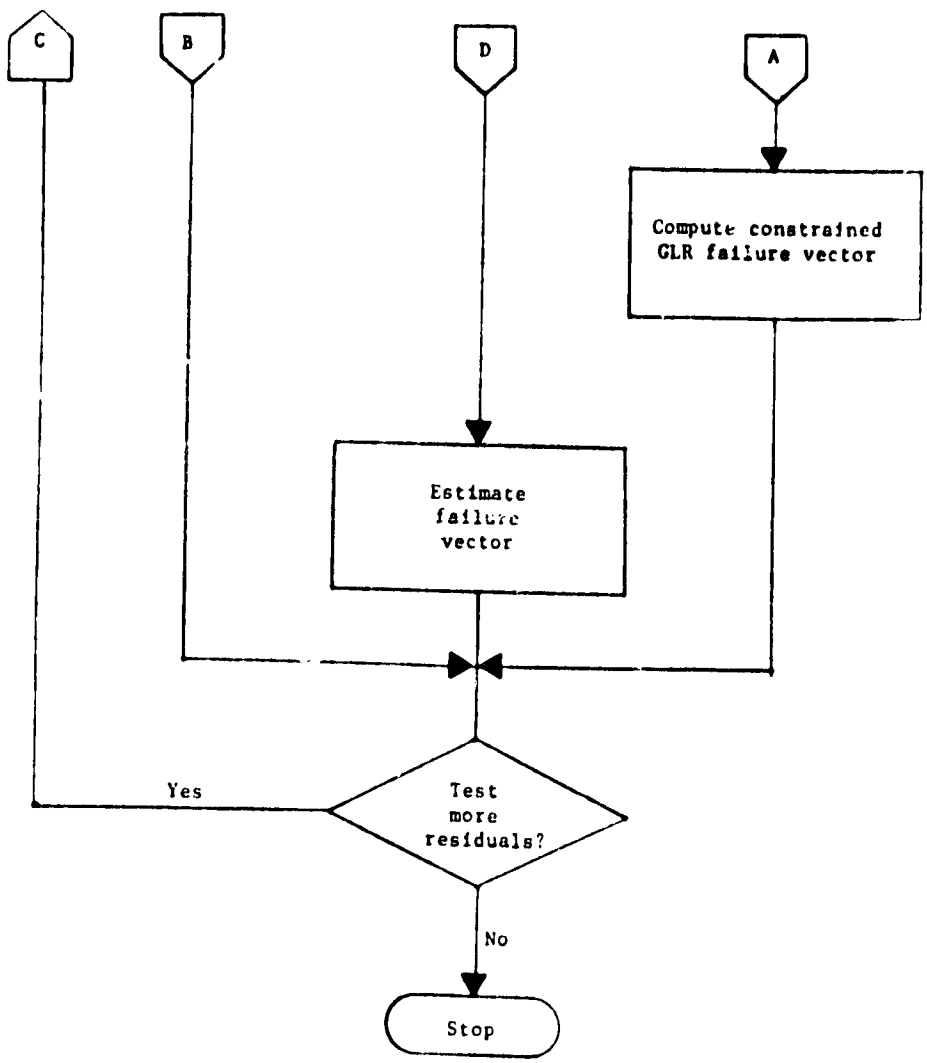

Figure 4.5 - Concluded. Logic flow diagram for the GLR detection program.

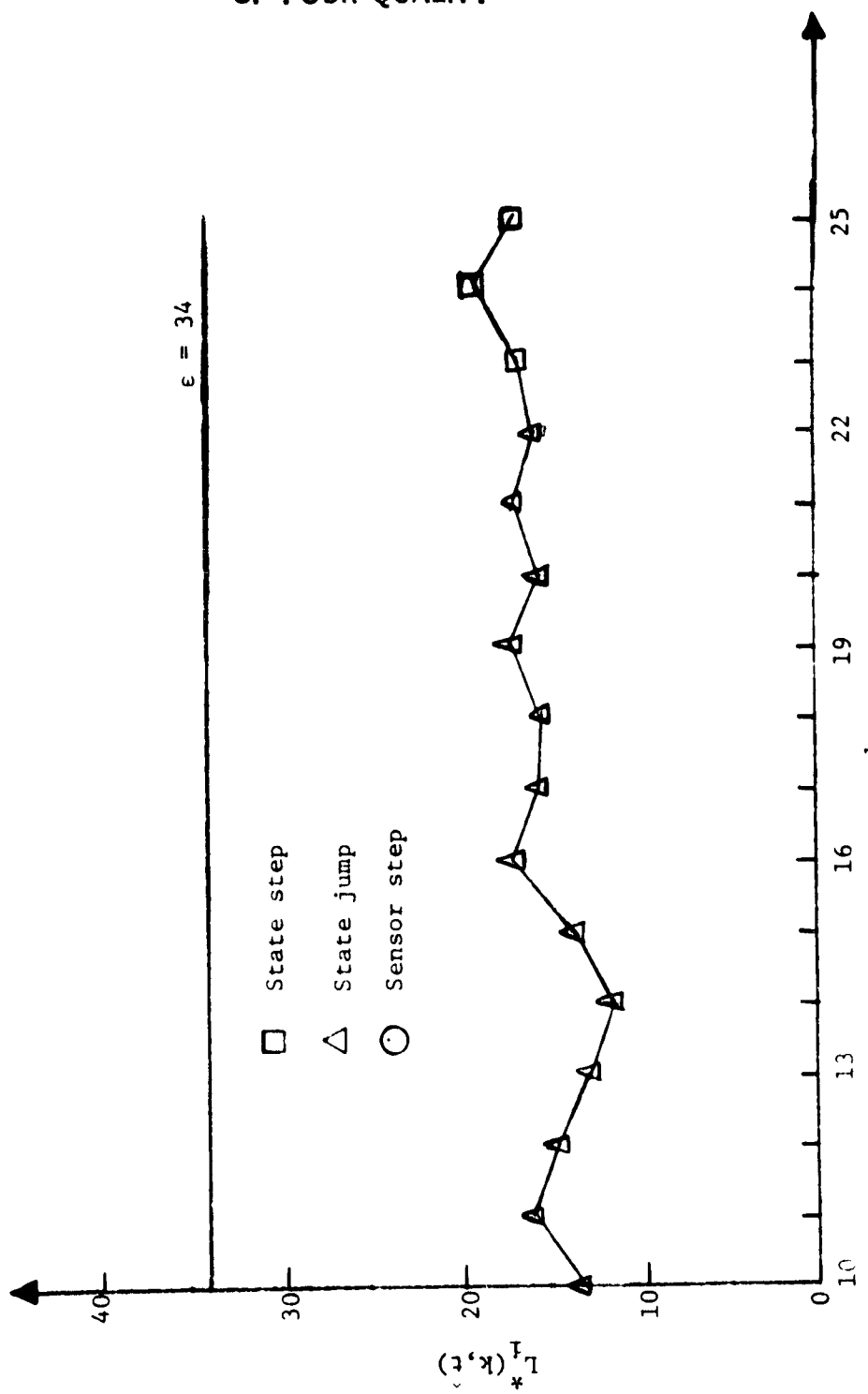

Figure 4.8. - Evolution of maximum GLR index when no failure has occurred (first noise sequence).

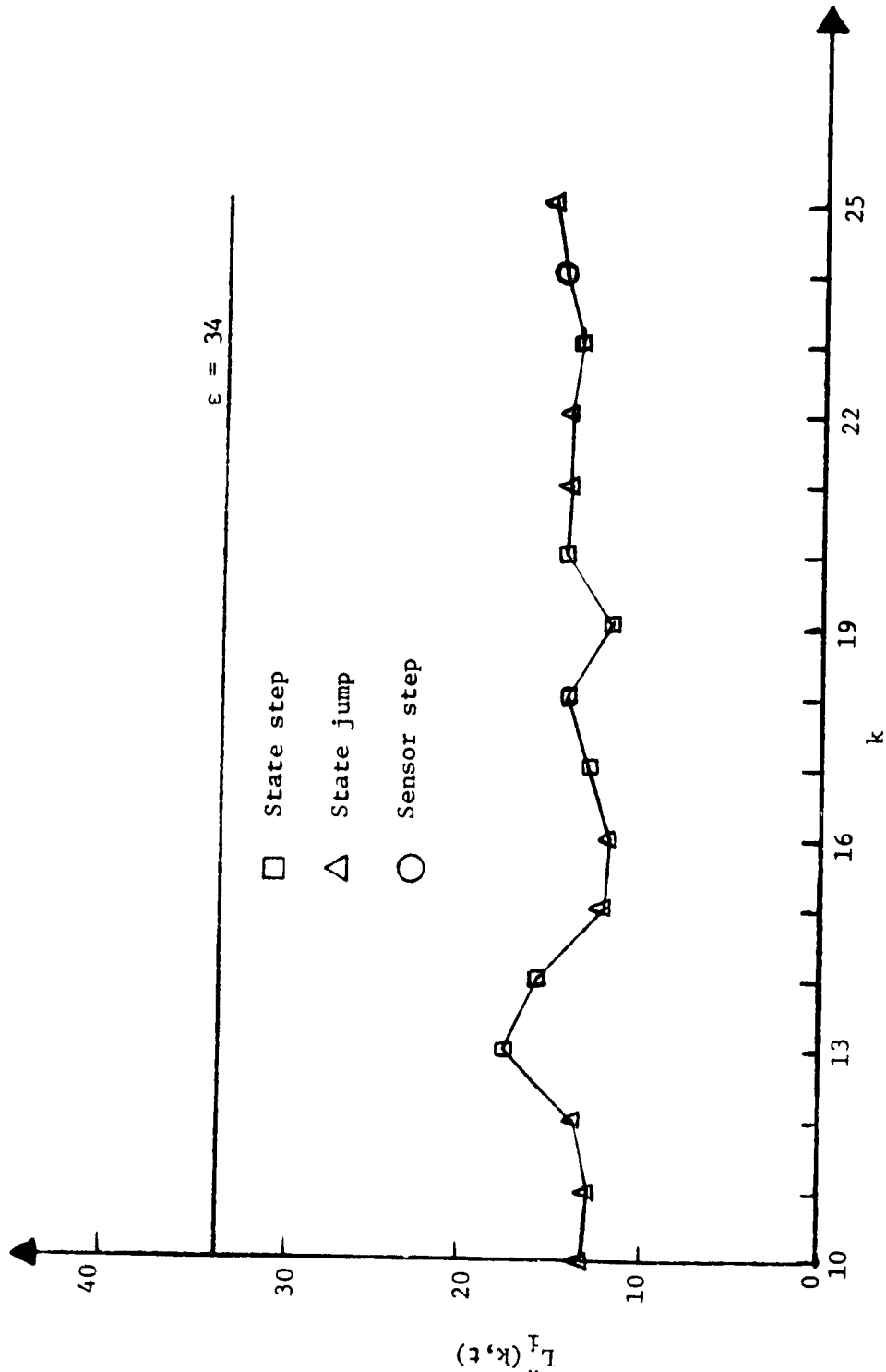

Figure 4.7. - Evolution of maximum GLR index when no failure has occurred (second noise sequence).

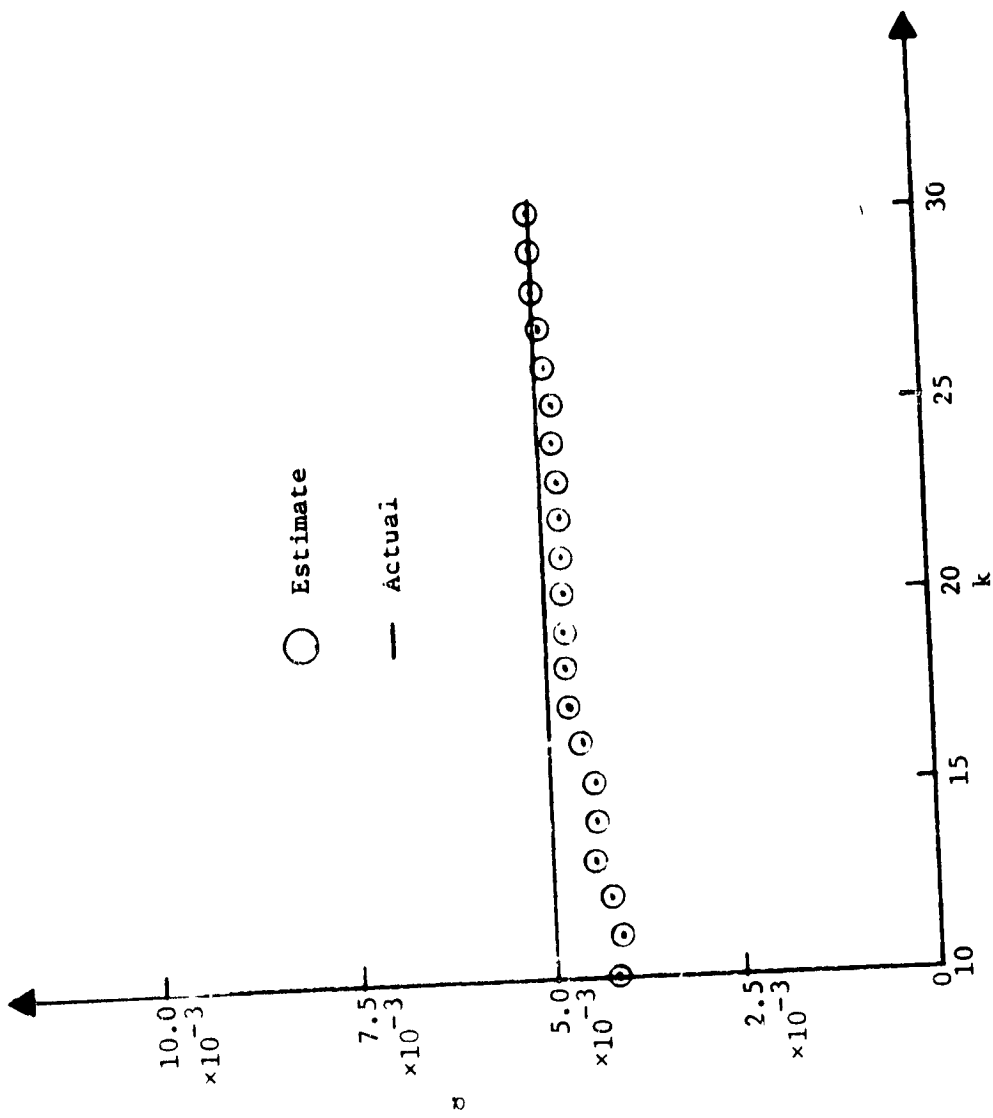

Figure 4.8. - Plot of actual failure size and the estimate of failure size for a single failure in PS11 sensor.

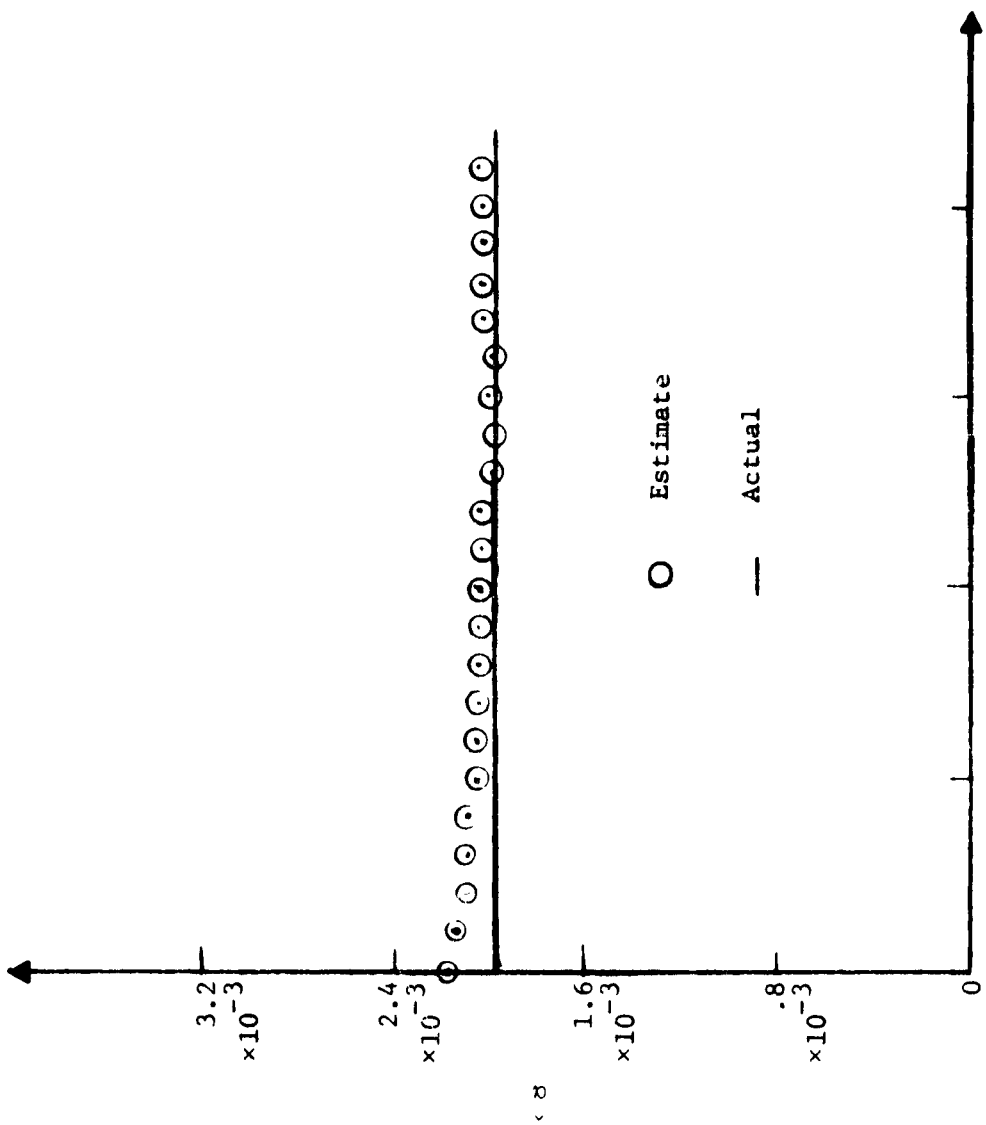

Figure 4.9. - Plot of failure size estimate in NL versus observation for single failure in NL.

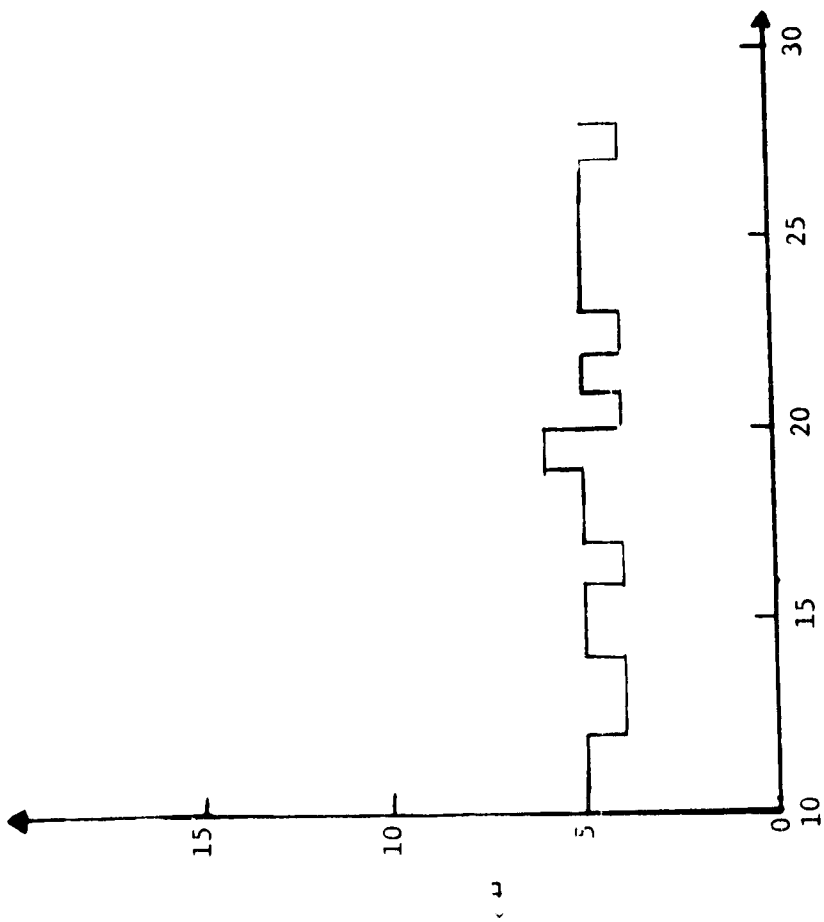

Figure 4.10. - Estimate of failure time versus observations for single step failure in THETA1.

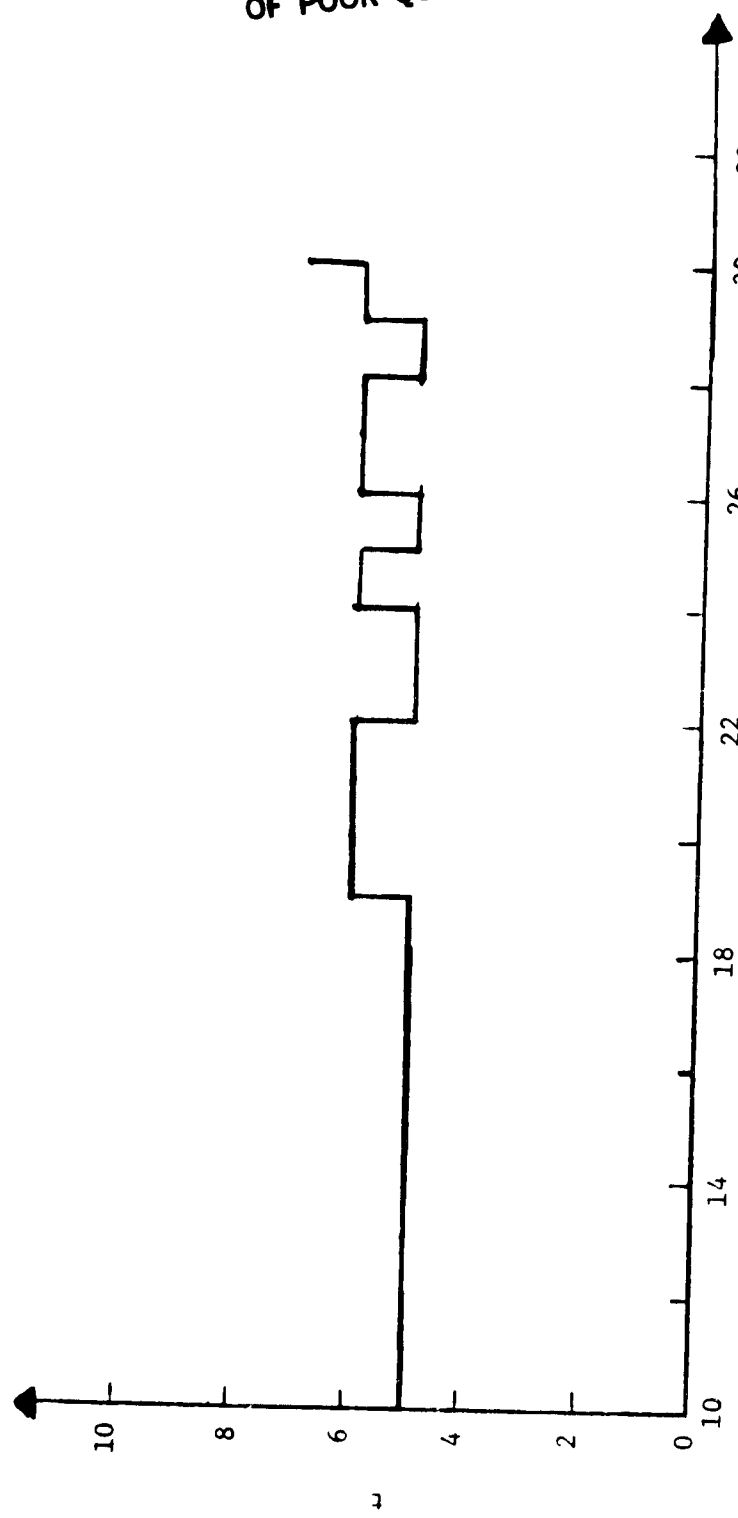

Figure 4.11. - Estimate of failure time versus observations for single-step failure in X18.

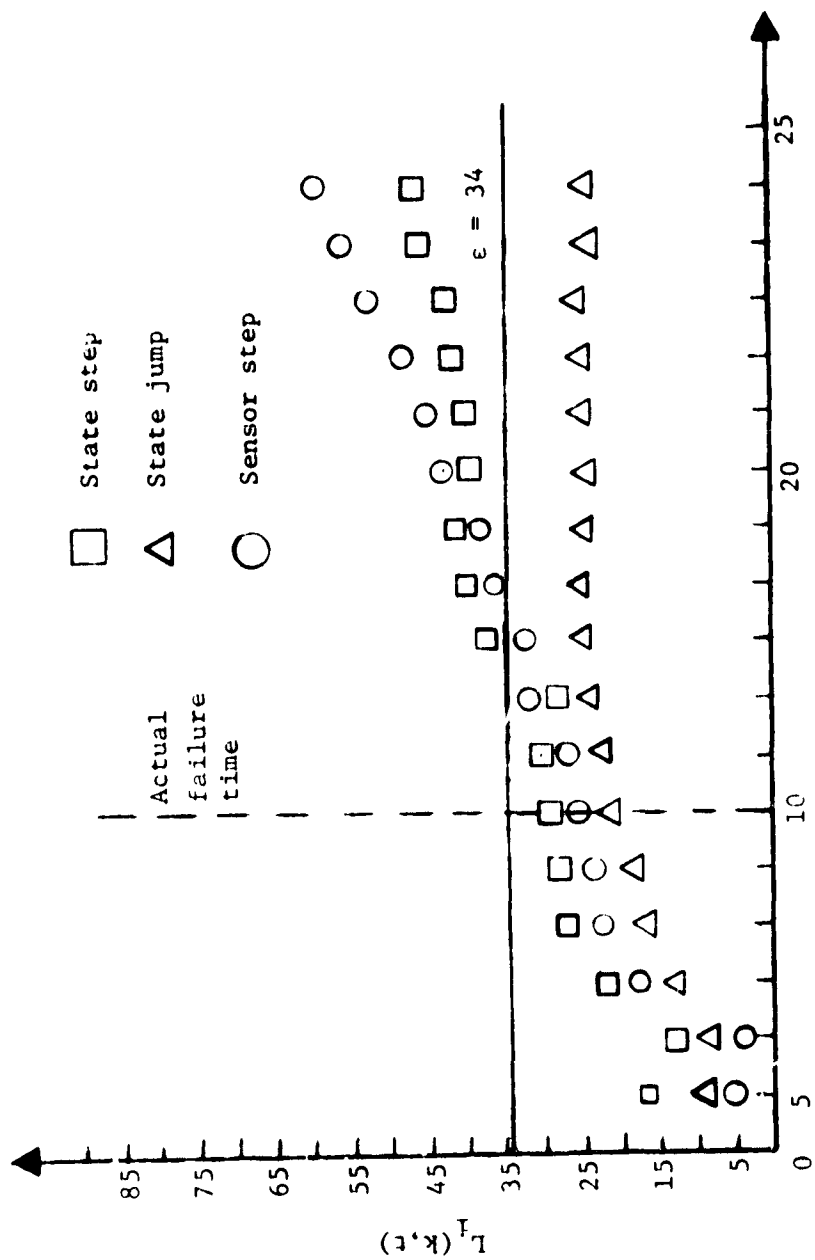

Figure 4.1.2. - Evolution of maximum GLR indices versus the number of observations for a hypothetical sensor failure case.

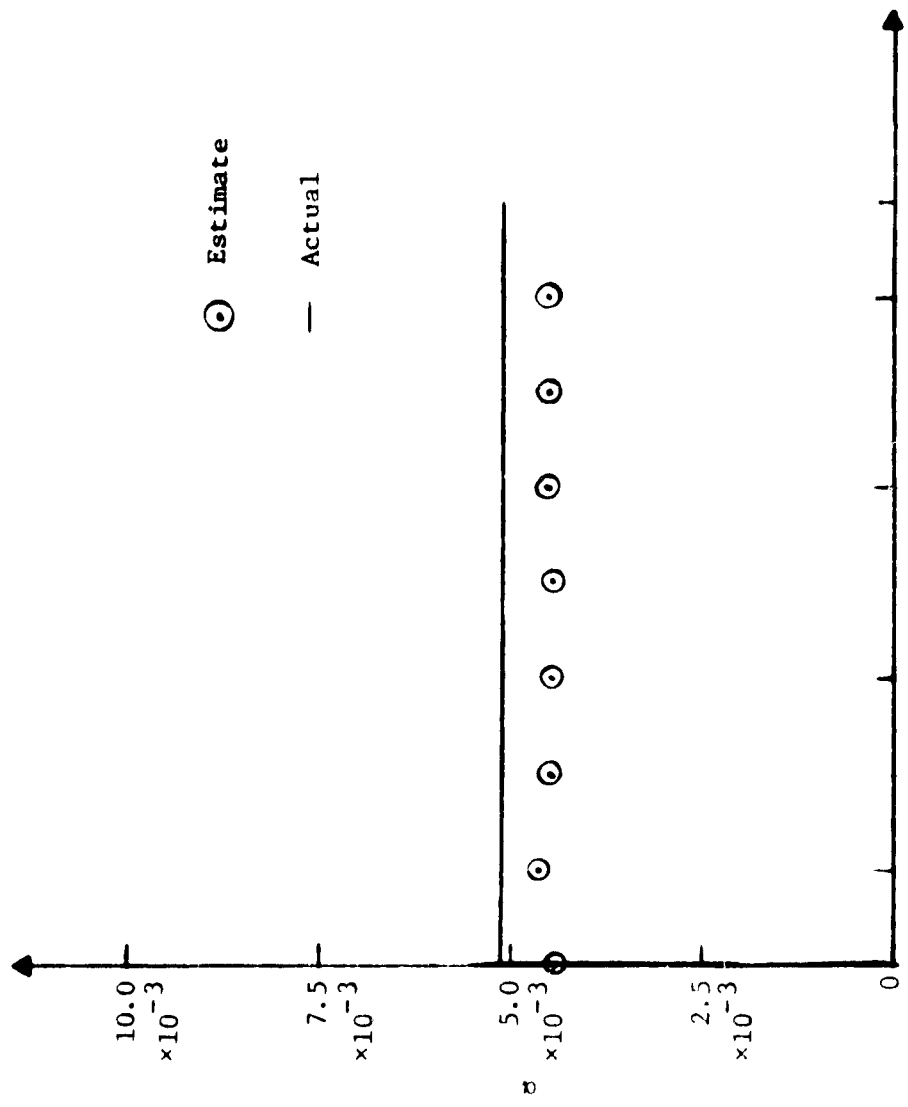

Figure 4.13. - Plot of the estimate of failure size for PS11 versus the number of observations.

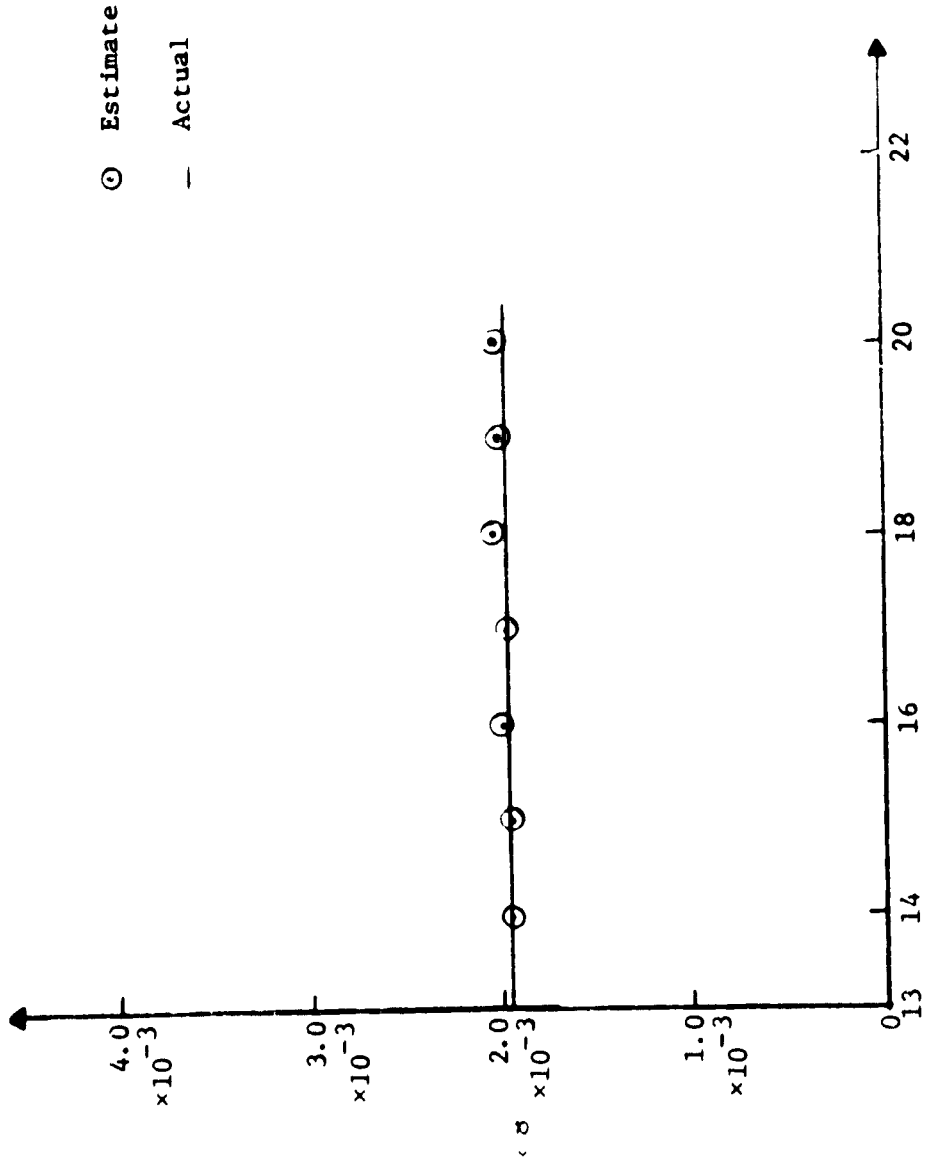

Figure 4.14. - Plot of the estimate of failure size for NH versus the number of observations.

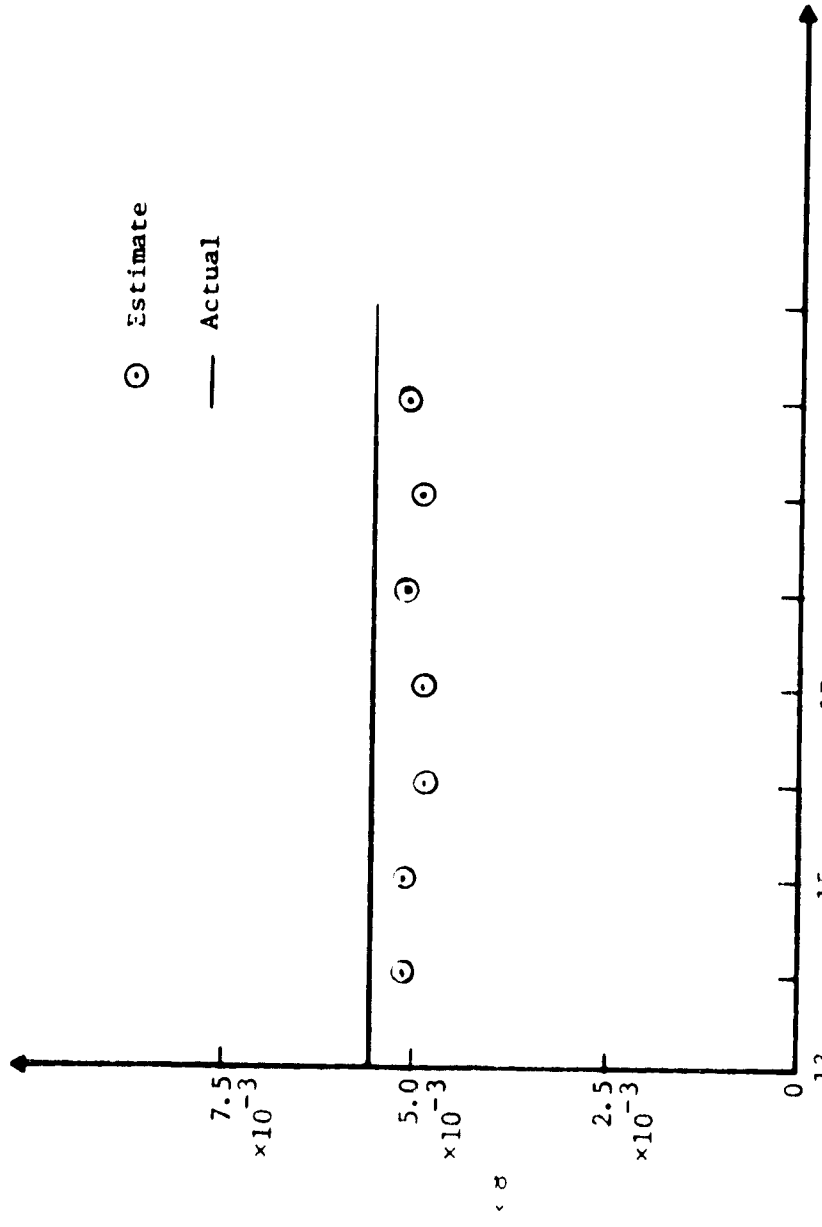

Figure 4.15. - Plot of the estimate of failure size in T3 versus observation for single failure in T3.

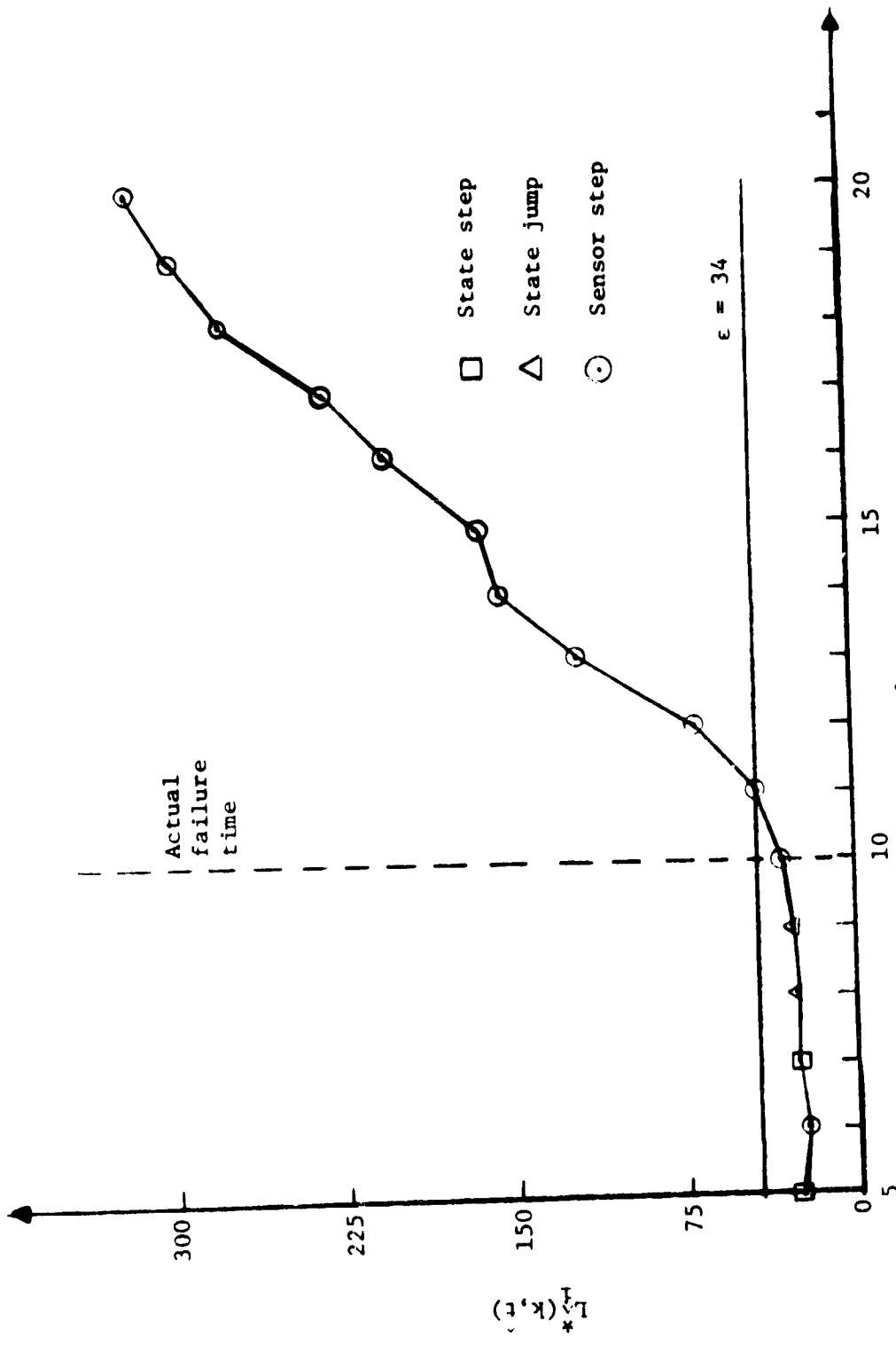

Figure 4.16. - Plot of maximum GLR index for sensor-step failure in PS11 versus observation number.

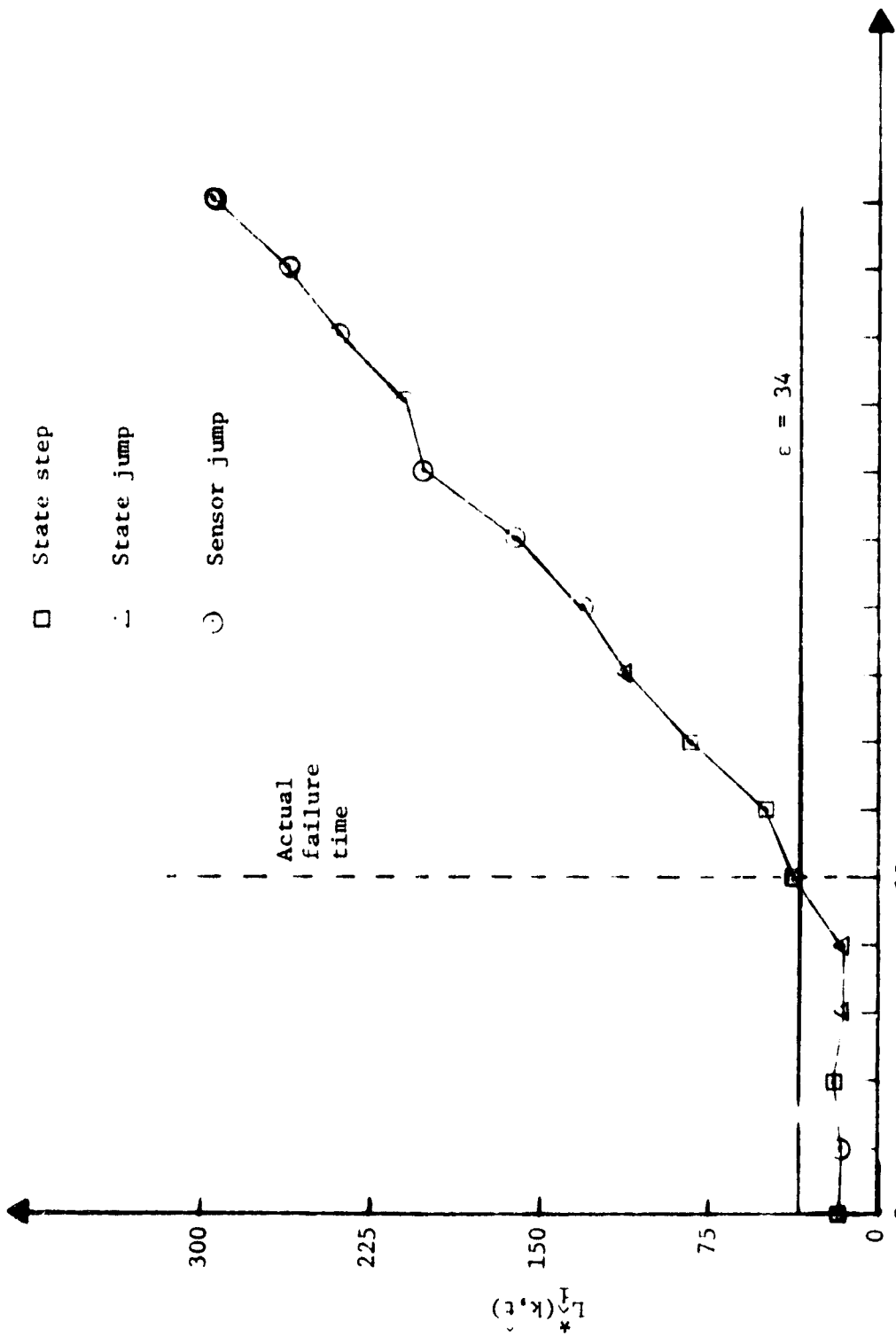

Figure 4.17. - Plot of maximum GLR index for NH sensor failure versus observation number.

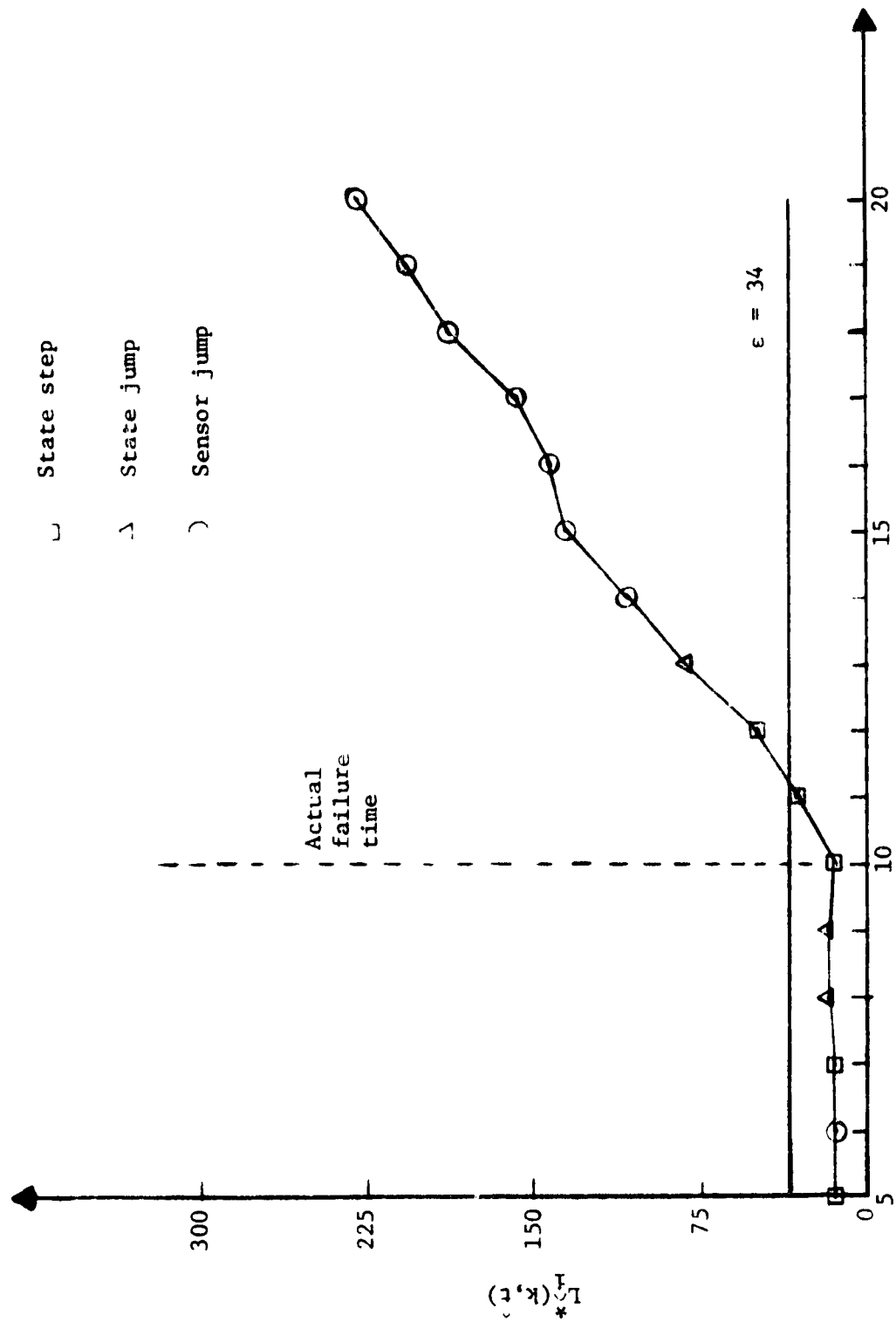

Figure 4.18. - Plot of maximum GLR index for sensor-step failure in T3 versus observation number.

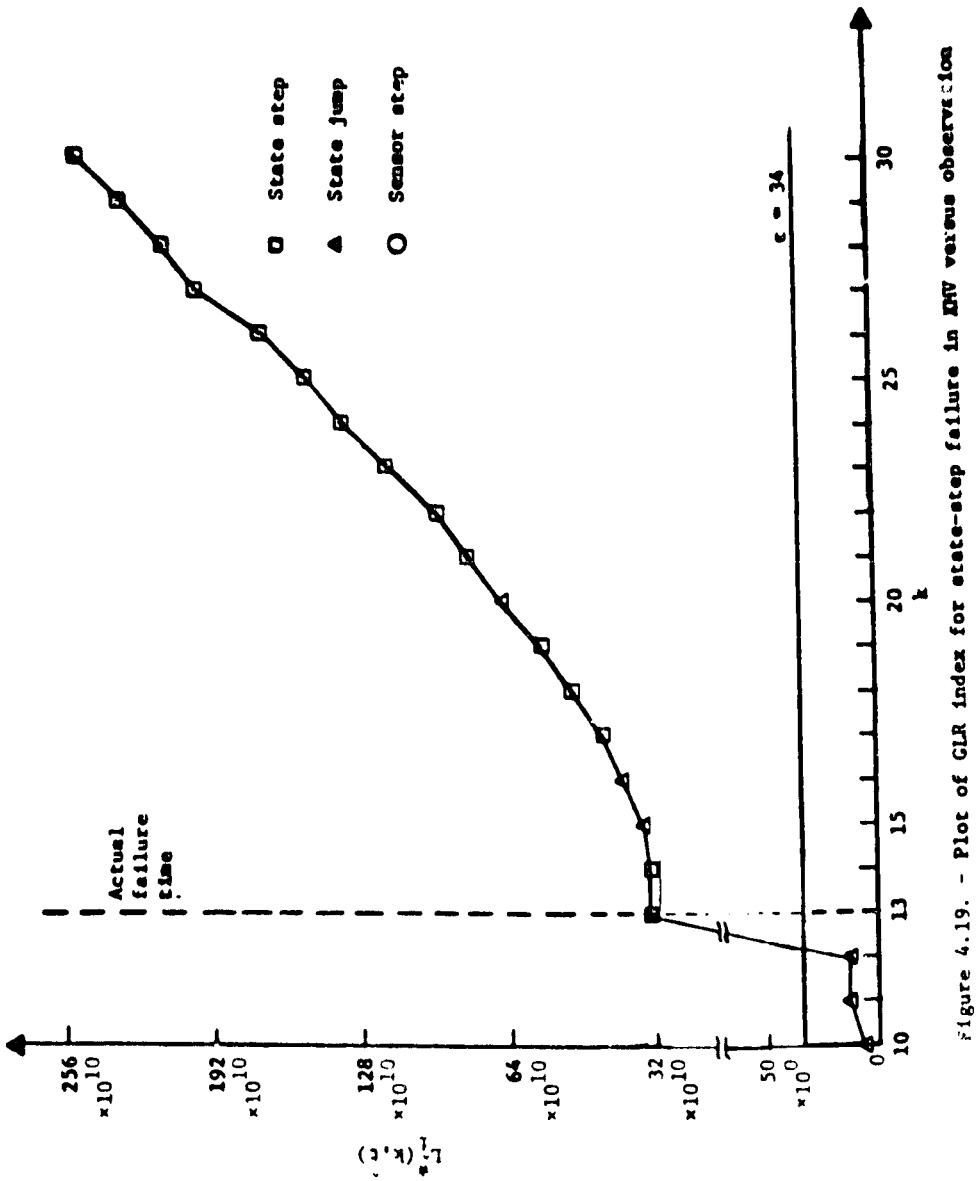

Figure 4.19. - Plot of GLR index for state-step failure in ENV versus observation number, k.

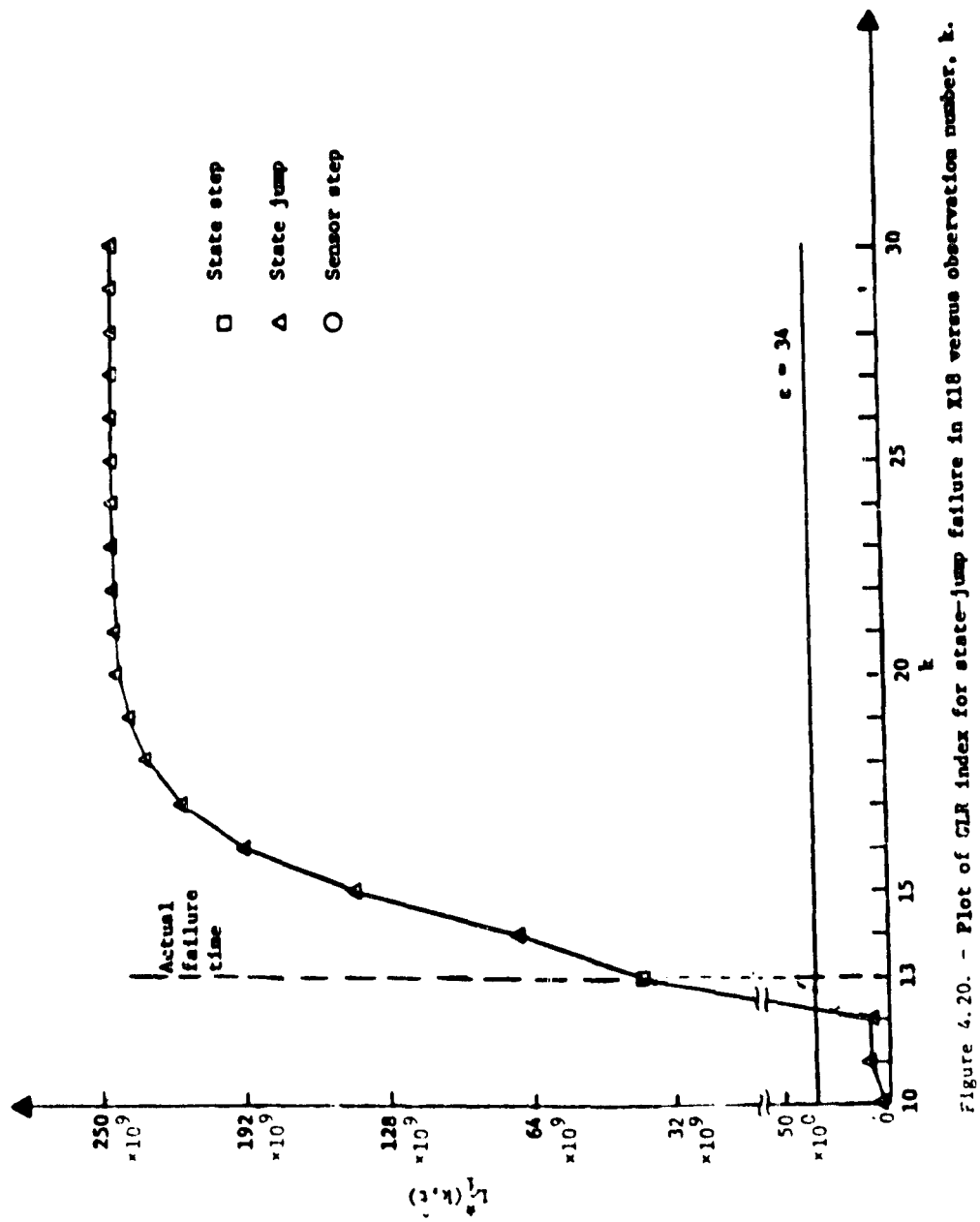

Figure 4.20. - Plot of GLR index for state-jump failure in X18 versus observation number, k.

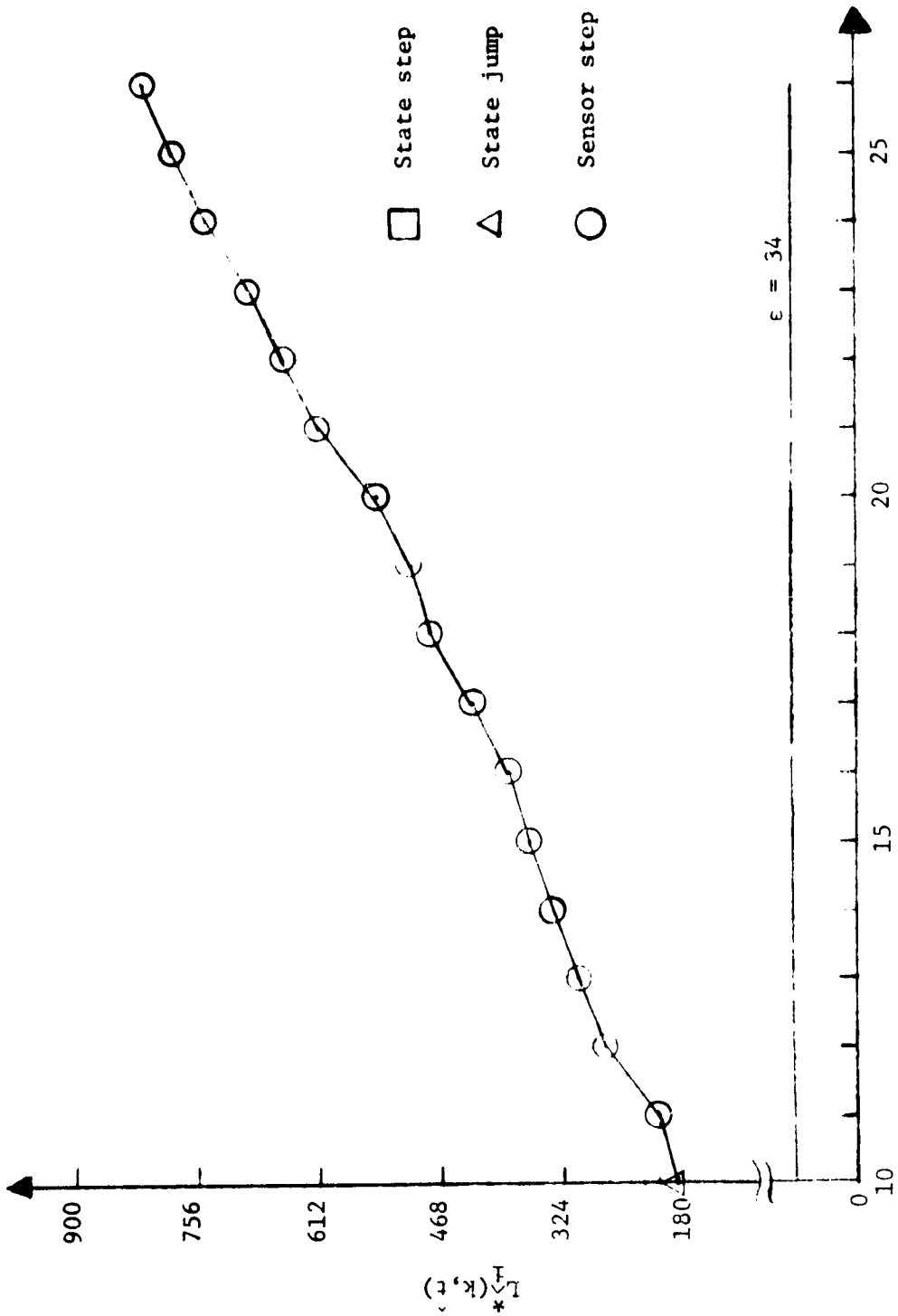

Figure 4.21. - Evolution of maximum GLR index for multiple failure in PS11 and NL sensors.

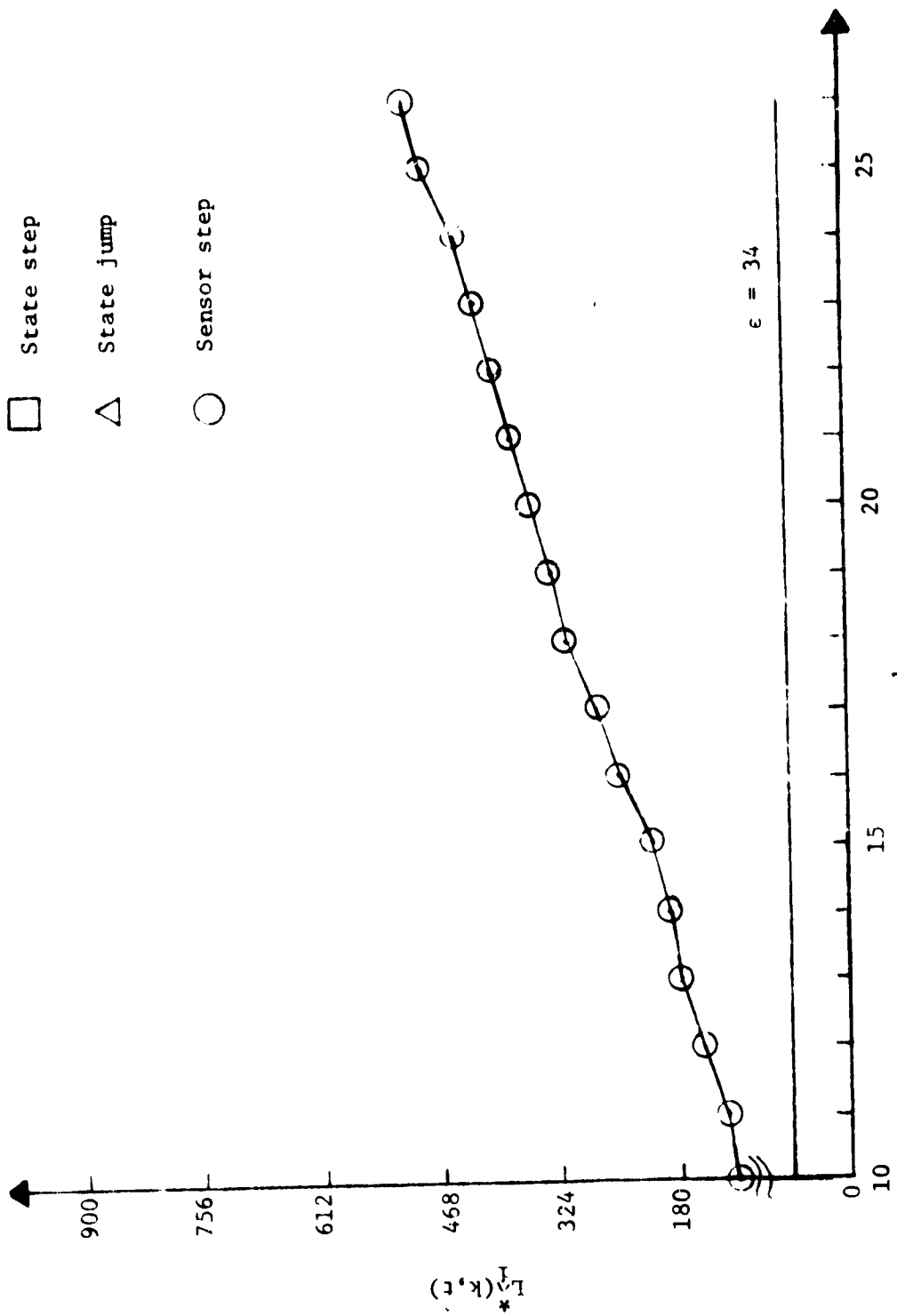

Figure 4.22. - Evolution of GLR index for single failure in PS11.

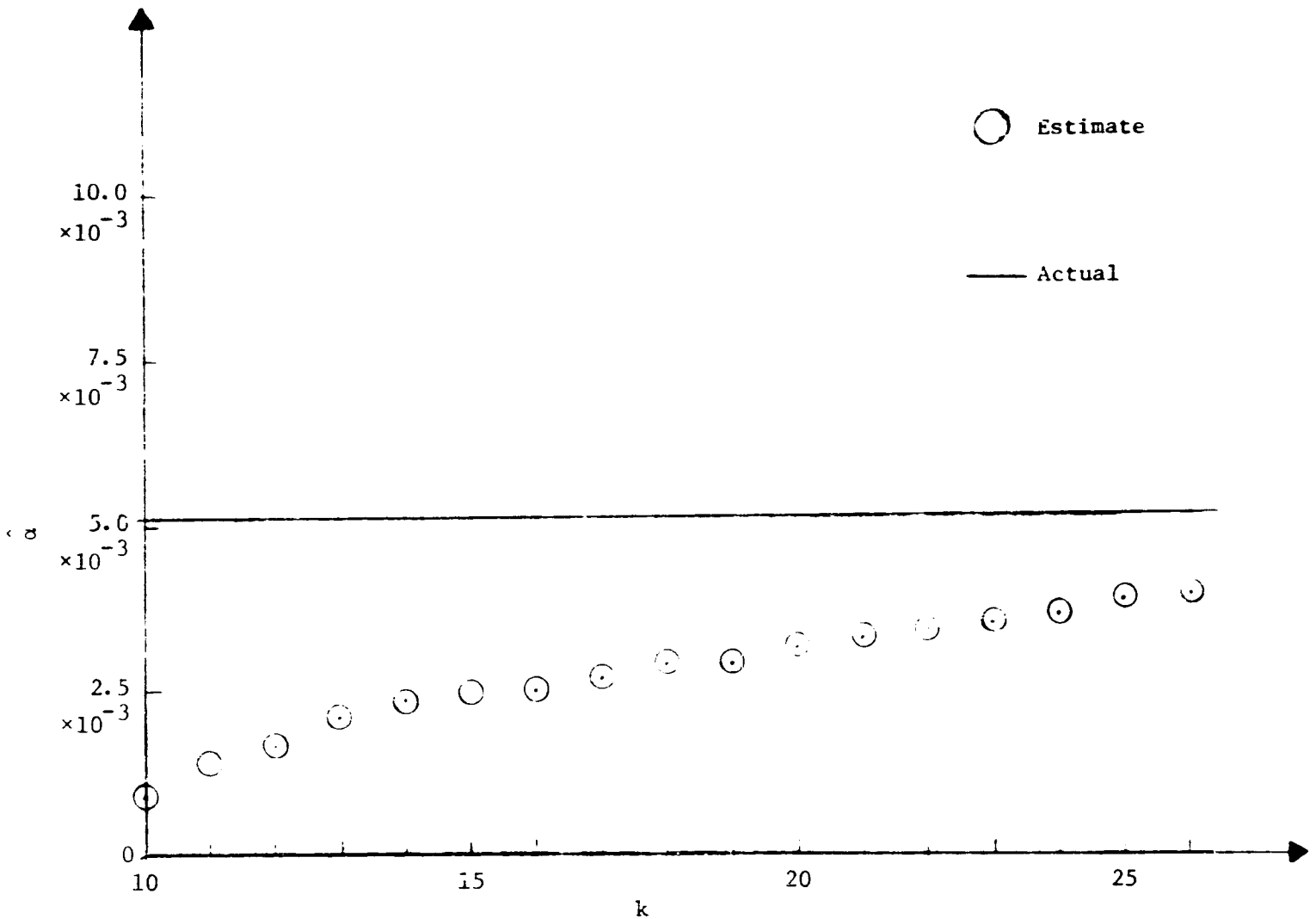

Figure 4.23. - Plot of the estimate of failure size in PS11 versus observation number k for simultaneous failures in PS11, NH, P12, and T3.

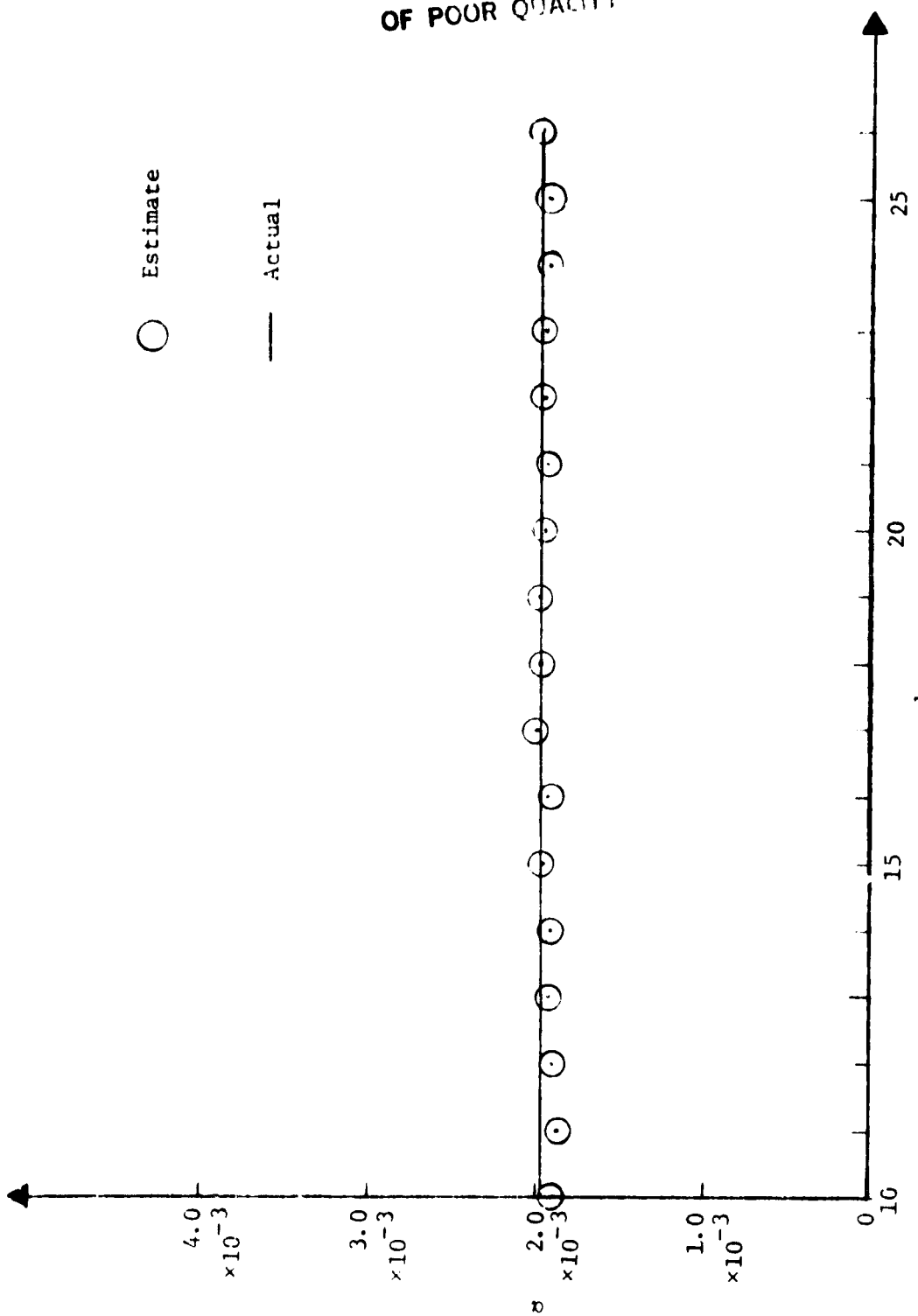

Figure 4.24. - Plot of the estimate of failure size NH versus observations for simultaneous failure in PS11, NH, P12, and T3.

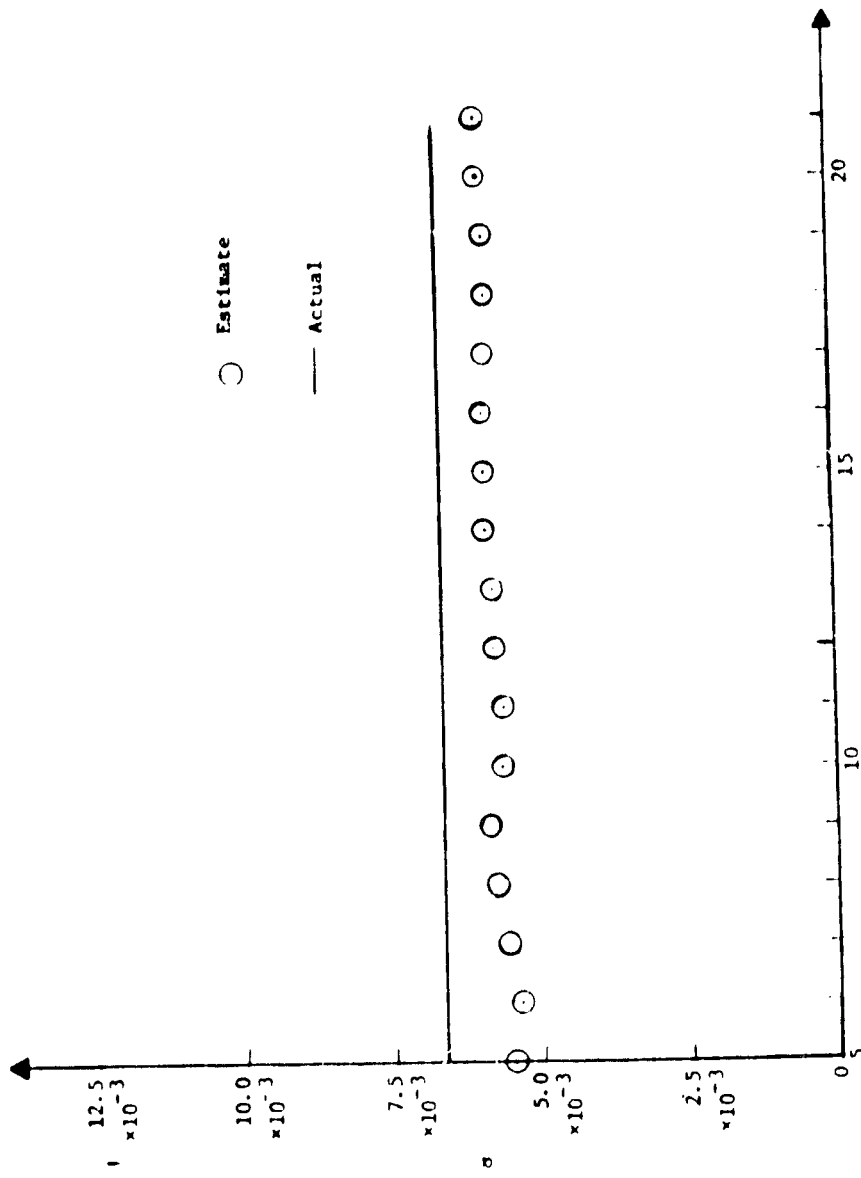

Figure 4.25. - Plot of the estimate of failure size in T2 versus observations for simultaneous failure in PS11, NH, PS11, and T3.

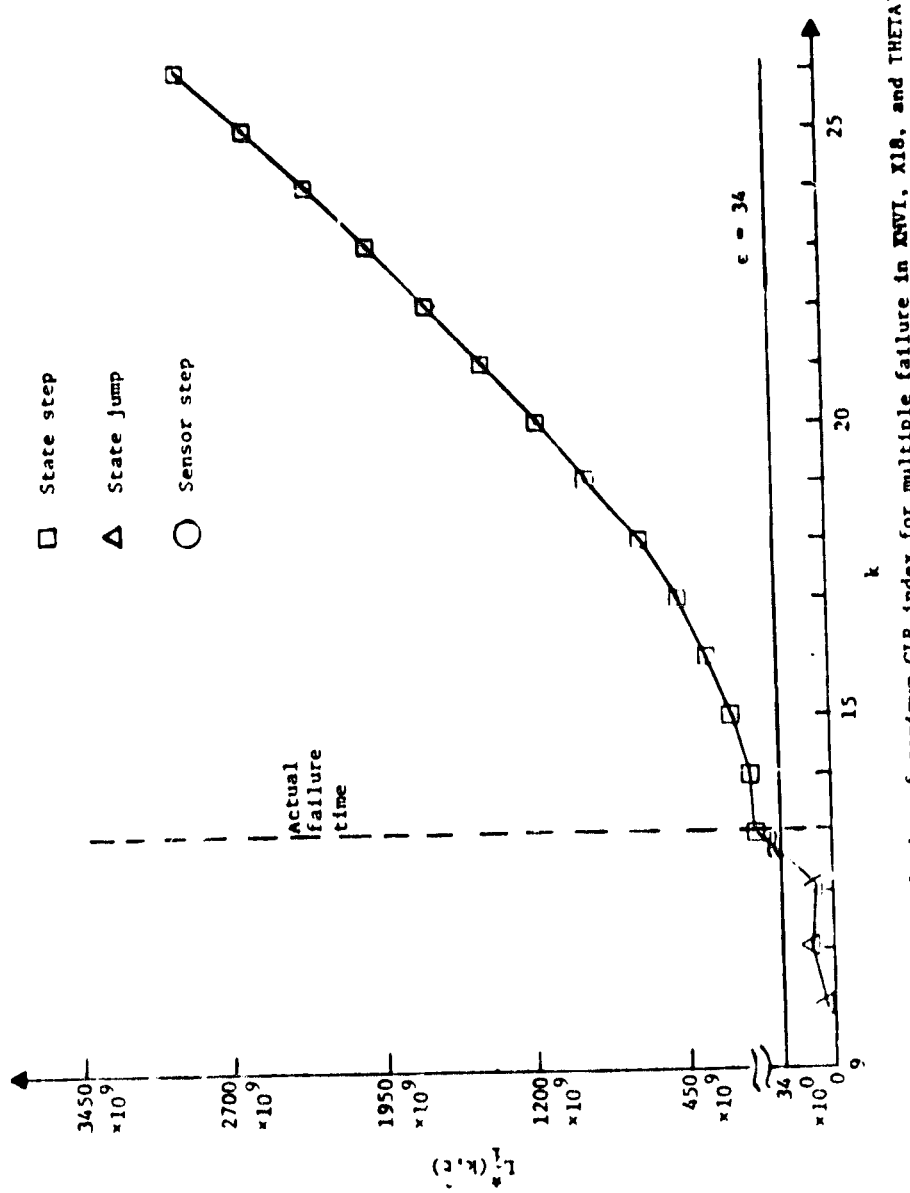

Figure 4.26. - Evolution of maximum GLR index for multiple failure in XNV1, X18, and THETA1.

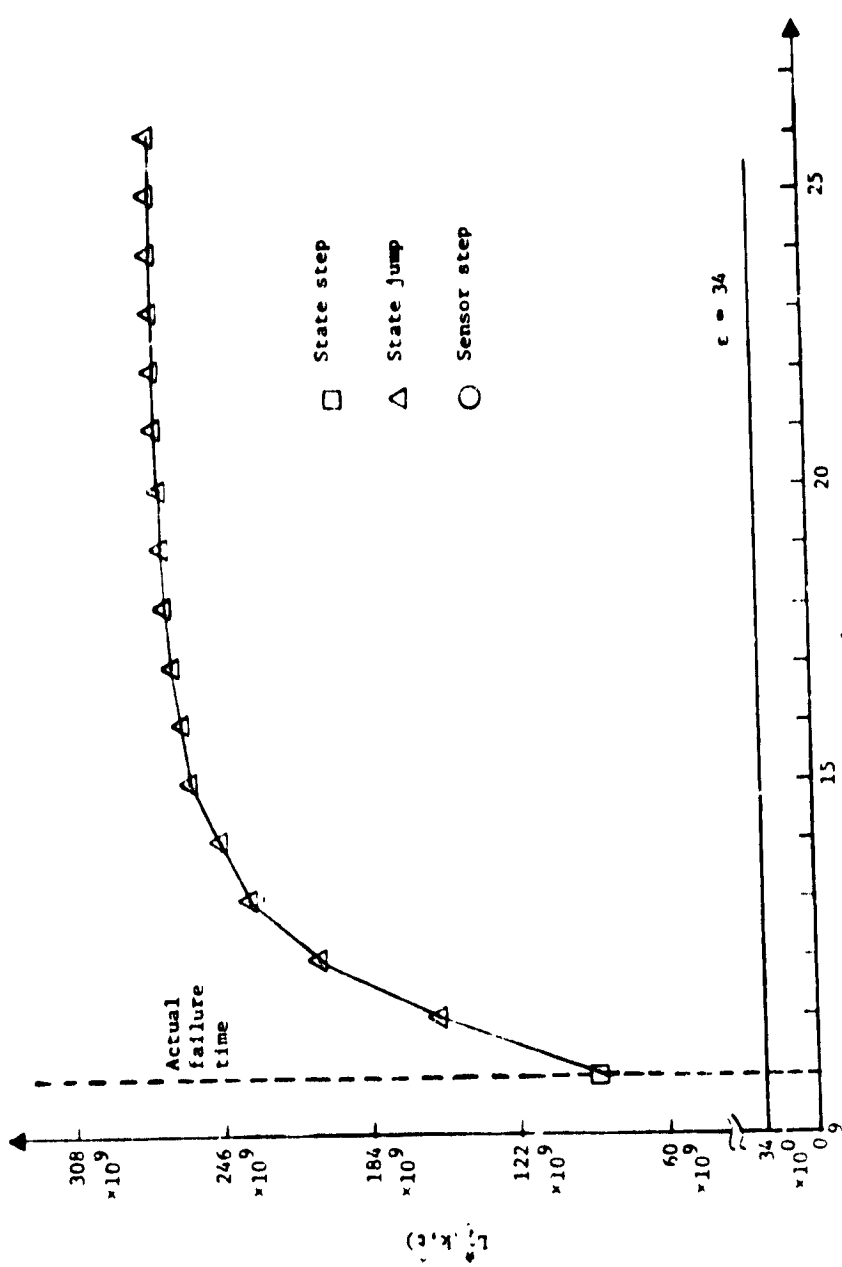

Figure 4.27. - Evolution of maximum GLR index for multiple jump failure in XHVI, X16, and THETAI.

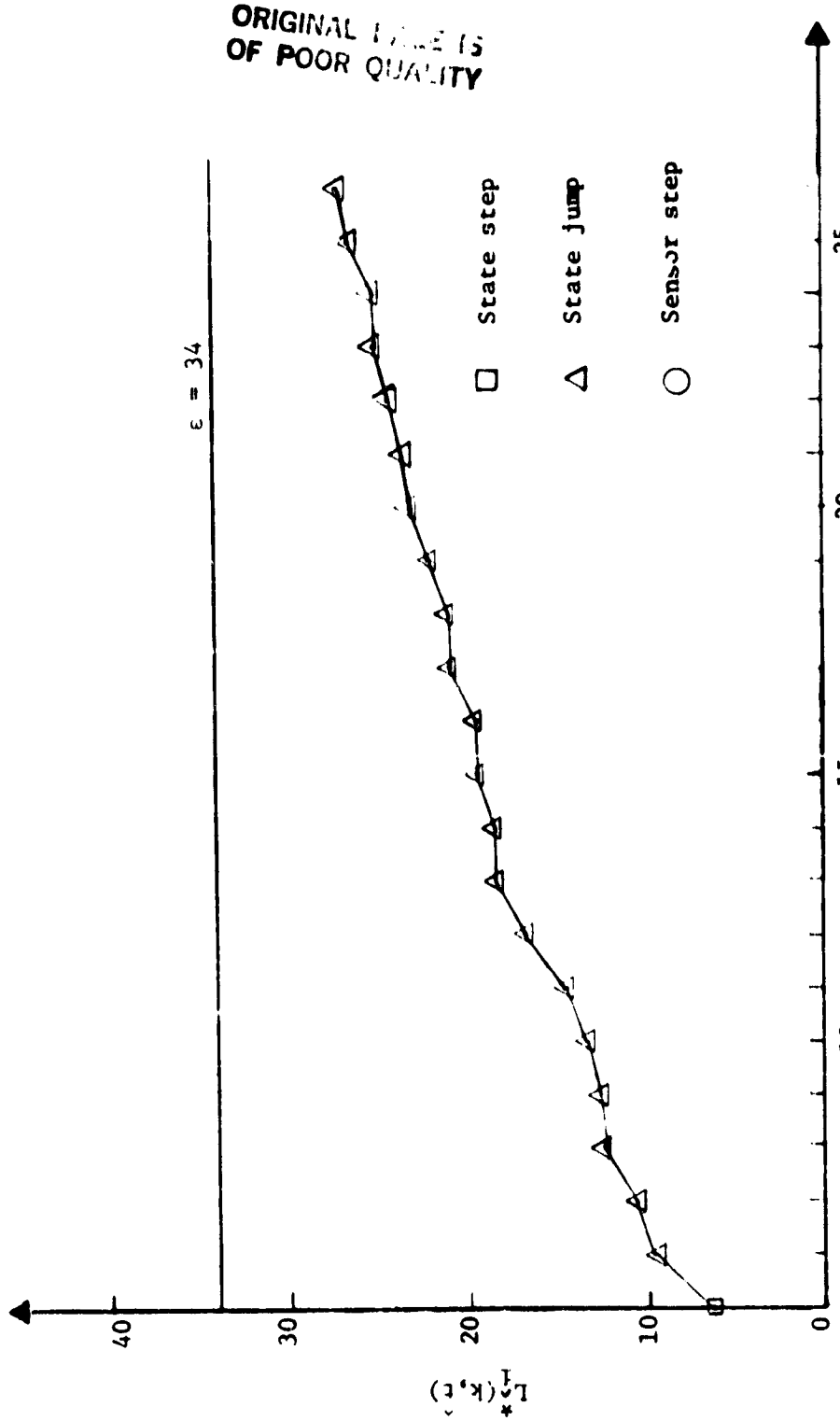

Figure 4.28. - Evolution of maximum GLR index for model degradation with no failure in sensors/actuators.

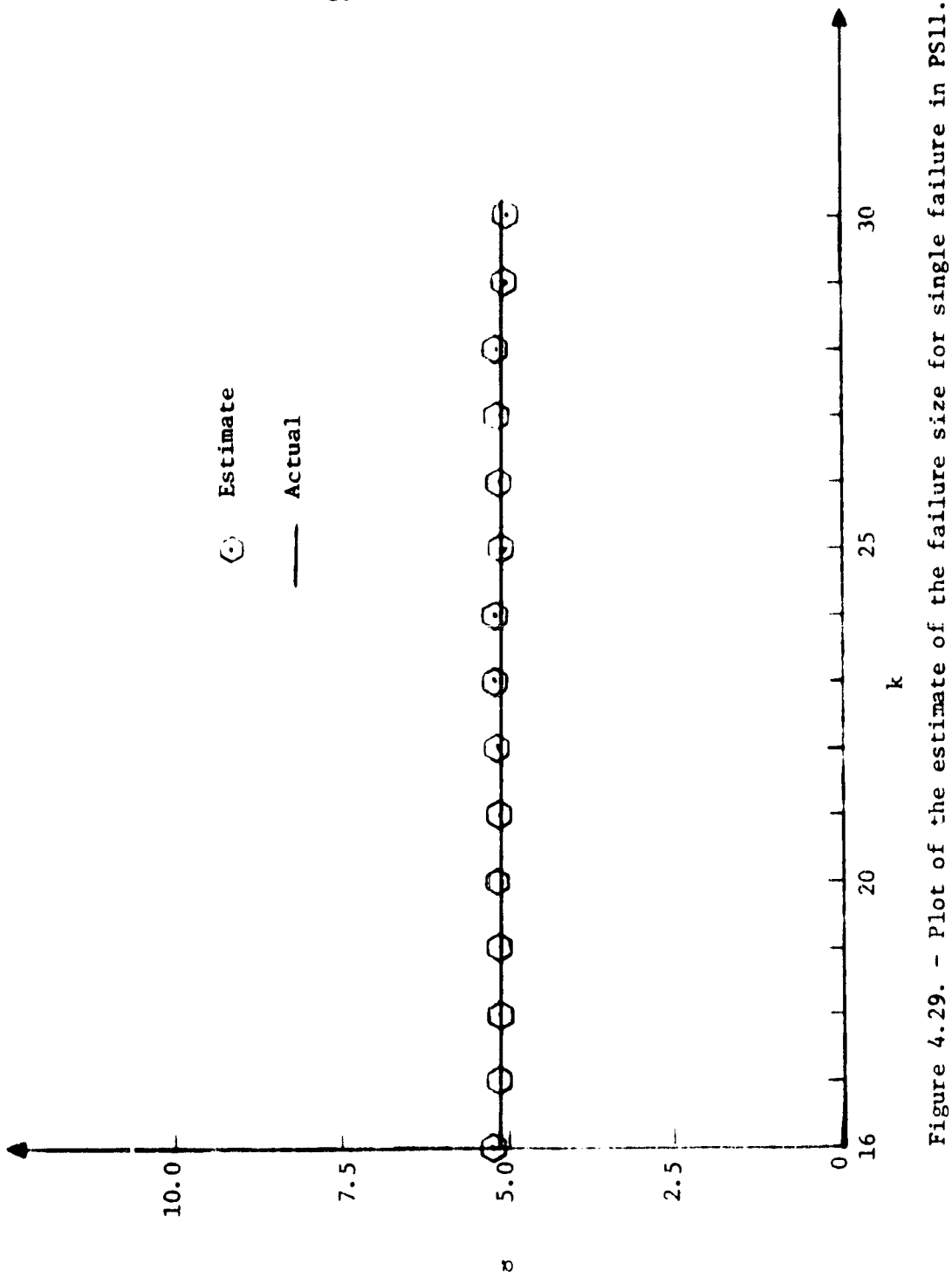

Figure 4.29. - Plot of the estimate of the failure size for single failure in PS11.

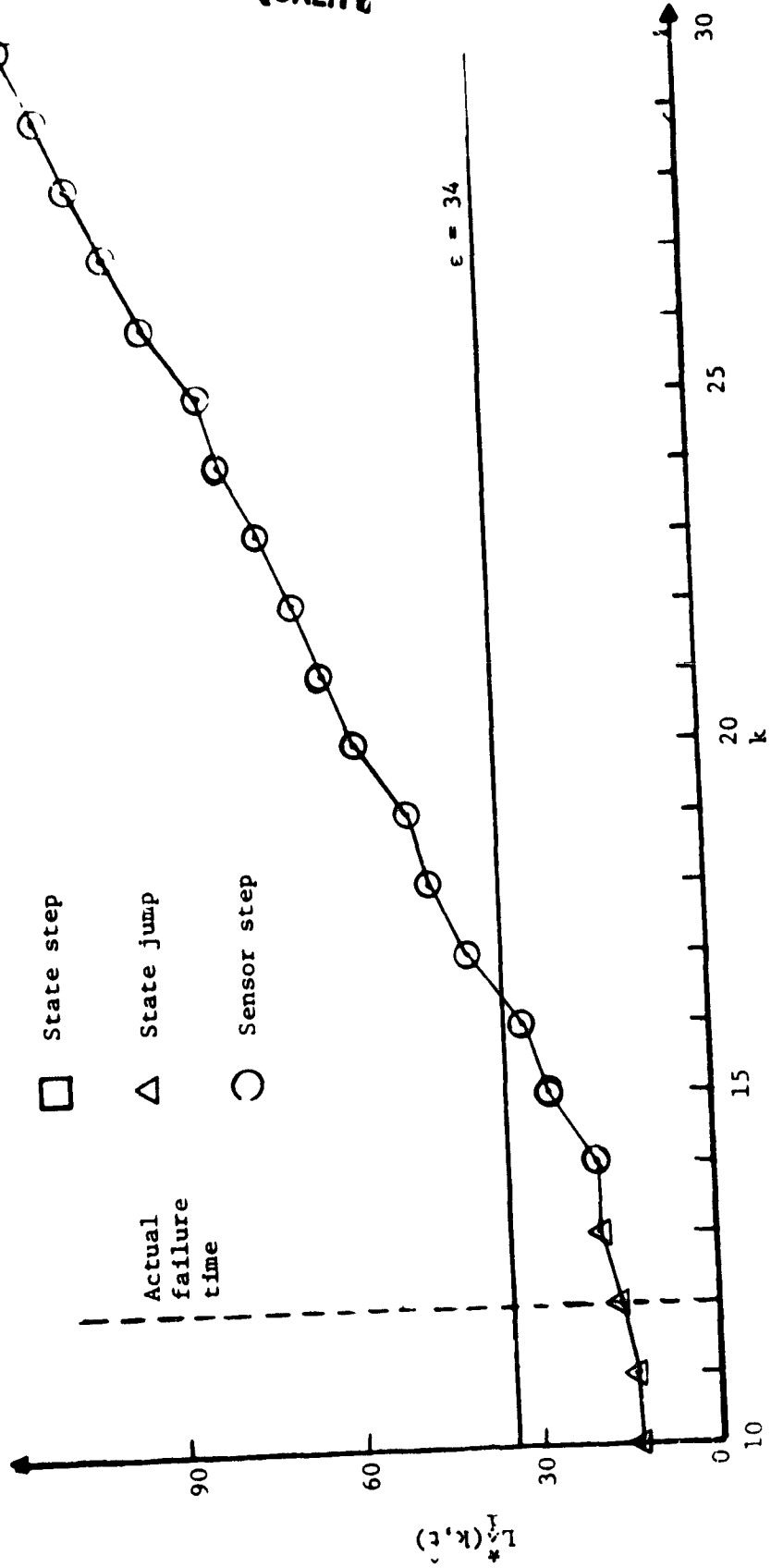

Figure 4.30. - Evolution of maximum GLR index for single sensor failure in PS11.

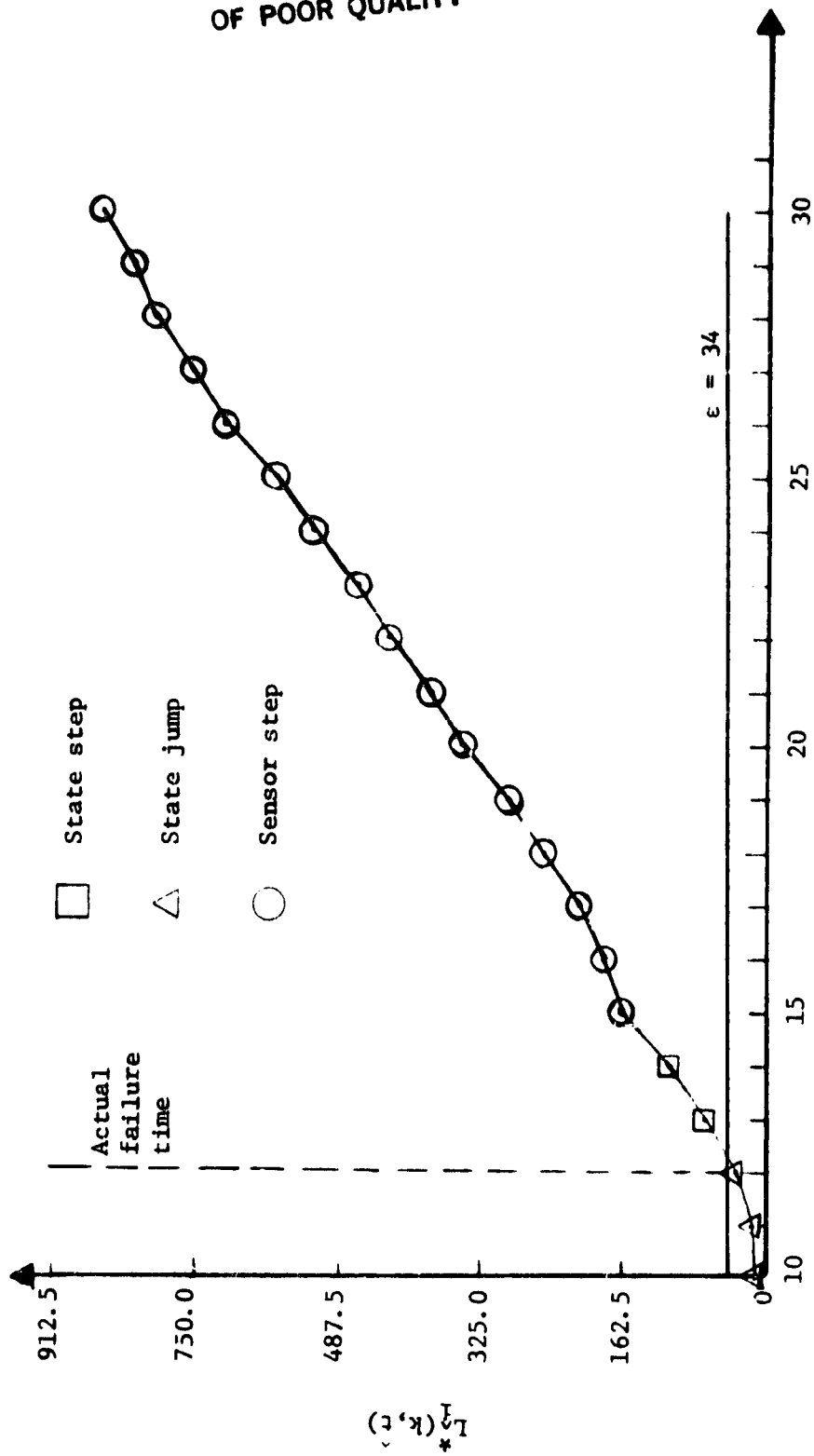

Figure 4.31. - Evolution of maximum GLR index for multiple failure in PS11, NL, NH, P12, P4, and T3 sensors.

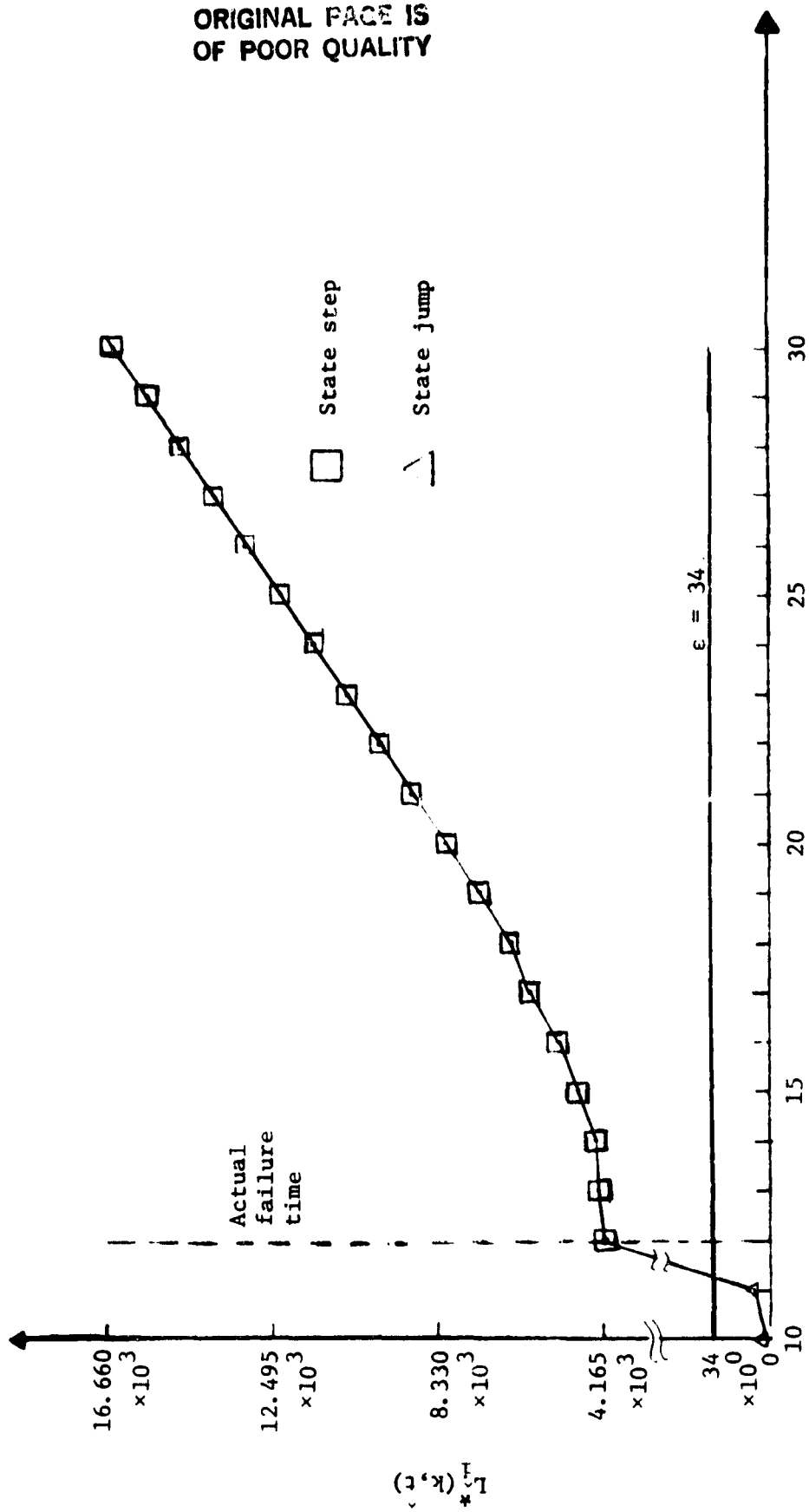

Figure 4.32. - Evolution of maximum GLR index for single step failure in THETAI.

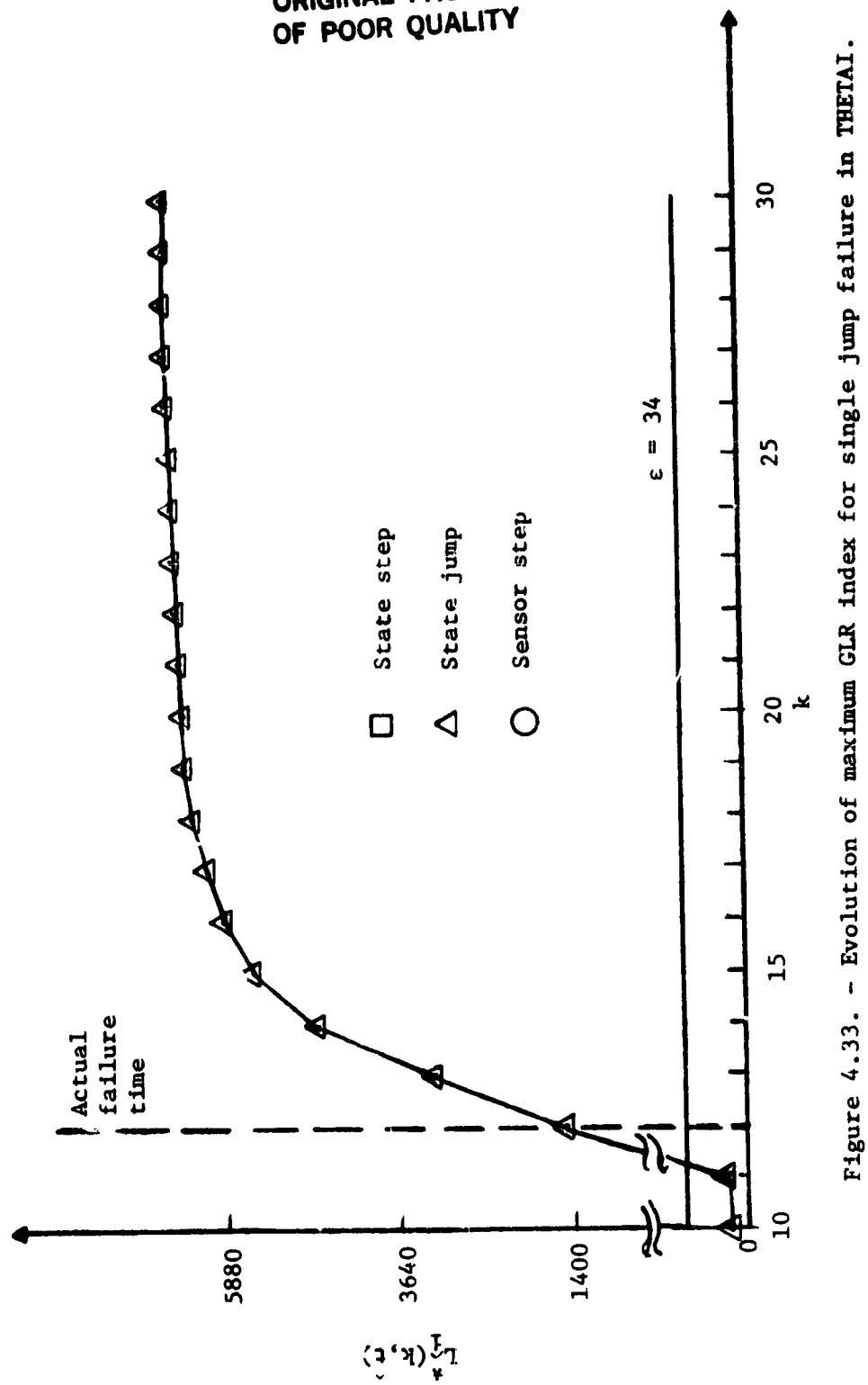

Figure 4.33. - Evolution of maximum GLR index for single jump failure in THETAI.

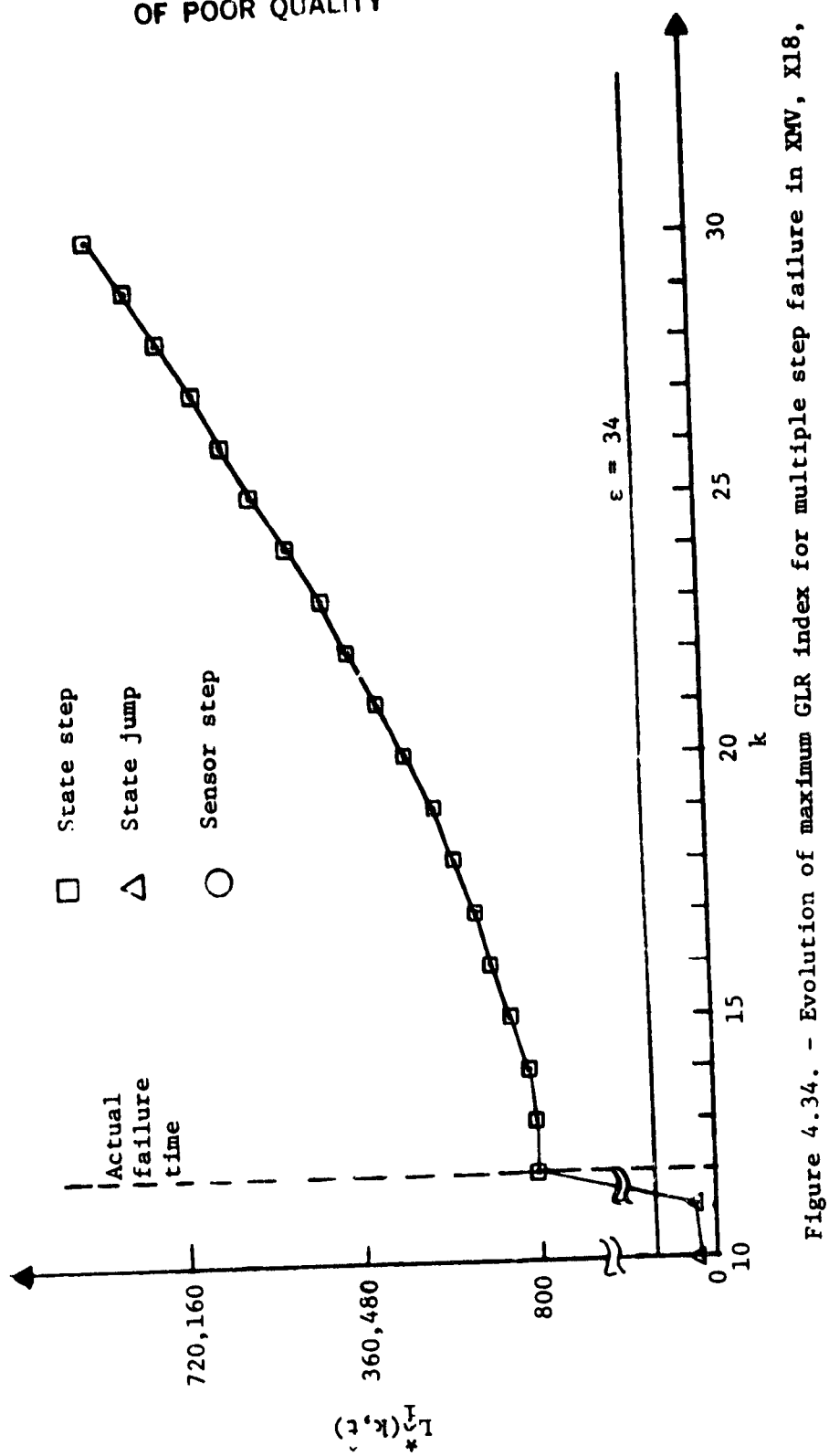

Figure 4.34. - Evolution of maximum GLR index for multiple step failure in XMV, X18, THETAI.

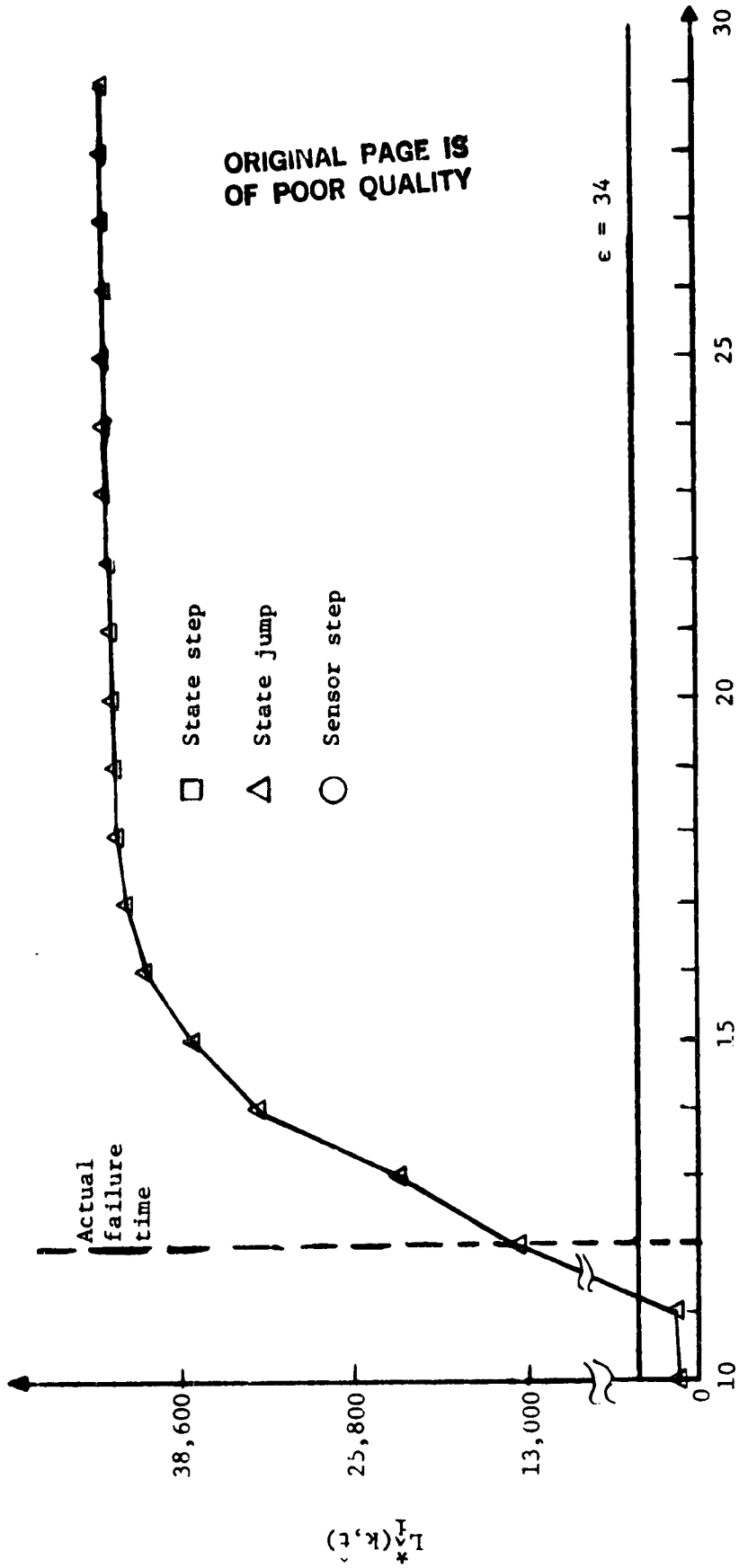

Figure 4.35. - Evolution of maximum GLR index for multiple jump failure in XMV, X18, THETAI.

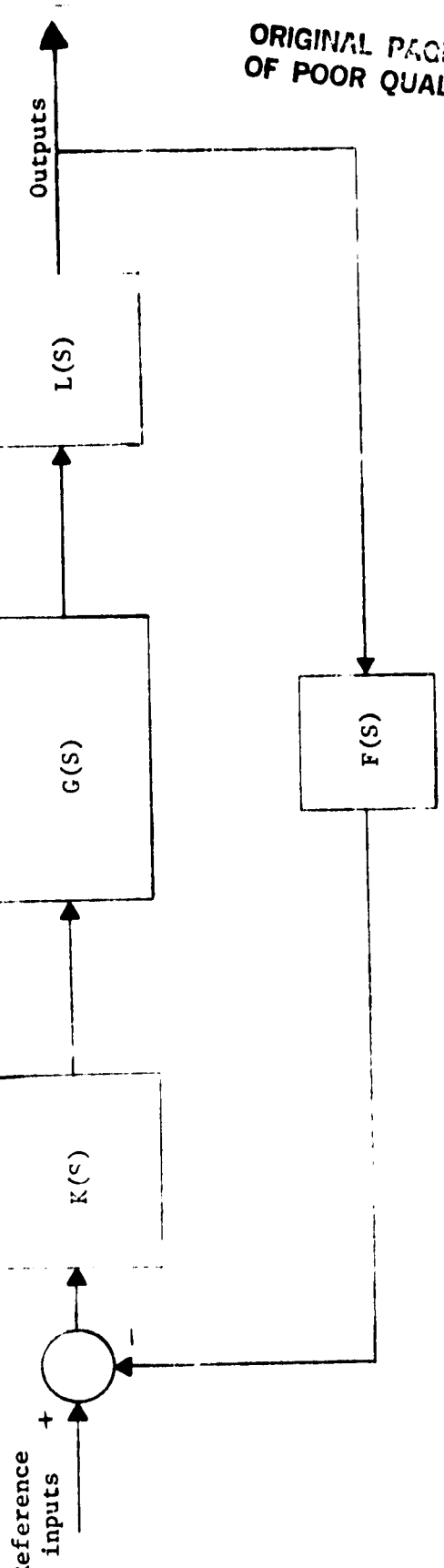

Figure 5.1. - Multivariable system configuration.

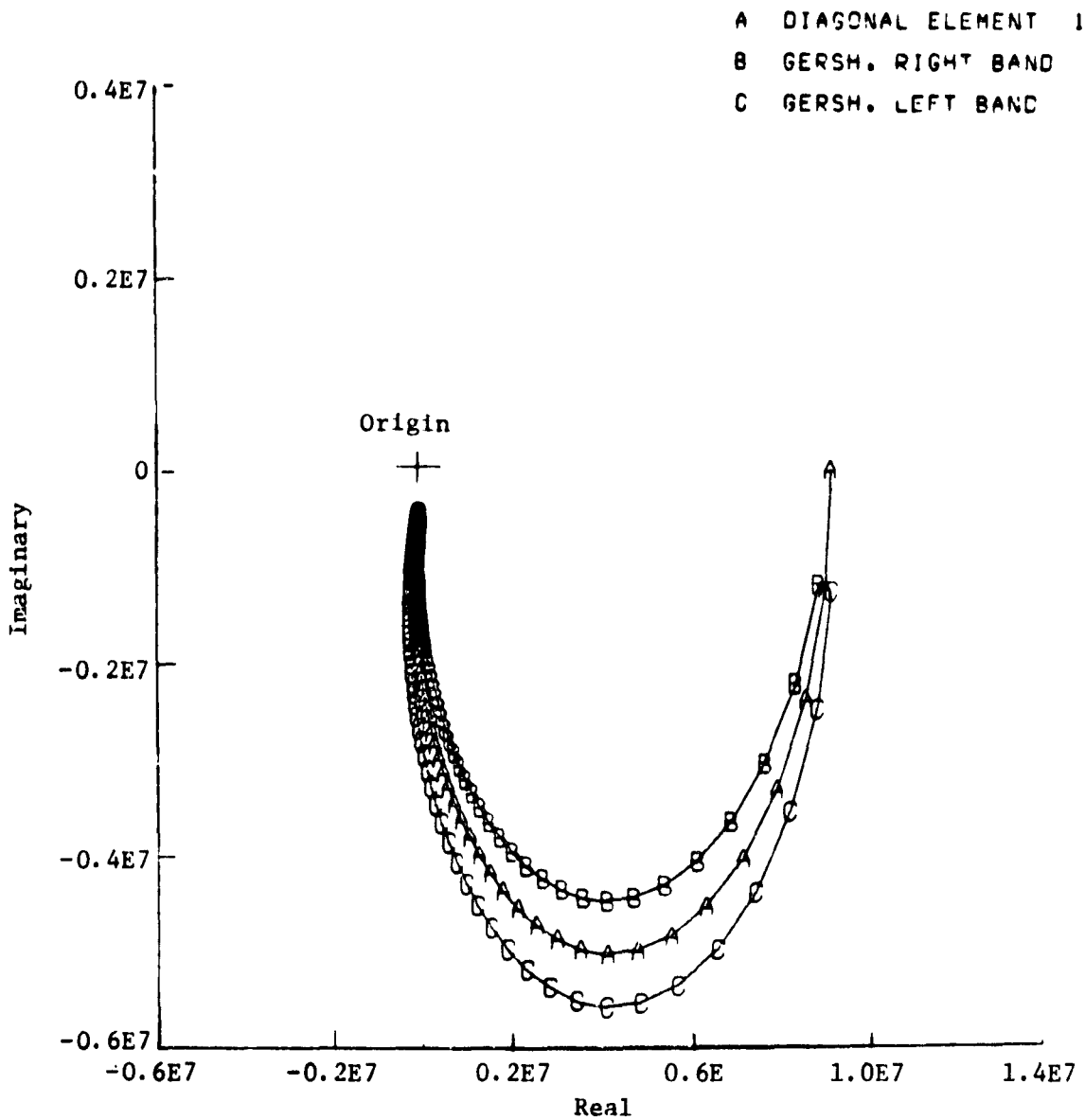

Figure 5.2. - Greshgorin bands for the first column (sensor failure case).

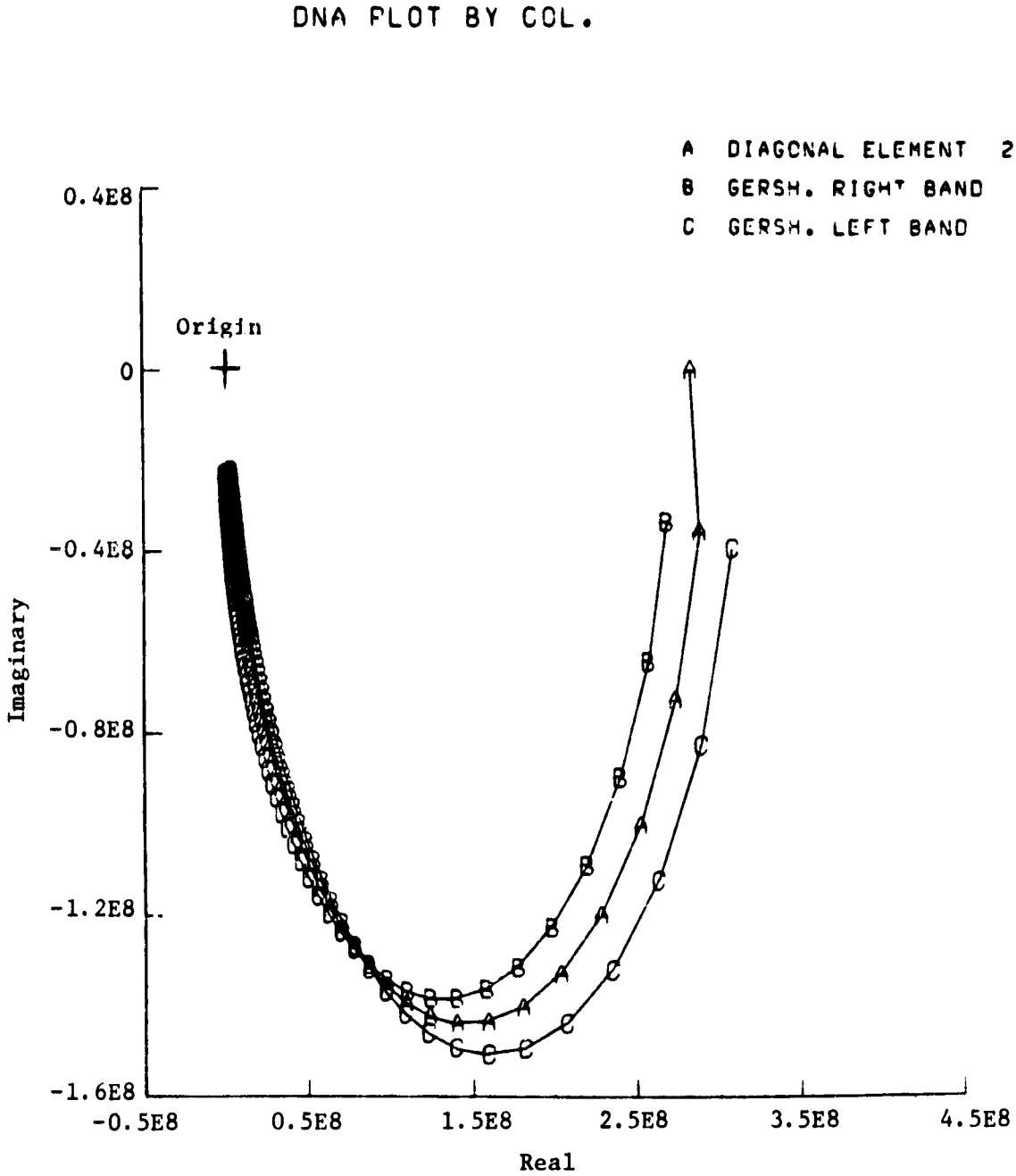

Figure 5.3. - Greshgorin bands for the second column (sensor failure case).

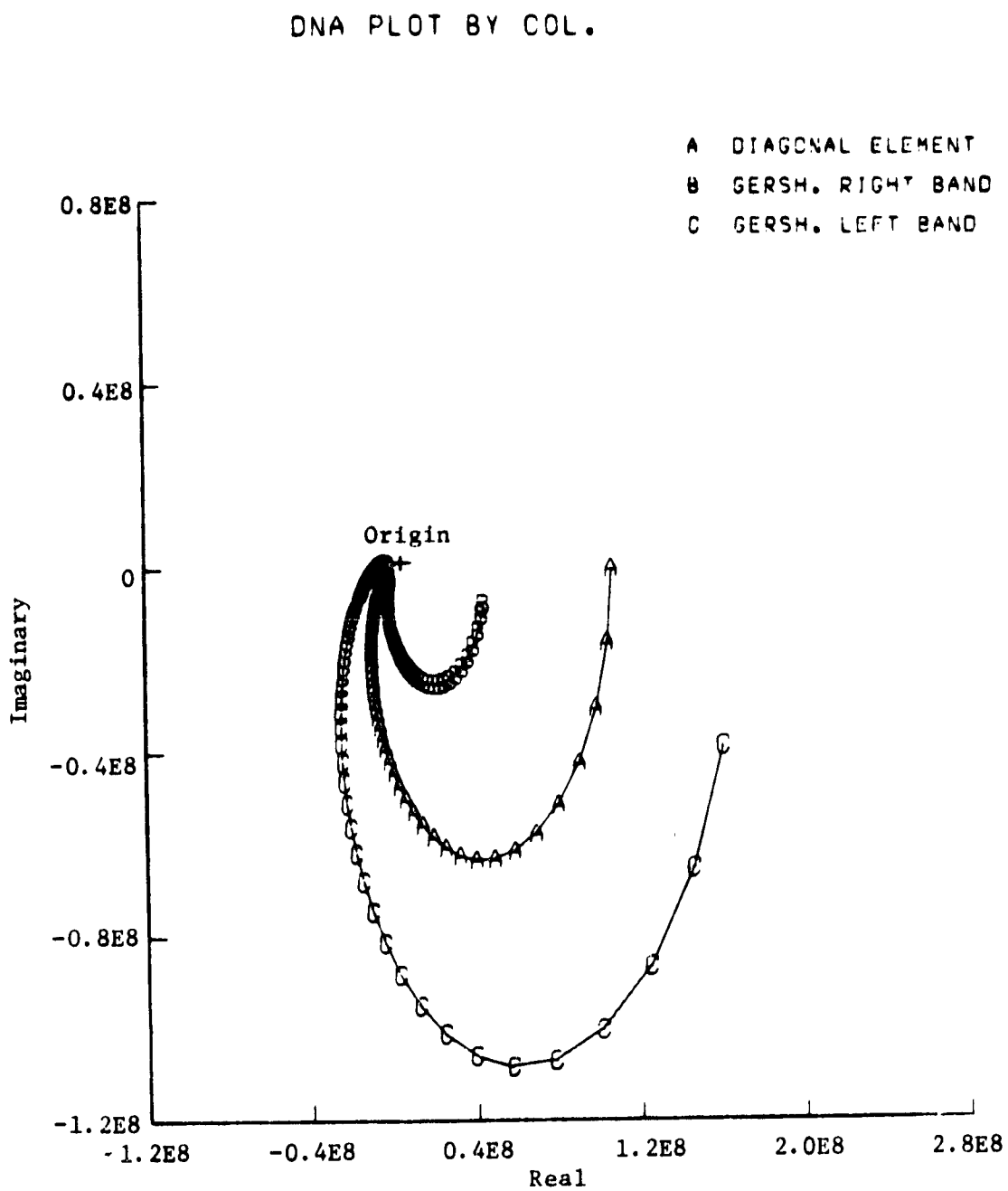

Figure 5.4. - Greshgorin bands for the first column (actuator failure case).

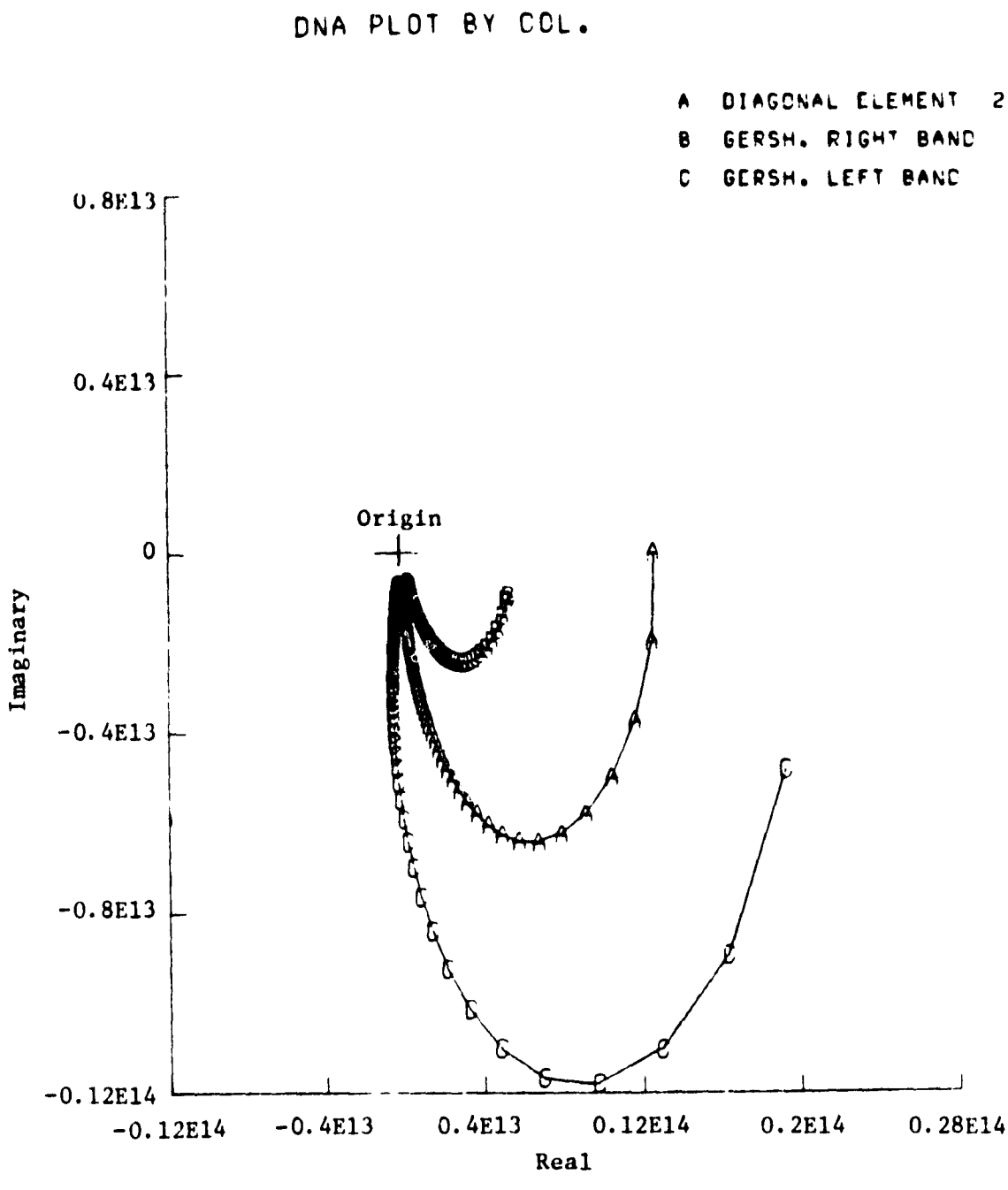

Figure 5.5. - Greshgorin bands for second column (actuator failure case).

APPENDIX B

FAILURE DETECTABILITY PROOFS

This appendix is comprised of two parts. In the first part a theorem concerning the sum of positive definite matrices is presented and in the second part various definitions and proofs concerning the matrix norms are given.

PART B.1:

Theorem: Let V_i for $i = 1, 2, \ldots, R$ be R positive definite matrices of order n then the matrix S_R defined as:

$$S_R = \sum_{i=1}^{R} V_i$$

is also positive definite.

Proof: The proof is given by induction. Since V_i is positive definite then by definition

$$x^T V_i x > 0 \tag{B-1}$$

for any nonzero vector x. Similarly let V_j be positive definite, hence,

$$x^T V_j x > 0 \tag{B-2}$$

for any nonzero vector x. Now adding the two inequalities in equations (B-1) and (B-2) results in

$$x^T V_i x + x^T V_j x > 0 \tag{B-3}$$

$$x^T (V_i x + V_j x) > 0 \tag{B-4}$$

or

$$x^T (V_i + V_j) x > 0 \tag{B-5}$$

Therefore the theorem is true for $R = 2$. Now let

$$S_{R-1} = \sum_{i=1}^{R-1} V_i$$

be positive definite. Then by applying equations (B-1) to (B-5) for S_{R-1} and V_R the proof will be completed.

PART B.2:

Definition: A norm is a function that assigns to every vector x in a given vector space a real number denoted by $||x||$ such that is satisfies the following conditions:

$$1 - ||x|| > 0 \quad \text{for} \quad x \neq 0 \tag{B-6}$$

$$2 - ||x|| = 0 \quad \text{for} \quad x = 0 \tag{B-7}$$

$$3 - ||ax|| = |a| \; ||x||$$

where a is scalar and $|a|$ is the absolute value of a

$$4 - ||x + y|| \leq ||x|| + ||y|| \quad \text{for all} \quad x \text{ and } y \tag{B-8}$$

$$5 - |(x,y)| \leq ||x|| \; ||y|| \tag{B-9}$$

where (x,y) is the inner product of x and y and $|(x,y)|$ is the absolute value of (x,y)

Definition: A norm of an $n \times n$ matrix A is defined as

$$||A|| = \text{Minimum } K \tag{B-10}$$

such that

$$||AX|| \leq K \; ||X|| \tag{B-11}$$

where $||A||$ denotes the norm of matrix A and K is a scalar.

Theorem: The norms of any two $n \times n$ matrices satisfy the following property

$$||AB|| \leq ||A||\ ||B|| \tag{B-12}$$

The proof is given in reference 6, however, it is repeated here for the sake of completeness. First it is necessary to show that for any vector x the following holds

$$||AX|| \leq ||A||\ ||X|| \tag{B-13}$$

This simply follows from the definition of $||A||$. Since $\min K = ||A||$ then by direct substitution in equation (B-11) the equation (B-13) will result. Now consider the vector $||ABX||$, by applying the equation (B-12) twice one can write

$$||ABX|| = ||A(BX)|| \leq ||A||\ ||BX|| \leq ||A||\ ||B||\ ||X||$$

Let

$$K = ||A||\ ||B||$$

then

$$||ABX|| \leq K\ ||X||$$

hence by equation (B-10) $||AB|| = \text{Min } K$ which proves that

$$||AB|| \leq ||A||\ ||B||$$

An immediate result of the above theorem is that

$$||A^R|| \leq ||A||^R.$$

APPENDIX C

SENSOR NOISE COVARIANCE ESTIMATE

Consider the logarithm of the likelihood ratio given in equation (2-96). It can be written as

$$\log L = \frac{t-k}{2} \log|S_1| + \frac{k-t}{2} \log|S_2| - \frac{1}{2} \mathrm{Tr}\, S_2 \sum_{j=t}^{k} r(j)r^T(j)$$

$$+ \frac{1}{2} \mathrm{Tr}\, S_1 \sum_{j=t}^{k} r(j)r^T(j) \qquad \text{(C-1)}$$

Differentiating with respect to S_2, the first and the last terms will be eliminated. The third term can be written as:

$$\mathrm{Tr}\, S_2 \sum_{j=t}^{k} r(j)r^T(j) = \sum_{i,j=1}^{n} S_{ij}\, q_{ij} \qquad \text{(C-2)}$$

where S_{ij} is the ijth element of S_2 matrix and q_{ij} represents the ijth element of the following matrix:

$$Q = \sum_{j=t}^{k} r(j)r^T(j) \qquad \text{(C-3)}$$

Therefore the terms involving S_2 in equation (C-1) can be written as

$$g = \frac{1}{2} (k-t) \log|S_2| - \frac{1}{2} \sum_{i,j=1}^{n} S_{ij}\, q_{ij} \qquad \text{(C-4)}$$

Now differentiating with respect to S_{ii} one can write

$$\frac{\partial g}{\partial S_{ii}} = \frac{1}{2} (k-t) \Big/ |S_2| \, \frac{\partial |S_2|}{\partial S_{ii}} - \frac{1}{2} q_{ii} \qquad \text{(C-5)}$$

Note that the term $\frac{\partial |S_2|}{\partial S_{ii}}$ is equal to the cofactor of S_{ii}. This is easily seen by expansion of $|S_2|$. Then

$$\frac{\partial g}{\partial S_{ii}} = \frac{1}{2}(k - t)\ \text{Cof}\ S_{ii}/|S_2| - \frac{1}{2} q_{ii} \tag{C-6}$$

Similarly when taking the partial derivative with respect to S_{ij}

$$\frac{\partial g}{\partial S_{ij}} = (k - t)\ \text{Cof}\ S_{ij}/|S_2| - q_{ij} \tag{C-7}$$

Setting $\frac{\partial g}{\partial S_{ii}}$ and $\frac{\partial g}{\partial S_{ij}}$ equal to zero results in the following

$$(k - t)\frac{\text{Cof}\ S_{ii}}{|S_2|} = q_{ii}$$

$$(k - t)\frac{\text{Cof}\ S_{ij}}{|S_2|} = q_{ij}$$

Using the fact that $\text{Cof}\ S_{ij}/|S_2|$ is the jith element of the inverse of the S_2 matrix one can write

$$\hat{S}_2 = (k - t)Q^{-1}$$

or

$$\hat{S}_2 = (k - t)\left[\sum_{j=t}^{k} r(j)r^T(j)\right]^{-1}$$

Note that we have used the fact that $q_{ij} = q_{ji}$.

APPENDIX D

COVARIANCE OF FAILURE VECTOR ESTIMATE

The failure vector estimate, $\hat{\nu}$, is used for both isolation and accommodation of the failure in the system. Hence it is important to obtain a measure of the accuracy of $\hat{\nu}$. In this appendix the covariance of $\hat{\nu}$ is calculated as the measure of the accuracy of $\hat{\nu}$. The approach used here follows the one in reference 3, however, for the sake of completeness it is presented here.

Consider the estimate of the failure vector derived in Section 2.3.3. For easy reference, it is repeated here as

$$\hat{\nu} = C_i^{-1}(k,t)D_i(k,t) \tag{D-1}$$

where

$$C_i(k,t) = \sum_{j=t}^{k} G_i^T(j,t)V^{-1}(j)G_i(j,t) \tag{D-2}$$

and

$$D_i(k,t) = \sum_{j=t}^{k} G_i^T(j,t)V^{-1}(j)r(j) \tag{D-3}$$

where $r(j)$ is the model residual defined as

$$r(j) = r_1(j) + G_i(j,t)\nu \tag{D-4}$$

where $r_1(j)$ is a zero mean white Gaussian noise process and $G_i(j,t)\nu$ is the bias in the residuals due to a type of failure. Define the following relation

$$\tilde{D}_i(k,t) = \sum_{j=t}^{k} G_i^T(j,t)V^{-1}(j)r_1(j) \tag{D-5}$$

The mean of $\tilde{D}_i(k,t)$ in equation (D-5) is zero and the cross covariance of $D_i(k,t)$ and $\tilde{D}_i(k,t)$ can be computed as

$$E\left[D_i(k,t)D_i^T(k,t)\right] = E\left\{\left[\sum_{j=t}^{k} G_i^T(j,t)V^{-1}(j)r_1(j)\right] \times \left[\sum_{j=t}^{k} G_i^T(j,t)V^{-1}(j)r(j)\right]^T\right\} \tag{D-6}$$

Substituting for $r(j)$ from equation (D-4) and using the whiteness property of $r_1(j)$, equation (D-6) can be written as

$$E\left[\tilde{D}_i(k,t)D^T(k,t)\right] = \sum_{j=t}^{k} G_i^T(j,t)V^{-1}(j)E\left[r_1(j)r_1^T(j)\right] V^{-1}(j)G_i(j,t)$$

or

$$E\left[\tilde{D}_i(k,t)D^T(k,t)\right] = \sum_{j=t}^{k} G_i^T(j,t)V^{-1}(j)G_i(j,t) \tag{D-7}$$

comparing equation (D-7) with equation (D-2) yields

$$E\left[\tilde{D}_i(k,t)D_i^T(k,t)\right] = C_i(k,t) \tag{D-8}$$

Now the equation (D-3) for $D_i(k,t)$ can be rewritten as

$$D_i(k,t) = \sum_{j=t}^{k} G_i^T(j,t)V^{-1}r_1(j) + \sum_{j=t}^{k} G_i^T(j,t)V^{-1}G_i(j,t)\nu \qquad \text{(D-9)}$$

or

$$D_i(k,t) = \tilde{D}_i(k,t) + C_i(k,t)\nu \qquad \text{(D-10)}$$

Next, consider the error in the Maximum Likelihood Estimate $\hat{\nu}$ (MLE) (given by eq. (D-1))

$$E\left[(\hat{\nu} - \nu)(\hat{\nu} - \nu)^T\right] = \nu\nu^T - E\left[\hat{\nu}\nu^T\right] - E\left[\nu\hat{\nu}^T\right] + E\left[\hat{\nu}\hat{\nu}^T\right] \qquad \text{(D-11)}$$

The second term on the right-hand side of equation (D-11) can be written as

$$E\left[\hat{\nu}\nu^T\right] = E\left[C_i^{-1}(k,t)D_i(k,t)\nu^T\right] \qquad \text{(D-12)}$$

Substituting for $D_i(k,t)$ from equation (D-10) results in

$$E\left[\hat{\nu}\nu^T\right] = E\left[C_i^{-1}(k,t)\tilde{D}_i(k,t)\hat{\nu}^T + C_i^{-1}(k,t)C_i(k,t)\nu\nu^T\right] \qquad \text{(D-13)}$$

Since the expected value of $\tilde{D}_i(k,t)$ is zero, equation (D-13) reduces to

$$E\left[\hat{\nu}\nu^T\right] = \nu\nu^T \qquad \text{(D-14)}$$

The third term on the right-hand side of equation (D-11) can be computed as

$$E\left[\nu\hat{\nu}^T\right] = E\left[\nu D_i^T(k,t)C_i^{-1}(k,t)\right] \qquad \text{(D-15)}$$

From equation (D-10) it follows that

$$E\left[\nu\hat{\nu}^T\right] = E\left\{\nu\left[\tilde{D}_i^T(k,t) + \nu^T C_i(k,t)\right]C_i^{-1}(k,t)\right\}$$

or

$$E\left[\nu\hat{\nu}^T\right] = \nu\nu^T \tag{D-16}$$

Finally the fourth term on the right-hand side of equation (D-11) becomes

$$E\left[\hat{\nu}\hat{\nu}^T\right] = E\left[C_i^{-1}(k,t)D_i(k,t)D_i^T(k,t)C_i^{-1}(k,t)\right] \tag{D-17}$$

Now substituting for $D_i(k,t)$ from equation (D-10) in equation (D-17) results in:

$$E\left[\hat{\nu}\hat{\nu}^T\right] = E\left\{C_i^{-1}(k,t)\left[\tilde{D}_i(k,t) + C_i(k,t)\nu\right]D_i^T(k,t)C_i^{-1}(k,t)\right\} \tag{D-18}$$

Multiplying the terms on the right-hand side of equation (D-18) and using the result in equation (D-8) yields

$$E\left[\hat{\nu}\hat{\nu}^T\right] = \left[C_i^{-1}(k,t) + \nu\nu^T\right] \tag{D-19}$$

Substituting for the terms on the right-hand side of equation (D-11) from equations (D-14), (D-16), and (D-19) yields

$$E\left[(\hat{\nu} - \nu)(\hat{\nu} - \nu)^T\right] = C_i^{-1}(k,t) \tag{D-20}$$

Equation (D-20) is the desired result.

APPENDIX E

QCSEE SYSTEM MATRICES

The system A matrix for QCSEE at 62.5% power level is

$$A = \begin{bmatrix}
-0.105085E\ 02 & 0.291846E\ 00 & 0.000000 & 0.000000 \\
0.106883E\ 02 & -0.168912E\ 02 & 0.000000 & 0.000000 \\
0.850184E\ 02 & 0.588016E\ 01 & -0.125307E\ 02 & 0.000000 \\
0.102389E\ 01 & 0.708155E-01 & -0.409882E-01 & -0.995042E\ 01 \\
0.895407E\ 03 & -0.799016E\ 03 & 0.337876E\ 01 & -0.144357E\ 03 \\
0.710867E\ 02 & 0.909366E\ 02 & -0.632545E\ 02 & -0.283151E\ 02 \\
-0.729535E\ 01 & 0.176629E\ 01 & 0.552433E\ 00 & 0.000000 \\
-0.137935E\ 02 & 0.333947E\ 01 & -0.601115E\ 01 & 0.000000
\end{bmatrix}$$

$$\begin{bmatrix}
-0.131467E-02 & 0.000000 & 0.000000 & 0.000000 \\
0.326249E-01 & -0.100647E-02 & 0.000000 & 0.000000 \\
0.000000 & 0.430649E\ 00 & 0.401042E-01 & 0.388458E-01 \\
0.000000 & 0.518529E-02 & 0.482993E-03 & 0.467838E-03 \\
-0.214287E\ 01 & 0.905415E\ 00 & 0.205227E\ 00 & 0.198787E\ 00 \\
0.000000 & -0.685347E\ 00 & -0.169765E\ 01 & 0.642603E\ 00 \\
0.000000 & 0.117756E-05 & -0.276006E\ 00 & 0.000000 \\
0.000000 & 0.794218E-06 & 0.971873E-01 & -0.619027E\ 00
\end{bmatrix}$$

The B matrix is

$$B = \begin{bmatrix}
-0.607894E-01 & 0.103031E-03 & 0.179767E-01 \\
0.132536E\ 01 & -0.709244E\ 01 & -0.446111E\ 00 \\
0.198737E\ 04 & 0.569287E-02 & -0.390624E-04 \\
0.240662E\ 02 & 0.631966E-04 & -0.439778E-06 \\
0.100854E\ 05 & 0.370906E\ 00 & 0.293014E\ 02 \\
0.329770E\ 05 & 0.108203E\ 00 & -0.179109E-02 \\
-0.731900E\ 02 & -0.196076E\ 00 & 0.341769E-02 \\
0.473328E\ 04 & -0.213886E\ 00 & 0.382312E-02
\end{bmatrix}$$

For the following outputs

$$\begin{pmatrix}
PS11 \\
P13 \\
P4 \\
P8 \\
NL \\
NH \\
T41C \\
FN
\end{pmatrix}$$

The C matrix is

$$C = \begin{bmatrix} -0.178340E\ 01 & 0.115550E\ 01 & 0.000000 & 0.000000 \\ 0.000000 & 0.100503E\ 01 & 0.000000 & 0.000000 \\ 0.000000 & 0.000000 & 0.100503E\ 01 & 0.000000 \\ 0.000000 & 0.000000 & 0.000000 & 0.100503E\ 01 \\ 0.000000 & 0.000000 & 0.000000 & 0.000000 \\ 0.000000 & 0.000000 & 0.000000 & 0.000000 \\ 0.000000 & 0.000000 & -0.959950E\ 01 & 0.000000 \\ 0.520969E\ 04 & -0.335492E\ 04 & -0.213724E\ 01 & 0.525182E\ 03 \end{bmatrix}$$

$$\begin{bmatrix} -0.498601E-02 & 0.000000 & 0.000000 & 0.000000 \\ 0.000000 & 0.000000 & 0.000000 & 0.000000 \\ 0.000000 & 0.000000 & 0.000000 & 0.000000 \\ 0.000000 & 0.000000 & 0.000000 & 0.000000 \\ 0.100503E\ 01 & 0.000000 & 0.000000 & 0.000000 \\ 0.000000 & 0.100503E\ 01 & 0.000000 & 0.000000 \\ 0.000000 & 0.000000 & 0.000000 & 0.000000 \\ 0.153103E\ 02 & -0.204418E\ 00 & 0.250473E-01 & 0.242613E-01 \end{bmatrix}$$

and the D matrix is

$$D = \begin{bmatrix} -0.148495E\ 00 & 0.377881E-02 & 0.680882E-01 \\ 0.000000 & 0.000000 & 0.000000 \\ 0.000000 & 0.000000 & 0.000000 \\ 0.000000 & 0.000000 & 0.000000 \\ 0.000000 & 0.000000 & 0.000000 \\ 0.000000 & 0.000000 & 0.000000 \\ 0.760177E\ 04 & 0.456472E\ 01 & -0.100396E\ 00 \\ 0.166154E\ 04 & -0.172886E\ 04 & -0.209075E\ 03 \end{bmatrix}$$

The discrete system matrix is

$$\Phi = \begin{bmatrix}
0.43374972 & 0.91925487E-02 & -0.21365763E-05 \\
0.33337976 & 0.22976518 & 0.16559224E-03 \\
2.7585373 & 0.22255993 & 0.32224697 \\
0.32082696E-01 & 0.25931691E-02 & -0.18636566E-02 \\
30.512177 & -30.267670 & 0.32382239E-01 \\
-4.1948767 & 3.0783167 & -3.0145245 \\
-0.27429551 & 0.77381611E-01 & 0.26782583E-01 \\
-1.5723992 & 0.63729227E-01 & -0.28649169
\end{bmatrix}$$

$$\begin{bmatrix}
0.28050621E-03 & -0.49036797E-04 & -0.27744363E \\
-0.69871278E-02 & 0.12374774E-02 & 0.16674167E \\
-0.21748357E-01 & 0.16706878E-03 & 0.20460729E \\
0.45085824 & 0.19714762E-05 & 0.23894686E \\
-7.1143742 & 0.79237133 & 0.64835548E \\
-1.4917765 & 0.52215196E-02 & 0.88539732 \\
-0.83617843E-03 & 0.13359095E-03 & 0.53711841E \\
0.31266294E-02 & 0.21572415E-03 & -0.57836771E
\end{bmatrix}$$

$$\begin{bmatrix}
-05 & -0.37991942E-06 & -0.55294595E-06 \\
-04 & 0.13773187E-04 & 0.12452469E-04 \\
-01 & 0.30427403E-03 & 0.24714542E-02 \\
-03 & 0.33591323E-05 & 0.28946321E-04 \\
-01 & 0.10082114E-01 & 0.15658051E-01 \\
 & -0.13323694 & 0.42157732E-01 \\
-03 & 0.97818661 & 0.59236045E-04 \\
-02 & 0.72414279E-02 & 0.95105529
\end{bmatrix}$$

APPENDIX F

QCSEE SENSOR NOISE CHARACTERISTICS

For the following sensors

PS11	psi
NL	rpm
NH	rpm
P4	psi
P12	psi
T3	^{o}R

the covariance matrix of the sensor noise is

$$V = \begin{pmatrix} 0.010147 & & & & \\ & 12.839860 & & 0 & \\ & & 12.839860 & & \\ & & & 0.010147 & \\ & 0 & & & 0.010147 \\ & & & & & 0.0171805 \end{pmatrix}$$

normalizing V with respect to the nominal value of the sensor measurements yields

$$V_n = \begin{pmatrix} 1.039941 & & & & \\ & 0.153229 & & 0 & \\ & & 0.153229 & & \\ & & & 1.039941 & \\ & 0 & & & 1.039941 \\ & & & & & 1.784873 \end{pmatrix} \times 10^{-6}$$

The following nominal values of the QCSEE actuator inputs at 62.5% power are used to compute the failure sizes in the actuators

XMV = 0.355 in.

X18 = 1.87 in.

THETAI = 119.32 deg.

The nominal value of the output sensors are

PS11 = 11.967 psia

NL = 2653.34 rpm

NH = 11958.60 rpm

P12 = 14.63 psia

P4 = 139.419 psia

T3 = 1090.17 ^{o}R

P8 = 15.538 psia

The sample mean vector of the generated noise sequence for PS11, NL, NH, P12, P4, and P8 are

$$\begin{pmatrix} 0.2927975 \\ -0.091251 \\ 0.312425 \\ 0.138931 \\ -2.19810 \\ 1.3842 \end{pmatrix} \times 10^{-4}$$

APPENDIX G

PROOF OF UNBIASED GLR ESTIMATION

In this appendix it will be proven that the failure vector estimate resulting from GLR technique is an unbiased estimate of the failure vector. To achieve this consider the expression for failure vector estimate from equation (2-37):

$$\hat{\nu} = C_i^{-1}(k,t)D_i(k,t) \tag{G-1}$$

where $C_i(k,t)$ and $D_i(k,t)$ are defined in equations (2-35) and (2-36). Substituting for $D_i(k,t)$ from equation (2-36) yields

$$\hat{\nu} = C_i^{-1}(k,t)\left[\sum_{q=1}^{k} G_i^T(q,t)V^{-1}r(q)\right] \tag{G-2}$$

Under type i failure hypothesis $r(q)$ is defined as in equation (2-27). Now substituting for $r(q)$ from equation (2-27) in equation (G-2) yields

$$\hat{\nu} = C_i^{-1}(k,t)\left[\sum_{q=1}^{k} G_i^T(q,t)V^{-1}(q)r_1(q)\right]$$

$$+ C_i^{-1}(q,t)\left[\sum_{q=1}^{k} G_i^T(q,t)V^{-1}G_i(q,t)\right]\nu \tag{G-3}$$

Taking expected value of both sides of the above equation results in

$$E[\hat{\nu}] = C_i^{-1}(k,t)\left[\sum_{q=1}^{k} G_i^T(q,t)V^{-1}G_i(q,t)\right]\nu \tag{G-4}$$

where the term inside the first bracket in equation (G-3) vanishes because $r_1(j)$ has a null expected value. On the other hand, the term

inside the bracket in equation (G-4) is equal to $C_i(k,t)$ (see eq. (2-35)), hence

$$E\left[\hat{\nu}\right] = \nu \tag{G-5}$$

Therefore $\hat{\nu}$ is an unbiased estimator of ν.

The estimate of failure size, $\hat{\alpha}$, resulting from the application of Constrained GLR (CGLR) technique, given in equation (2-43), is also unbiased. To show this, consider the expression for $\hat{\alpha}$ from equation (2-43):

$$\hat{\alpha} = \frac{f_j^T D_i(k,t)}{f_j^T C_i(k,t) f_j} \tag{G-6}$$

where f_j is the jth direction of the prespecified directions and $C_i(k,t)$ and $D_i(k,t)$ are the same as in equations (2-35) and (2-36). Substituting for $D_i(k,t)$ in equation (G-6) from equation (2-36) yields

$$\hat{\alpha} = \frac{f_j^T\left[\sum_{q=1}^{k} G_i^T(q,t)V^{-1}(q)r_1(q)\right]}{f_j^T C_i(k,t) f_j} + \frac{f_j^T\left[\sum_{q=1}^{k} G_i^T(q,t)V^{-1}(q)G_i(q,t)\right]f_j\alpha}{f_j^T C_i(k,t) f_j} \tag{G-7}$$

Now taking the expected value of both sides of equation (G-7) results in

$$E\left[\hat{\alpha}\right] = \frac{f_j^T\left[\sum_{q=1}^{k} G_i^T(q,t)V^{-1}(q)G_i(q,t)\right]f_j\alpha}{f_j^T C_i(k,t) f_j} \qquad \text{(G-8)}$$

In the above equation the term inside the bracket is $C_i(k,t)$; thus equation (G-8) can be written as

$$E\left[\hat{\alpha}\right] = \alpha \qquad \text{(G-9)}$$

Hence $\hat{\alpha}$ is an unbiased estimator of the failure size α.

A useful result of the above analysis is that as k the number of observations increases the estimate of the failure vector improves. However, if the mean of the model residual is different from zero when no failure has occurred then the failure vector estimate is not unbiased. This can be easily seen from equation (G-3); specifically

$$E\left[\hat{\nu}\right] = \nu + C_i^{-1}(k,t)\left\{\sum_{q=1}^{k} G_i^T(q,t)V^{-1}(q)E\left[r_1(q)\right]\right\} \qquad \text{(G-8)}$$

Similarly if CGLR technique is applied to the residuals with nonzero mean the estimate of the failure size will be biased and it is given by

$$E\left[\hat{\alpha}\right] = \alpha + \frac{f_j^T\left\{\sum_{q=1}^{k} G_i^T(q,t)V^{-1}(q)E\left[r_1(q)\right]\right\}}{f_j^T C_i(k,t) f_j} \qquad \text{(G-9)}$$

In all of the above analysis no assumption regarding the type of the failure was made; hence, the above results are valid for all three types of failure. Also the derivation is for time-varying systems but clearly is applicable to time-invariant systems.

BIBLIOGRAPHY

1. Willsky, A.S.; and Jones, H.L.: A Generalized Likelihood Ratio Approach to the Detection and Estimation of Jumps in Linear Systems, IEEE Trans. Automatic Control, Vol. AC-21, No. 1, Feb. 1976.

2. Boeno, R. A.: Performance and Sensitivity Analysis of the Generalized Likelihood Ratio Method for Failure Detection, Master Thesis, M.I.T., Cambridge, Mass., February,1977.

3. Chow, E. Y.: Analytical Studies of The Generalized Likelihood Ratio Technique For Failure Detection, Master Thesis, M.I.T., Cambridge, Mass., February, 1976.

4. Chien, T. T.: An Adaptive Technique for a Redundant Sensor Navigation System, Ph.D Thesis, Report T-560, Draper Laboratories, Cambridge, Mass., February, 1972.

5. Anderson, T. W.: An Introduction to Multivariable Statistical Analysis, John Wiley & Sons., Inc., New York, 1962.

6. Merrill, W. C.: An Application of Modern Control Theory To Jet Propulsion Systems, NASA TMX-71726, May, 1975.

7. Cwynar, D. S.; and Batterton, P. G.: Digital Implementation of TF30-P-3 Turbofan Engine Control, NASA TMX-3105, 1975.

8. Loft, A.: SPEEDTRONIC - Tomorrow's Analog and Digital

Gas Turbine Control System, IEEE Transaction on Industry and General Applications, Vol. IGA-5, No. 4.

9. Kuhlberg, J. F.; and Newirth, D. M.: The Digital Electronic Propulsion Control System - Problems and Payoffs, AIAA Paper No. 74-1068.

10. Sevich, G. J.; and Newirth, D. M.: Economic Benefits of Digital Electronic Propulsion Controls for Advanced Commercial Aircraft, Society of Automotive Engineers, Air Transport Meeting, May 18-20, 1976.

11. Yafee, M. L.: Fuel Saving Engine Controls Studied, Aviation Week and Space Technology, June 7, 1976, pp. 65-67,

12. Montgomery, R. C.; and Price, D. B.: Management of Analytical Redundancy in Digital Flight Control Systems for Aircraft, AIAA Paper 74-887.

13. Michael, G.; and Farrar, F.. Development of Optimal Control Modes for Advanced Technology Propulsion Systems, United Aircraft Research Laboratories (UARL) Report NO. M9-11620-1.

14. McMorran, P. D.: Design of Gas-Turbine Controller Using Inverse Nyquist Method, Proceedings of IEE. Vol. 117, No. 10, October, 1970.

15. MacFarlane, A.G.J.; McMorran, P. D.; Dixon, B. H.; and Hodge, S. S.: Application of Multivariable Control Techniques to Aircraft Gas Turbines, Conference on Multivariable Control System Design and Applications, England, 1971.

16. Sain, M. K.; Peczkowski, J. J.; Melsa, J. L.: Alternatives for Linear Multivariable Control, National Engineering Consortium, Inc., Chicago, 1978.

17. Rosenbrock, H. H.: Design of Multivariable Control Systems Using The Inverse Nyquist Array, Proc. IEE, Vol. 116.

18. Rosenbrock, H. H.: Computer Aided Control System Design, Academic Press, London, 1974.

19. Leininger, G. G.: Diagonal Dominance For The Multivariable Nyquist Array Using Function Minimization, Final Report NASA Grant 3063 and University of Toledo Report TR 7701, May, 1977.

20. Leininger, G. G.: Diagonal Dominance For Multivariable Nyquist Array Methods Using Function Minimization, Automatica Journal, May, 1979.

21. Spang, H. A.: Insight Into The Application of The Inverse Nyquist Array Method to Turbofan Engine Control, Alternatives for Linear Multivariable Control, NEC Inc., 1978.

22. Lehtinen, B.; DeHoff, R. L.; and Hackney, R. D.: Multivariable Control Altitude Demonistration on the F100 Turbofan Engine, AIAA Paper No. 79-1204, Presented at Fifteenth Joint Propulsion Conference, Co-sponsored by AIAA, SAE and ASME, Las Vegas, Nevada, June 18-20, 1979.

23. Leininger, G. G.: The Multivariable Nyquist Array: The Concept of Dominance Sharing, NEC International Forum on Alternatives for Linear Multivariable Control, Oct. 1977, Chicago, Illinois.

24. Leininger, G. G.: New Dominance Characteristics For The Multivariable Nyquist Array Method, International Journal of Control, Vol. 30, No. 3, 1979.

25. Gillmore, J. P.; and McKern, R. A.: A Redundant Strapdown Inertial System Mechanization - SIRU, AIAA Paper 70-1027, Aug. 1970.

26. Pejsa, A. J.: Optimum Orientation and Accuracy of Redundant Sensor Arrays, AIAA 9th Aerospace Science Meeting, New York, Jan. 25-27, 1971.

27. Kalman, R. E.; and Bucy, R.: New Results in Linear Filtering and Prediction Theory, Trans. ASME, Journal of Basic Engineering, Vol. 83D, pp. 95-108, March, 1961.

28. Jazwinski, A. H.: Stochastic Processes and Filtering Theory, Academic Press, New York, 1970.

29. Kerr, T. H.: A Two Ellipsoid Overlap Test for Real Time Failure Detection and Isolation by Confidence Regions, Pittsburgh Conf. on Modeling and Simulation, April 24-26, 1974.

30. Willsky, A. S.: A Survey of Design Methods for Failure Detection In Dynamic Systems, Systems Reliability Issues for Future Aircrafts, NASA Publication CP-003, Aug. 18-20, 1975.

31. Sage, A. P.; and Melsa, J. L.: Estimation Theory with Application To Communication and Control, McGraw-Hill Company, 1971.

32. Montgomery, R. C.; and Caglayan, A. K.: A Self-Reorganizing Digital Flight Control System for Aircraft, AIAA Paper 74-21, 1974.

33. Mehra, R. K.; and Peschon, J.: An Innovation Approach to

Fault Detection and Diagnosis in Dynamic Systems, Automatica, Vol. 7, No. 5, Sept. 1971, pp. 637-640.

34. Willsky, A. S.; Deyst, J. J.; and Crawford, B. S.: Adaptive Filtering and Self-Test Methods for Failure Detection and Compensation, Proc. of the 1974 JACC, Austin, Texas, June 19-21, 1974.

35. Corley, R. C.; and Spang, H. A., III: Failure Detection and Correction for Turbofan Engines, Joint Automatic Control Conference, San Francisco, California, June, 1977.

36. Van Trees, H. L.: Detection, Estimation, and Modulation Theory, Part I: Detection Estimation and Linear Modulation Theory, John Wiley & Sons, Inc., New York, 1968.

37. Willsky, A. S.; Jones, H. L.: A Generalized Likelihood Ratio Approach to State Estimation in Linear Systems Subject to Abrupt Changes, Proc. of the 1974 IEEE Conference on Decision and Control, Phoenix, Arizona, November, 1974.

38. Gustafson, D. E.; Willsky, A. S.; and Wang, J. Y., Final Report: Cardiac Arrythmia Detection and Classification Through Signal Analysis, Rept. R-920, The Charles Stark Draper Labs., Cambridge, Mass., July 1975.

39. MacFarlane, A.G.J.: Commutative Controller: A New Technique For The Design of Multivariable Control Systems, Electronic Letters 6, pp. 121-123, 1970.

40. Hill, R. G.; and Peterson, C. R.: Mechanics and Thermodynamics of Propulsion, Third Printing, Addison Wesley Pub. Co., Inc., 1970.

41. Kerrebrock, J. L.: Aircraft Engines and Gas Turbines, The M.I.T. Press, Cambridge, Mass., 1977.

42. Beattie, E.; and Spock, W.: Application of Multivariable Optimal Control Techniques to a Variable Area Turbine Engine, 1976 JACC Paper, Purdue University, Lafayette, Indiana, July 27-30, 1976.

43. DeHoff, R. L.; and Hall, W. E., Jr.: Optimal Control of Turbine Engines Winter Annual Meeting, San Francisco, California, Dec. 10-15, 1978.

44. Sain, M. K.; Leake, R. J.; Basso, R.; Gejji, R.; Maloney, A.; and Seshardi, V.: Alternative Methods for The Design of Jet Engine Control Systems Proceedings of the 1976 JACC, Purdue University, Lafayette, Indiana, July 27-30, 1976.

45. Sobey, A.; and Suggs, A.: Control of Aircraft and Missile Power Plants, John Wiley & Sons, Inc., New York, 1963.

46. Gibra, I. A.: Probability and Statistical Inference for Scientists and Engineers, Prentice Hall, Inc., Englewood Cliffs, New Jersey, 1973.

47. Miller, R. J.; and Hackney, R. D.: F-100 Multivariable Control System Engine Models/Design Criteria, Technical Report AFAPL-TR-76-74, Pratt & Whitney Aircraft Group Government Products Division, West Palm Beach, Florida.

48. Quiet Clean Short-Haul Experimental Engine Under-The-Wing Engine Digital Control System Design Report, Advanced Engineering and Technology Programs Department, General Electric Company, NASA CR-134920, R75AEG483, Jan. 1978.

49. Mihaloew, J. R.; and Hart. C. E.: Real Time Digital Propulsion System Simulation For Manned Simulators, NASA TM-78959, Presented at Fourteenth Propulsion Conference Co-sponsored by AIAA and SAE, Las Vegas, Nevada, July 25-27, 1978.

50. Hoel, P. G.; Port, S. C.; and Stone, C. J.: Introduction to Statistical Theory, Houghton Mifflin Pub. Co., 1971.

51. Hines, W. W.; and Montgomery, D. C.: Probability and Statistics In Engineering and Management Science, Ronald Press Company, 1972.

52. Rosenbrock, H. H.: State-Space and Multivariable Theory, Nelson Pub. Co., 1970.

53. Ogata, K.: State Space Analysis of Control Systems, Prentice-Hall, Inc., Englewood Cliffs, New Jersey, 1967.

54. Schafer, R. M.; and Sain, M. K.: A Dynamic Approach To The Diagonal Dominance, International Forum on Alternatives for Linear Multivariable Control, Chicago, 1978.

55. Rosenbrock, H. H.; and Storey, C.: Mathematics of Dynamic Systems, Nelson Pub. Co., 1970.

56. Powell, M.J.D.: An Efficient Method for Finding the Minimum of a Function of Several Variables Without Calculating Derivatives, Computer Journal, Vol. 7, 1964.

57. Zangwill, W. I.: Minimizing a Function Without Calculating Derivatives, Computer Journal, Vol. 10, 1967.

58. Beard, R. V.: Failure Accommodation in Linear Systems Through Self Reorganization, Rept. MVT-71-1, Ph.D. Thesis, M.I.T., Cambridge, Mass., Feb. 1971.

59. Jones, H. L.: Failure Detection in Linear Systems, Ph.D. Thesis. M.I.T., Cambridge, Mass., Sept. 1973.

60. Wells, W. R.: Detection of Sensor Failure and Output Reconstruction For Aircraft Controls, AIAA Paper No. 78-4, 1978.

61. Fisz, M.: Probability Theory and Mathematical Statistics, John Wiley & Sons, 1963.

62. Fletcher, R.: Function Minimization Without Calculating Derivatives - A Review. Computer Journal, Vol. 8,1965.

63. Crossley, T. R.: Envelope Curves for Inverse Nyquist Array Diagrams, International Journal of Control, Vol. 22, No. 1.

64. The Aircraft Gas Turbine Engine and its Operation, Pratt and Whitney Aircraft, Marketing Support, East Hartford, Connecticut, May 1974.